

Phase behavior, kinetics and structural aspects of (semi-) clathrate hydrate systems

Citation for published version (APA):

Torres Trueba, A. (2014). *Phase behavior, kinetics and structural aspects of (semi-) clathrate hydrate systems*. [Phd Thesis 1 (Research TU/e / Graduation TU/e), Chemical Engineering and Chemistry]. Technische Universiteit Eindhoven. <https://doi.org/10.6100/IR769557>

DOI:

[10.6100/IR769557](https://doi.org/10.6100/IR769557)

Document status and date:

Published: 27/03/2014

Document Version:

Publisher's PDF, also known as Version of Record (includes final page, issue and volume numbers)

Please check the document version of this publication:

- A submitted manuscript is the version of the article upon submission and before peer-review. There can be important differences between the submitted version and the official published version of record. People interested in the research are advised to contact the author for the final version of the publication, or visit the DOI to the publisher's website.
- The final author version and the galley proof are versions of the publication after peer review.
- The final published version features the final layout of the paper including the volume, issue and page numbers.

[Link to publication](#)

General rights

Copyright and moral rights for the publications made accessible in the public portal are retained by the authors and/or other copyright owners and it is a condition of accessing publications that users recognise and abide by the legal requirements associated with these rights.

- Users may download and print one copy of any publication from the public portal for the purpose of private study or research.
- You may not further distribute the material or use it for any profit-making activity or commercial gain
- You may freely distribute the URL identifying the publication in the public portal.

If the publication is distributed under the terms of Article 25fa of the Dutch Copyright Act, indicated by the "Taverne" license above, please follow below link for the End User Agreement:

www.tue.nl/taverne

Take down policy

If you believe that this document breaches copyright please contact us at:

openaccess@tue.nl

providing details and we will investigate your claim.

Phase Behavior, Kinetics and Structural Aspects of (Semi-) Clathrate Hydrate

PROEFSCHRIFT

ter verkrijging van de graad van doctor aan de Technische Universiteit
Eindhoven, op gezag van de rector magnificus prof.dr.ir. C.J. van Duijn,
voor een commissie aangewezen door het College voor Promoties, in het
openbaar te verdedigen op donderdag 27 maart 2014 om 16:00 uur

door

Alondra Torres Trueba

geboren te Mexico City, Mexico

Dit proefschrift van het proefontwerp is goedgekeurd door de promotoren en de samenstelling van de promotiecommissie is als volgt:

voorzitter: prof.dr.ir. J.C. Schouten
1^e promotor: prof.dr.ir. M.C. Kroon
2^e promotor: prof.dr.ir. C.J. Peters
leden: prof.dr.ir. R.A.J. Janssen
prof.dr. J.A. Ripmeester (University of British Columbia)
prof.dr. B. Dam (TU Delft)
prof.dr. G.-J. Kroes (Leiden University)
dr. I.R. Radović (Belgrade University)

A catalogue record is available from the Eindhoven University of Technology Library
ISBN: 978-90-386-3571-2

Cover photograph courtesy of Þröstur Þór Ágústsson
Ice walk facebook, Breiðamerkurjökull ice cave, Iceland.

Summary

In the transition from fossil fuels to alternative energy carriers, the capture and storage of carbon dioxide (CO₂) and hydrogen (H₂) is of utmost importance. CO₂ capture is necessary for reducing anthropogenic greenhouse gas emissions by combustion of fossil fuels, while an efficient and safe H₂ storage medium is required for the establishment of a so-called H₂ economy. Conventional CO₂ capture and H₂ storage processes have several disadvantages, such as the high energy consumption required or the low storage capacity obtained. This thesis focuses on the use of clathrate hydrates, which are crystalline inclusion compounds consisting of networks of water (H₂O) molecules with cavities, as alternative capture and storage media without the drawbacks of the conventional processes. Specifically, thermodynamic, kinetic, structural and molecular studies are performed in order to determine the key aspects that could enable the improvement of clathrate hydrate properties for H₂ storage and CO₂ sequestration.

The thesis presents five different studies on clathrate systems. The first study involves the measurement of phase equilibria of H₂ clathrate hydrates. The aim was to determine the influence of several organic compounds, so-called promoters, on the phase equilibrium conditions of the hydrate phase. For this purpose, the hydrate equilibrium conditions of five mixed (H₂ + organic volatile compound) clathrate hydrates at the stoichiometric concentration of the organic compound were measured. The results showed that the mixed (H₂+organic volatile compound) clathrate hydrates present a considerably higher stability, not only in comparison with the single H₂ hydrate but also in comparison with the single clathrate hydrates of the organic compounds tested. Although the results are encouraging in terms of stability, recent studies report that the maximum H₂ storage capacity of sII mixed (H₂+organic volatile compound) hydrate is not higher than ~1.0 wt% at the stoichiometric concentration of the organic volatile compound. Therefore, it is evident that a mixed (H₂ + additive) sII clathrate hydrate is still far from reaching the required capacity of at least 5 wt% or higher.

The second and third study focus on the kinetic features of semi-clathrate hydrates. Semi-clathrate hydrates or semi hydrates are another class of crystalline inclusion compounds. Similarly to clathrate hydrates, semi-hydrates also consist of networks of cavities. However, these networks are formed by mixtures of H₂O and quaternary ammonium salts (instead of H₂O only). Semi-hydrates present higher stability than clathrate hydrates. Some studies have reported that CO₂ and H₂ can be stored in such structures. However, so far no study has addressed the kinetic properties of these materials. Therefore, the kinetics of formation of three semi-hydrate systems were studied: H₂-tertbutylammonium bromine (TBAB), H₂-tertbutylammonium fluoride (TBAF) and CO₂-TBAF. The aim was to determine the factors influencing the amount of H₂ and CO₂ stored in the semi-clathrate hydrates. The results indicated that the induction time, the rate of hydrate formation and the amount of H₂ stored were favored at higher pressures and higher solute concentrations. No influence of the formation method on the hydrate growth and amount of H₂ stored was observed. The results also showed that mass transfer limitations hindered the gas transport into the hydrate phase and consequently the amount of gas stored was significantly reduced. For the CO₂-TBAF semi-hydrates the concentration of TBAF did not show a large influence, and pressure only displayed a major influence on the formation rate. Instead, the induction time and the amount of CO₂ stored were favored at low temperatures as a result of the increased subcooling. As in the case of H₂, mass transfer played a major role in the total amount of gas uptake. Although it also seems unlikely that semi-clathrate hydrates can be used to develop a viable H₂ storage technology, the results indicated that CO₂-TBAF semi-hydrates have the potential to be applied in novel separation technologies e.g., for the purification of flue gases (CO₂ removal). For instance, CO₂-TBAF semi-hydrate formation displayed shorter induction times and higher formation rates compared to H₂-TBAF semi-hydrate formation. Moreover, at low pressures the CO₂ content in the hydrate phase was considerably higher than the H₂ content.

The fourth and fifth study applied NMR spectroscopy and molecular dynamic simulations to identify specific features of fluoromethane (CH₃F) –

methane (CH_4) – TBME (*tert* –butyl-methylether) sH clathrate hydrates. The aim was to determine the ability of the two dodecahedral cages ($\text{D}-5^{12}$ and $\text{D}'-4^35^66^3$) of sH to discriminate between the two guest molecules (CH_4 and CH_3F) that are slightly different in size. ^{13}C NMR studies showed a small preference for CH_3F for the D' cage compared to the D cage. However, a more interesting feature was observed. At high temperatures, the ^{13}C NMR spectra associated with CH_3F showed a merging of the doublet structures characteristic of CH_3F in the non-spherical environments of the sII and sH cages. This merging of the doublet peaks implies a local migration of CH_3F and CH_4 between neighboring cages. Additional measurements of the ^2H NMR powder lineshapes of tetrahydrofuran (THF) - *deuterated* fluoromethane (CD_3F) hydrates at different temperatures confirmed the migration of CD_3F between neighboring cages. This phenomenon of rapid motion of the guest between cages can be attributed to water vacancies in the confining symmetry of the cages. Therefore, the results suggest that the combination of TBME and CH_3F and THF and CH_3F at temperatures above 250 K gives rise to fast dynamics of the water lattice in sII and sH. Although guest exchange between neighboring cages may also occur in other systems, this is the first report of such motion in a NMR spectrum. On the other hand, molecular dynamics calculations of the hydrogen bond dynamics and small guest rotation dynamics showed that CH_3F enhances hydrogen bonding between TBME and THF with the water framework. This could be due to the larger size of CH_3F molecules and the resulting weakening of the water hydrogen bonding network in the cages hosting CH_3F , leading to an enhanced hydrogen bonding of the large cage guests with the water framework.

Despite the unfavorable results for H_2 storage in clathrate hydrates, the knowledge gained over the last few years on the subject can open opportunities to new technological developments. For instance, the deeper understanding of the structure and interactions among guests and hosts is of particular interest. From this knowledge, new materials with higher H_2 storage capacity can be developed. The interactions of the guest with the H_2O molecules of the hydrate framework can induce defects in the structure.

These defects affect the mechanical and physical properties of the structure and motion of the guests. This study proves that in order to fully understand the behavior of these materials, further research addressing specific targets, such as the effect of a certain guest molecules or guest mixtures on the cell volume and structure, the development of methods for the incorporation of molecules on the framework and the study of the factors affecting cage occupancy, is necessary.

Alondra Torres Trueba

Samenvatting

In de overgang van fossiele brandstoffen naar alternatieve energiedragers is de opvang en opslag van koolstofdioxide (CO_2) en waterstof (H_2) uiterst belangrijk. CO_2 opvang is nodig om de antropogene broeikasgasemissie te reduceren die door de verbranding van fossiele brandstoffen, terwijl een efficiënt en veilig H_2 opslagmedium nodig is om een zogenoemde H_2 economie op te richten. Conventionele CO_2 opvang en H_2 opslagprocessen hebben enkele nadelen, zoals het benodigde hoge energieverbruik of de lage behaalde opslagcapaciteit. Deze thesis richt zich op het gebruik van clathrate hydraten, wat kristallijne insluitingsmedia zijn, bestaande uit een netwerk van water (H_2O) moleculen met holtes, als alternatief opvang- en opslagmedium zonder de nadelen van conventionele processen. In het bijzonder zijn thermodynamische, kinetische, structurele en moleculaire onderzoeken verricht om de sleutelaspecten te bepalen die de verbetering van clathrate hydraat eigenschappen voor H_2 opslag en CO_2 scheiding mogelijk te maken.

Deze thesis toont vijf verschillende onderzoeken naar clathrate hydraat systemen. De eerste studie had te maken met het fasenevenwicht van H_2 clathrate hydraten. Het doel was het bepalen van de invloed van verschillende organische stoffen, zogenoemde promotors op de condities van het fasenevenwicht van de hydraat fase. Daarvoor zijn de condities gemeten voor hydraat-evenwicht van vijf gemengde clathrate hydrates (H_2 + vluchtig organisch stof) bij de stoichiometrische concentratie. De resultaten laten zien dat het gemengde clathrate hydrate (H_2 + vluchtige organische stof) een aanzienlijke hogere stabiliteit liet zien, niet alleen in vergelijking met het eenzijdige H_2 hydraat, maar tevens in vergelijking met het eenzijdige hydraat van de geteste organische stof. Hoewel de resultaten aanmoedigend zijn in hun stabiliteit, laten recente studies een maximale opslagcapaciteit van slechts ~1.0 massa-% H_2 zien in sII gemengde hydraten (H_2 + vluchtige organische stof), in een stoichiometrische concentratie van de vluchtige organische stof. Het is evident dat een gemengd (H_2 – additief) sII clathrate hydraat nog ver van de benodigde capaciteit van 5 massa-% of hoger verwijderd is.

De tweede en derde studie richtten zich op de kinetische kenmerken van semi-clathrate hydrates. Semi-clathrate hydraten of semi hydraten behoren tot een andere klasse van stoffen met kristallijne insluiting. Net als clathrate hydraten bestaan semi-hydraten ook uit een door H_2O moleculen gevormd netwerk van holtes. Echter, semi-hydraten worden gevormd in mengsels van H_2O en quaternaire ammoniumzouten (in plaats van enkel H_2O). Semi-hydraten laten een hogere stabiliteit zien dan clathrate hydrates. Enkele studies melden dat CO_2 en H_2 opgeslagen kunnen worden in zulke structuren. Desalniettemin zijn in geen enkele studie de kinetische eigenschappen van deze materialen beschreven. Daarom zijn de vormingskinetica van drie semi-hydraat systemen bestudeerd: H_2 -tertbutylammonium bromine (TBAB), H_2 -tertbutylammonium fluoride (TBAF) en CO_2 -TBAF. Het doel was om de factoren te bepalen die invloed hebben op de opslagcapaciteit van H_2 en CO_2 in semi-clathrate hydrates. De resultaten laten een betere inductietijd, vormingssnelheid en de hoeveelheid opgeslagen H_2 zien onder hoge druk en hoge oplossingsconcentratie. Invloed van de vormingsmethode op de hydraatgroei en de opslaghoeveelheid van H_2 werd niet opgemerkt. De resultaten laten zien dat de grens in de massatransport de verplaatsing van het gas in de hydraatfase verhindert en als gevolg daarvan de gasopslaghoeveelheid significant verlaagt. Voor de CO_2 -TBAF semi-hydraten liet de concentratie van TBAF geen grote invloed zien; enkel de druk liet een grote invloed op de vormingssnelheid zien. In tegenstelling daartot werden inductietijd en CO_2 opslaghoeveelheid gunstiger bij lage temperatuur als gevolg van de toegenomen onderkoeling. Net als met H_2 speelt massatransport een grote rol in de totale opname. Hoewel het tevens onwaarschijnlijk lijkt dat semi-clathrate hydrates gebruikt kunnen worden om een levensvatbare H_2 opslagtechnologie te ontwikkelen, wijzen de resultaten erop dat CO_2 -TBAF semi-hydraten potentie hebben om in nieuwe scheidingstechnologieën toegepast te worden, bv. voor de zuivering van rookgassen (verwijdering van CO_2). Bijvoorbeeld liet CO_2 -TBAF semi-hydraat vorming een kortere inductietijd en een hogere vormingssnelheid zien dan bij H_2 -TBAF semi-hydraten. Bovendien is het gehalte CO_2 in de hydraatfase bij lage druk aanzienlijk hoger dan het H_2 gehalte.

De vierde en vijfde studie hebben NMR spectroscopie en moleculaire dynamische simulaties toegepast om specifieke eigenschappen te identificeren van de fluormethaan (CH_3F) – methaan (CH_4) – TBME (tert-butylmethylether) sH clathrate hydrate. Het doel was het bepalen van het vermogen tot onderscheiding tussen de twee gastmoleculen (CH_4 and CH_3F), die lichtelijk afwijkend in grootte zijn, in de twee dodecahdrale holtes (D-5¹² and D'-4³⁵⁶⁶³) van sH. ¹³C NMR studies lieten een lichte voorkeur van CH_3F zien voor de D' holte in vergelijking tot de D holte. Er werd echter een interessanter kenmerk geobserveerd. Bij hoge temperaturen lieten de ¹³C NMR spectra, gerelateerd met CH_3F , een samenvoeging van de doublet structuren zien, karakteristiek voor CH_3F in niet-bolvormige omgeving van de sII en sH holtes. Het samenvoegen van de doublet pieken impliceert een lokale migratie van CH_3F en CH_4 tussen buurholtes. Aanvullende metingen van de ²H NMR poeder lijnvormen van het tetrahydrofuran (THF) / Deuteriumfluormethaan (CD_3F) hydraat bij afwijkende temperaturen bevestigde de migratie van CD_3F tussen buurholtes. Dit fenomeen van snelle beweging van de gast tussen holtes kan worden toegewezen aan leegstand van water in de opsluitingssymmetrie van de holtes. Daarom suggereren de resultaten dat de combinatie van TBME en CH_3F , en THF en CH_3F bij temperaturen boven 250K snelle dynamica van het waterrooster in sII en sH veroorzaken. Hoewel uitwisseling van de gast tussen buurholtes tevens in andere systemen voor kunnen komen, is dit de eerste rapportage van zo'n beweging in een NMR spectrum. Aan de andere kant lieten moleculair-dynamische berekeningen aan de dynamica van waterstofbindingen en rotatiedynamica van de kleine gast zien dat CH_3F waterstofbindingen tussen TBME en THF met het waterrooster bevordert. Dit zou gevolg kunnen zijn van de grotere afmeting van CH_3F moleculen en als gevolg de verzwakking van het water-waterstof-bindingsnetwerk in de holtes die CH_3F behuizen, wat voortvloeit in een bevordering van de waterstofbindingen met het waterrooster van de holtes van de grote gast.

Ondanks de ongunstige resultaten in H₂ opslag in clathrate hydrates, kan de kennis die de laatste paar jaar op dit onderwerp is opgedaan kansen openen naar nieuwe technologische ontwikkelingen. Met name een groot begrip van de structuur en wisselwerking tussen gast en waard is erg interessant. Met deze kennis kunnen nieuwe materialen met hogere H₂-opslagcapaciteit worden ontwikkeld. De wisselwerking tussen de gast en de H₂O moleculen van het hydratrooster kan afwijkingen in de structuur inbrengen. Deze afwijkingen hebben invloed op de mechanische en fysische eigenschappen van de structuur en beweging van de gasten. Deze studie bewijst dat aanvullend onderzoek nodig is om het gedrag van deze materialen te begrijpen, die zich richten op specifieke doelen zoals het effect van een zeker gastmolecuul of gastmengsel op het volume van de holte en de structuur, de ontwikkeling van methodes voor de inlijving van moleculen in het rooster en het bestuderen van factoren die invloed hebben op holte benutting.

Alondra Torres Trueba

Table of Contents

1. Introduction	1
1.1 Problem definition	2
1.1.1 Carbon dioxide (CO ₂) capture and sequestration (CCS)	3
1.1.2 The “hydrogen (H ₂) economy” and the problem of H ₂ storage	4
1.2 Gas hydrates for CO ₂ capture and sequestration and H ₂ storage	5
1.2.1 Gas hydrates as energy source	6
1.2.2 Gas storage in gas hydrates	6
1.2.3 Challenges in gas storage with clathrate hydrates	7
1.3 Another class of hydrates for gas storage	7
1.4 Scope of the thesis	8
1.5 References	9
2. Fundamentals of clathrate hydrates and semi-clathrate hydrates	13
2.1 Introduction	14
2.1.1 Early history	14
2.1.2 Definition	15
2.1.3 Characteristics of the hydrate cavities	16
2.1.4 Clathrate hydrate structures	18
2.1.5 Semi-clathrate hydrates	19
2.2 Stability of clathrate hydrates	20
2.2.1 Phase equilibrium and phase diagrams	20
2.2.2 The Gibbs’ phase rule	21
2.2.3 Clathrate hydrates phase behavior	23
2.3 Hydrate formation	28
2.3.1 Hydrate nucleation	29
2.3.2 Hydrate growth	30
2.4 Characterization techniques to determine structural aspects of clathrate hydrates	32
2.4.1 Powder X-ray diffraction	32
2.4.2 Raman spectroscopy	34

2.4.3 Nuclear magnetic resonance	36
2.5 References	38
3. Experimental methodology	45
3.1 Introduction	46
3.2 Phase behavior measurements	46
3.2.1 Sample preparation	46
3.2.2. Experimental set-up	47
3.2.3 Experimental procedure	48
3.3. Kinetics of formation of clathrate and semi-clathrate hydrates	51
3.3.1 Experimental set-up	51
3.3.2 Experimental procedure	52
3.4 Characterization techniques of clathrate hydrates	53
3.4.1 Sample preparation	53
3.4.2 Powder X-ray diffraction measurements	54
3.4.3 Nuclear magnetic resonance spectroscopy measurements	55
3.5 References	55
4. Phase equilibrium of structure II clathrate hydrates of hydrogen with various promoters	57
4.1 Introduction	58
4.2 Background	58
4.3 Experimental methodology	60
4.3.1 Materials	60
4.3.2 Experimental procedure	60
4.4 Results and discussion	60
4.5 Conclusions	70
4.6 References	70
5. Kinetics measurements and <i>in situ</i> Raman spectroscopy of formation of hydrogen-tetrabutylammonium bromide semi-hydrates	75
5.1 Introduction	76
5.2 Background	76
5.3 Methodology	78
5.3.1 Materials	78

5.3.2	<i>Experimental set-up and procedure</i>	78
5.4	Results and discussion	79
5.4.1	<i>The T-cycle and the T-constant methods</i>	79
5.4.2	<i>Induction time</i>	81
5.4.3	<i>Rate of formation and amount of H₂ consumed</i>	82
5.4.4	<i>sII H₂-THF clathrate hydrates Raman spectroscopic studies</i>	86
5.4.5	<i>H₂-TBAB semi-hydrate Raman spectroscopic studies</i>	88
5.5	Conclusions	91
5.6	References	92
6.	Kinetic measurements and <i>in situ</i> Raman spectroscopy study of the formation of TBAF semi-hydrates with hydrogen and carbon dioxide	95
6.1	Introduction	96
6.2	Background	96
6.3	Methodology	97
6.3.1	Materials	97
6.3.2	Experimental apparatus and procedure	97
6.4	Results and discussion	98
6.4.1	<i>Induction time</i>	98
6.4.2	<i>Rate of formation and total amount of guest gas consumed</i>	102
6.4.3	<i>H₂-TBAF semi-hydrate Raman spectroscopic studies</i>	106
6.4.4	<i>CO₂-TBAF semi-hydrate Raman spectroscopic studies</i>	111
6.5	Conclusions	113
6.6	References	114
7.	Inter-cage dynamics in structure I, II, and H fluoromethane hydrates as studied by ¹³C and ²H NMR	119
7.1	Introduction	120
7.2	Background	120
7.3	Materials and methods	121
7.4	Results and discussion	122
7.5	Conclusions	131
7.6	References	132

Table of Contents

8. Molecular dynamics study of sII and sH fluoromethane and methane hydrates	137
8.1 Introduction	138
8.2 Computational methods	138
8.3 Thermodynamics of the guest substitution	142
8.4 Results and discussion	144
8.5 Conclusions	156
8.6 References	156
9. Conclusions and outlook	159
Appendix A	165
Personal Information	169
List of Publications	170
Conference proceedings and book abstracts	172
Acknowledgments	174

Chapter 1

Introduction



1. Introduction

1.1 Problem definition

Ever since the Industrial Revolution took place in the 18th century, fossil fuels have been used massively to power our economy. In fact, the birth of our industrial civilization was possible due to the high availability, low cost and versatility of fossil fuels. This has result on a strong worldwide dependence to oil, coal and natural gas. For instance, in 2012, these three fuels contributed with 87% of the global energy demand, while other sources like hydroelectric, nuclear and renewable only contributed with 13 % (see Figure 1.1).

The worldwide dependence on fossil fuels as a primary energy source entails several severe consequences. Firstly, fossil fuels reserves are limited and due to continued population growth and due to the increasing consumption of the emerging economies, the conventional reserves of fossil fuels are close to be depleted. As a result oil companies have been forced to perform and develop more complex extraction methods in deeper deposits. However, despite the efforts of the oil companies to find newer and unconventional deposits, in the long term, unavoidable will be necessary to switch to different alternatives to satisfy the global energy requirements. Secondly, in our current economic system, growth is only possible by high energy consumption. As a consequence, there is an increasing competition for fossil fuels. This creates tensions between producing and consuming countries, which in extreme cases may lead to acts of war or to social and economic instability [2]. Thirdly, exploitation of fossil fuels creates pollution on local, regional and global scales. Therefore, the major concerns of the current globalized world are the development of alternatives to reduce the global energy dependence on fossil fuels and the creation of measures to diminish their polluting effects. Few of such measures are described in the following sections.

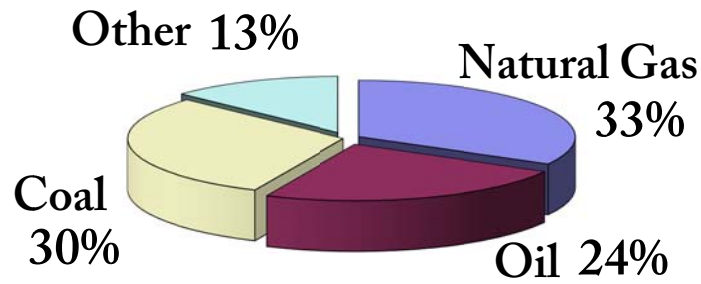


Figure 1.1. Distribution of energy consumption in 2012 [1].

1.1.1 Carbon dioxide (CO_2) capture and sequestration (CCS)

The combustion of fossil fuels releases greenhouse gases, whose main component is CO_2 (See Figure 1.2). Anthropogenic greenhouse gas emissions, especially carbon dioxide (CO_2) emissions, are associated with global warming, which is a threat to the global climate and may lead to major environmental degradation [4]. Furthermore, emissions from the combustion of fossil fuels are also responsible for local air pollution, which is becoming a serious problem due to the hazardous effects to human health [5].

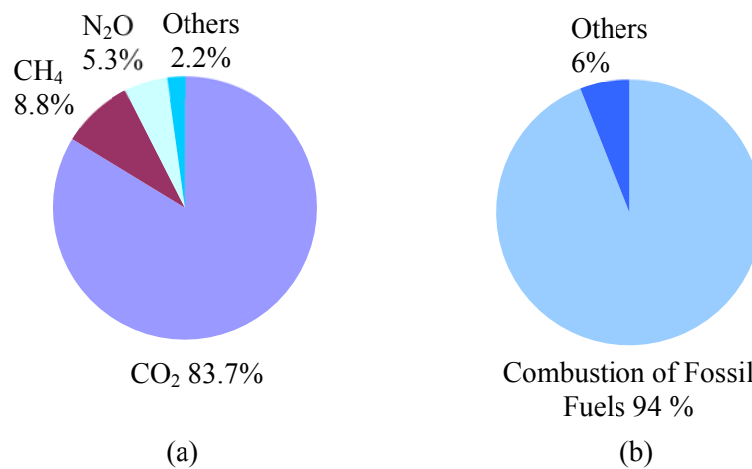


Figure 1.2. (a) Greenhouse gas emissions in U.S. by gas 2011. (b) Sources of CO_2 gas emissions in U.S. in 2011 [3].

In order to mitigate these effects, policies penalizing the release of CO₂ to the atmosphere and encouraging the removal and sequestration of CO₂ from waste streams, have been implemented. As a result, conventional technologies for CO₂ capture and sequestration (CCS), such as: absorption, adsorption and membrane separation [6], have gained importance. However, these technologies have also raised environmental concerns due to their intensive energy requirements, the amount of chemical consumption and emissions, and the significant infrastructure requirements. Therefore, the development of new technologies for CCS and with minimal environmental impacts [7] keeps attracting worldwide research efforts. In section 1.2 one of these innovative solutions is presented.

1.1.2 The “hydrogen (H₂) economy” and the problem of H₂ storage

In the search for alternatives to reduce the dependence on fossil fuels several options have been proposed. One of these alternatives is the establishment of the so-called “H₂ economy”, namely the substitution of fossil fuels by H₂ as a secondary energy form. The H₂ economy might be a viable option since H₂ offers numerous benefits over all conventional fuels. For instance, it is the most abundant element and with the highest energy content per mass in the universe [8,9]. Additionally, H₂ is not toxic and the product of its combustion is water (H₂O). Currently, H₂ is produced by steam reforming from hydrocarbons but it can also be produced from renewable technologies [10]. Moreover, H₂ can be produced from any locally available primary energy source, thus reducing the dependence on fossil fuels and providing energy security.

However, despite all the advantages, the H₂ economy faces several technical obstacles. A major barrier is to find an effective, safe, and stable H₂ storage medium [11]. The main problem is that although H₂ has a high energy density by mass, its energy density by volume is very poor. Therefore, it requires larger (heavier) storage than conventional fuels to provide the same amount of energy. For example, the H₂ content of 1 L of gasoline (main fuel for vehicles) is 116 g whereas 1 L of pure H₂ contains 71 g of H₂. This

implies that 1 L of gasoline possesses 64% more energy than the same volume of liquid H₂, without taking into account the energy contribution of the carbon content in gasoline [12]. As a result, several technologies for H₂ storage have been considered and studied. Nevertheless, despite some promising achievements all materials and methods still present some essential drawbacks. For instance, materials such as: metal hydrides, metal nitrides and metal imides are very expensive; some of them present irreversible H₂ absorption/desorption while others require of high temperatures for H₂ release. Materials like metal organic frameworks, hollow glass microspheres, carbon based materials and zeolites [13], present low H₂ storage capacity especially under mild operating conditions [12]. Therefore, further options are required to achieve an efficient and safer method for H₂ storage.

1.2 Gas hydrates for CO₂ capture and sequestration and H₂ storage

A possible solution for both CO₂ and H₂ storage, are clathrate hydrates. Clathrate hydrates or gas hydrates are nanoporous crystalline materials in which, gas molecules occupy cages in a water framework. The framework consists of cages formed by hydrogen bonds between water molecules. The cages are stabilized by van der Waals forces between the water molecules and the guest molecule [14] (See Figure 1.3). All molecules of the right size can form gas hydrates by their gas, liquid or solid, normally at low temperature conditions (≤ 300 K) [15]. Gas hydrates can be formed either by synthetic or natural methods and can be found in earth and elsewhere in the universe [16]. The main component of naturally occurring gas hydrates, in addition to water, is methane, although other hydrocarbon gases such as ethane and propane are also present. Part of this thesis is aimed to explore the potential of gas hydrates and semi-hydrates as an alternative solution for CO₂ and H₂ storage.

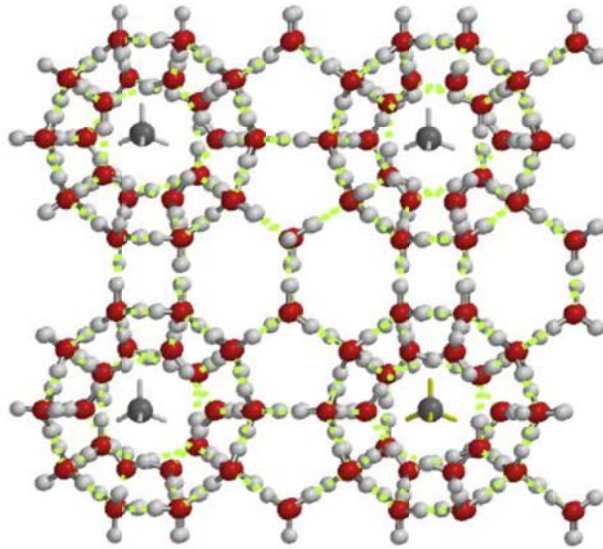


Figure 1.3. Schematic representation of clathrate hydrates.

1.2.1 Gas hydrates as energy source

Natural gas hydrates are considered to be an unconventional energy source. Vast reserves are present all over the world mainly in deep-water subsea sediments, frozen permafrost but also in some inland lakes [15,17]. Additionally, some natural gas hydrates reserves have the advantage, unlike conventional reserves of natural gas, of presenting high purity methane and less harmful gases; therefore, the environmental pollution is lower. Furthermore, methane gas hydrates have higher energy density [18] than conventional natural gas.

1.2.2 Gas storage in gas hydrates

In addition to the enormous potential of natural gas hydrates as energy source, another aspect of particular interest for gas hydrates is the study and development of hydrate based technologies for gas storage and sequestration [15,19]. Due to their physical properties, gas hydrates are an attractive medium for both H₂ storage and CO₂ storage and sequestration [13]. For

instance, a volume of gas hydrates can contain as much as 160 volumes of gas at standard temperature and pressure conditions. Moreover, capture and sequestration of CO₂ by hydrate formation is less energy demanding and more environmentally friendly compared to the other techniques available. What is more, H₂ storage in hydrates is safer, costs less, and presents higher reversibility than other potential H₂ storage materials.

1.2.3 Challenges in gas storage with clathrate hydrates

Nevertheless, the high pressure conditions associated with hydrate formation and its low storage capacity have hindered the development of hydrate based technologies. In order to reduce the pressure conditions necessary and to accelerate the hydrate phase formation, a second type of hydrate former that changes the hydrate structure, a so-called promoter, can be added. The resulting material is a mixed clathrate hydrate (promoter + gas + H₂O) which is more stable than single gas hydrates. The addition of a promoter however, significantly reduces the H₂ storage capacity since some cavities are occupied by the promoter. The inclusion of the promoter or additive presents other drawbacks, in addition to the reduction of the (gas) storage capacity, like health and safety concerns due to the chemical nature of the promoter and contamination of the gas phase.

1.3 Another class of hydrates for gas storage

Other class of crystalline inclusion compounds has also been object of intense research, the salt hydrates, nowadays also named semi-clathrate hydrates or semi-hydrates. These materials are formed by H₂O molecules and quaternary ammonium salts. Unlike conventional clathrate hydrates, in which the cages are formed exclusively by H₂O molecules, the cage frame of semi-hydrates consists not only of H₂O molecules but also by the anions of the salt. The tetrabutylammonium cations play the role of host molecules and are placed inside super cages composed of four large (T, P, H) cavities. The cavity space between the four cavities is connected by having water molecules missing

from the vertices. Semi-hydrates also have several kinds of D cages where guest molecules, such as CO₂ and H₂, can be hosted. These features provide higher stability to semi-hydrates compared to mixed clathrate hydrates.

For instance, hydrogen tetrabutylammonium fluoride (TBAF) semi-hydrates are stable at room temperature and atmospheric pressure. Additionally, the semi-hydrate formation process is reversible and the quaternary ammonium salts used as additives are non-volatile. Therefore, the gas phase is not contaminated upon dissociation of the semi-hydrate. Despite the above, studies on gas-semi-hydrate systems are scarce. Moreover, the H₂ and CO₂ storage capacity of such materials is still unknown as well as their kinetic properties.

1.4 Scope of the thesis

This thesis presents the study of several properties of clathrate hydrate and semi-hydrate systems in order to supplement their potential and technical feasibility for gas storage with a main focus on H₂. As starting point, Chapter 2 provides the theoretical aspects of clathrate hydrates. The thermodynamic, kinetic and structural properties of clathrate hydrates are reviewed, together with a brief description of the fundamentals and methods for characterization. In Chapter 3, a detailed description of the different experimental set-ups and methodologies followed in each study, are reported.

Chapter 4 presents the study of the role of five organic compounds with different features on the stability conditions of sII H₂ clathrate hydrates. The phase equilibrium of the resulting mixed (organic compound-H₂) clathrate hydrates are reported and analyzed. Additionally the phase equilibrium conditions of the binary systems “H₂O + organic compound” up to pressures of 14.0 MPa are presented.

Chapters 5 and 6 study the kinetics of formation of semi-clathrate hydrates of tetrabutylammonium bromide (TBAB) with H₂ and tetrabutylammonium

fluoride (TBAF) with H₂ and with CO₂. The effect of pressure, concentration and formation method on the induction time, formation rate and gas storage capacity is reported. Additionally the Raman spectrum collected *in situ* during the formation and dissociation of the different semi-hydrates systems is analyzed.

Chapter 7 presents a study based on ¹³C NMR measurements to explore the ability of the two dodecahedral cages of structure H to distinguish between CH₄ and fluoromethane (CH₃F). Additionally, an uncommon behavior of rapid exchange of guest molecules between the dodecahedral cages of sH is investigated by ¹³C NMR and ¹H NMR.

In order to complement the experimental work of the current thesis, Chapter 8 presents a molecular dynamics study. The thermodynamic substitution of CH₄ by CH₃F in the small and middle cages of structure H was studied with the aim to corroborate whether there is a cage preference for the two molecules. In addition, a molecular study of hydrogen bonding in the double TBME/CH₃F and TBME/CH₄ sH clathrate hydrates was performed in order to support the observations of the NMR study presented in the Chapter 7.

Finally, Chapter 9 summarizes the conclusions and presents recommendations and the perspective on future clathrate hydrate research.

1.5 References

- [1] BP Statistical Review of World Energy June 2012.
- [2] Ball M., Wietschel M. The future of hydrogen - opportunities and challenges. *International Journal of Hydrogen Energy*. 2009;34:615-27.
- [3] Agency U. S. E. P. Inventory of U.S. Greenhouse Gas Emissions and Sinks: 1990-2011. 2013.
- [4] Barbir F. Transition to renewable energy systems with hydrogen as an energy carrier. *Energy*. 2009;34:308-12.

- [5] Brunekreef B. Air Pollution and Human Health: From Local to Global Issues. In: Jun Y., editor. *Harmony of Civilization and Prosperity for All*. Amsterdam: Elsevier Science Bv; 2010. p. 6661-9.
- [6] Li B. Y., Duan Y. H., Luebke D., Morreale B. Advances in CO₂ capture technology: A patent review. *Applied Energy*. 2013;102:1439-47.
- [7] Singh B., Stromman A. H., Hertwich E. G. Scenarios for the environmental impact of fossil fuel power: Co-benefits and trade-offs of carbon capture and storage. *Energy*. 2012;45:762-70.
- [8] McWhorter S., Read C., Ordaz G., Stetson N. Materials-based hydrogen storage: Attributes for near-term, early market PEM fuel cells. *Current Opinion in Solid State & Materials Science*. 2011;15:29-38.
- [9] Fayaz H., Saidur R., Razali N., Anuar F. S., Saleman A. R., Islam M. R. An overview of hydrogen as a vehicle fuel. *Renewable and Sustainable Energy Reviews*. 2012;16:5511-28.
- [10] Mazloomi K., Gomes C. Hydrogen as an energy carrier: Prospects and challenges. *Renewable & Sustainable Energy Reviews*. 2012;16:3024-33.
- [11] Conte M., Iacobazzi A., Ronchetti M., Vellone R. Hydrogen economy for a sustainable development: state-of-the-art and technological perspectives. *Journal of Power Sources*. 2001;100:171-87.
- [12] Lim K. L., Kazemian H., Yaakob Z., Daud W. R. W. Solid-state Materials and Methods for Hydrogen Storage: A Critical Review. *Chemical Engineering & Technology*. 2010;33:213-26.
- [13] Di Profio P., Arca S., Rossi F., Filippini M. Comparison of hydrogen hydrates with existing hydrogen storage technologies: Energetic and economic evaluations. *International Journal of Hydrogen Energy*. 2009;34:9173-80.
- [14] Desmedt A., Bedouret L., Pefoute E., Pouvreau M., Say-Liang-Fat S., Alvarez M. Energy landscape of clathrate hydrates. *European Physical Journal-Special Topics*. 2012;213:103-27.
- [15] Ning F. L., Yu Y. B., Kjelstrup S., Vlugt T. J. H., Glavatskiy K. Mechanical properties of clathrate hydrates: status and perspectives. *Energy & Environmental Science*. 2012;5:6779-95.
- [16] Maslin M., Owen M., Betts R., Day S., Jones T. D., Ridgwell A. Gas hydrates: Past and future geohazard? *Philosophical Transactions of the Royal*

Society A: Mathematical, Physical and Engineering Sciences. 2010;368:2369-93.

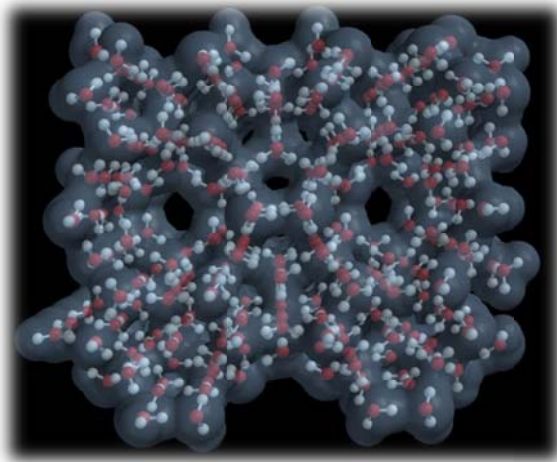
[17] Makogon Y. F. Natural gas hydrates – A promising source of energy. *Journal of Natural Gas Science and Engineering*. 2010;2:49-59.

[18] Zhang J. S., Lee J. W. Equilibrium of Hydrogen plus Cyclopentane and Carbon Dioxide plus Cyclopentane Binary Hydrates. *Journal of Chemical & Engineering Data*. 2009;54:659-61.

[19] Eslamimanesh A., Mohammadi A. H., Richon D., Naidoo P., Ramjugernath D. Application of gas hydrate formation in separation processes: A review of experimental studies. *Journal of Chemical Thermodynamics*. 2012;46:62-71.

Chapter 2

Fundamentals of Clathrate Hydrates and Semi-Clathrate Hydrates



2.1 Introduction

This chapter provides the fundamentals of clathrate hydrates. In section 2.1.1 a brief history of the motivation behind hydrate research is presented. Sections 2.1.2 – 2.1.4 provide the description, general properties and structures of clathrate hydrates. In section 2.1.5 the characteristics of semi-hydrates are presented. Section 2.2 provides the principles and thermodynamic properties of clathrate hydrates. Section 2.3 presents a general overview of hydrate formation kinetics, including nucleation and growth. Finally, section 2.4 presents a description of the characterization techniques used to elucidate hydrate structure.

2.1.1 Early history

Clathrate hydrates or gas hydrates have been object of intensive research since they were discovered in 1810 by Sir Humphrey Davy [1]. Most of the structures known nowadays were synthesized in the nineteenth century. These early studies focused on the identification of the molecules forming clathrate hydrates, and their formation conditions. Later on, in 1930, hydrocarbon clathrate hydrates also invoke considerable amount of applied research. In this occasion the studies were the consequence of a major problem faced by of the oil and gas industry; the plugging of transportation pipelines by gas hydrates [2]. As a result, intensive research was supported by the oil and gas industry with the aim to prevent hydrate formation. This field of research gave origin to the discipline of flow assurance [3]. Investigations on hydrate structure and formation conditions followed, as well as the development and verification of thermodynamic models. In addition, several hydrate thermodynamic inhibitors and promoters were identified. In the middle 60's, the discovery of the first natural gas hydrate deposit triggered the interest on the kinetics of clathrate hydrates. Extensive research was performed in understanding hydrate formation and decomposition, mainly with the aim to develop a method for natural gas production from clathrate hydrate sediments. The study of the kinetic properties also lead to the development of kinetic inhibitors. Nowadays this area of study still attracts a

considerable interest due to the economic potential of natural gas reserves. Other areas that are now subject of research on the field are: the sequestration and the storage of carbon dioxide and the separation of pre-combustion and post-combustion gases. These topics are the result of new policies aimed to reduce environmental pollution. Gas storage on clathrate hydrates has also become an important area of research. Finally, other fields of research include the study of clathrate hydrates properties as a refrigerants, for water desalination processes [4, 5] as well as the study of hydrates in the outer space [6].

2.1.2 Definition

Clathrate hydrates can be described as crystalline solid compounds formed in mixtures of water (H_2O) and non- or slightly polar low molecular gases or volatile liquids [7]. Clathrate hydrates tend to form under conditions of low temperature and high pressure. The hydrogen bonds of the water molecules form networks of cavities that are partially filled with the hydrate forming molecules, also known as ‘guest molecules’. Depending on the properties and characteristics of the guest molecule, clathrate hydrates may adopt different structures [8]. These structures are the result of the grouping of two or more cavities sharing faces in a certain ratio. The three common structures are: (i) structure I (sI), (ii) structure II (sII), and (iii) structure H (sH). The unit cell is the smallest repeating unit of a crystal structure [9]. The unit cell of sI is composed by 46 H_2O molecules forming 2 pentagonal dodecahedrons (5^{12}) and 6 tetrakaidecahedrons ($5^{12}6^2$). The unit cell of sII is composed by 136 H_2O molecules forming 16 pentagonal dodecahedrons (5^{12}) and 8 hexakaidecahedrons ($5^{12}6^4$). Finally, the unit cell of sH is composed by 34 H_2O molecules forming; 3 pentagonal dodecahedrons (5^{12}), 2 irregular dodecahedrons ($4^35^66^3$) and 1 icosahedron ($5^{12}6^8$). The geometric parameters and characteristics of the three structures are given in Table 2.1. There are different notations for the polyhedral present in the three clathrate hydrate structures. The most convenient, is the one related to their number of faces. For instance, the pentagonal dodecahedron due to its 12 faces is denoted as the D cavity, the tetrakaidecahedron is denoted as the T cavity, the

hexakaidecahedron as the H cavity, and the icosahedron as the E cavity. Some structures have different kinds of D or T cages, which are distinguished by primes. For example, the irregular dodecahedron in sH is denoted as D'. The following section presents a detailed description of the hydrate cavities.

2.1.3 Characteristics of the hydrate cavities

The hydrate cavities are formed by hydrogen bonds between H₂O molecules. Each H₂O molecule forms a hydrogen bond with four nearest neighbor molecules, of which, three form edges of a specific cavity and the fourth is directed outward from the cavity. The D cavity is energetically the most advantageous and it is present in almost all the clathrate structures [11]. This cavity can accommodate species as small as H₂ and He, as well as molecules with an average diameter of 5.2 Å, such as xenon, hydrogen sulfide, CH₄ and CO₂. However, the D cavity requires the presence of larger cavities with greater energy capacity to fill the space available, such as the T, H and E cavities. Experimental data on the structures compositions [11] and distribution of the guest molecules among the cavities, have shown that the degree of filling of the large cavities in all structures is close to unity while the D cavities are either vacant or partially occupied. The T cavity hosts molecules with an average diameter ≤ 6.0 Å and it presents an oblate geometry similar to an ellipsoid. Due to this feature, guest shape is essential in cavity stability [10]. The H cavity hosts molecules with an average diameter ≤ 6.6 Å and it is the most spherical of all clathrate hydrate cavities. The E cavity is the largest of the three common clathrate hydrate structures, it can host molecules of size between 7.1 and 9 Å. However due to its particular shape, efficient space filling in addition to suitable size is required for cavity stability [12]. Figure 2.1 shows the polyhedra present in the different structures of clathrate hydrates. Polyhedra with higher sizes can be encountered in hydrate structures, such cavities are characteristic of semi-clathrate hydrate structures. These larger polyhedra are formed by the combination of several cavities. Further description of semi-clathrate hydrates and their structure will be presented in section 2.1.5.

Table 2.1. Characteristics of the three structures of clathrate hydrates. Data modified from Sloan and Koh 2008 [10].

Hydrate Crystal Structure	I		II		H		
	Small	Large	Small	Large	Small	Medium	Large
Cavity Description	5 ¹² (D)	5 ¹² 6 ² (T)	5 ¹² (D)	5 ¹² 6 ⁴ (H)	5 ¹² (D)	4 ³ 5 ⁶ 6 ³ (D')	5 ¹² 6 ⁸ (E)
Number of cavities per unit cell	2	6	16	8	3	2	1
Average cavity radius (Å)	3.95	4.33	3.91	4.73	3.94	4.04	5.79
Variation in radius (%)	3.4	14.4	5.5	1.73	4.0	8.5	15.1
No. of water molecules per cavity	20	24	20	28	20	20	36
Crystal system	Cubic		Cubic		Hexagonal		
Space group	Pm3n		Fd3m		P6/mmm		
Lattice parameters	a = 12 Å α = β = γ = 90°		a = 17.3 Å α = β = γ = 90°		a = 12.2 Å c = 10.1 Å α = β = 90°, γ = 120°		

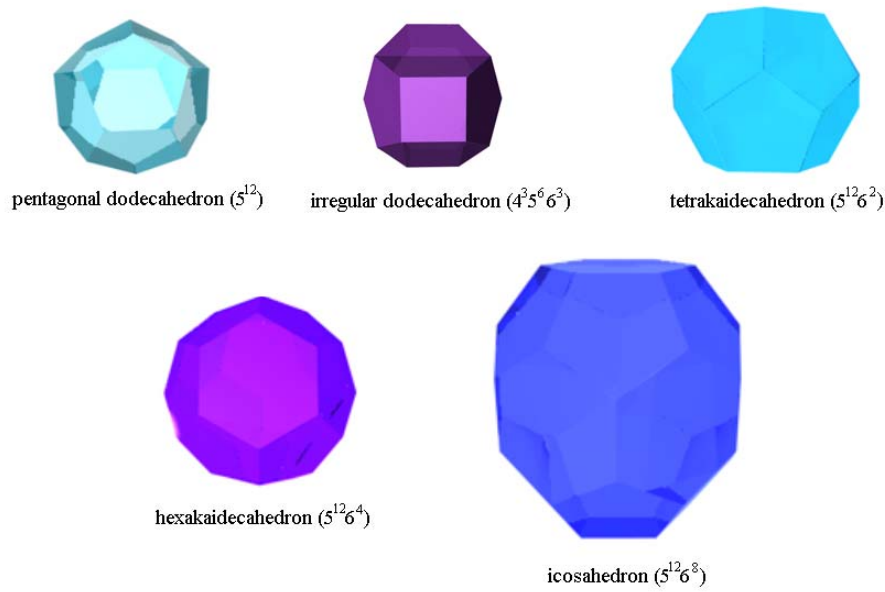


Figure 2.1. Polyhedra present in the different structures of clathrate hydrates.

2.1.4 Clathrate hydrate structures

As it was mentioned before, clathrate hydrate structures are formed by the combination of two or more cavities sharing faces in a certain ratio. The crystal structure I consists of a primitive cubic lattice [13] with parameters presented in Table 2.1. A representation of sI is displayed in Figure 2.2. In sI, the H cavity shares the two hexagonal faces and eight of the twelve pentagonal faces with other H cavities. The remaining pentagonal phases are shared with D cages. There is no direct face sharing among the D cages. The structure can thus be constructed from the vertices of the face sharing H cavities that are arranged in columns, with the H cavities sharing their opposing hexagonal phases. These columns are stacked so, they share each a pentagonal face between each pair of H cavities and the remaining spaces are the D cavities.

The crystal structure II consists of a face-centered cubic lattice [14] with parameters also presented in Table 2.1. A representation can also be observed in Figure 2.2. In sII, the D and T cavities share faces in the ratio 2:1. There

is a three dimensional face-sharing arrangement of the D cavities, in which the residual voids are the T cavities. A convenient way to picture the structure is to consider it build by stacked layers. One layer is composed by face sharing D cavities while the other layer is composed by H and D cavities.

The crystal structure H is hexagonal of space group P6/mmm. The lattice parameters are presented in Table 2.1 and a representation is displayed in Figure 2.2. sH is also represented by alternating layers. One layer consists of pentagonal face sharing D cavities, this layer alternates with a layer of square face-sharing D' cages, the residual voids are the E cavities.

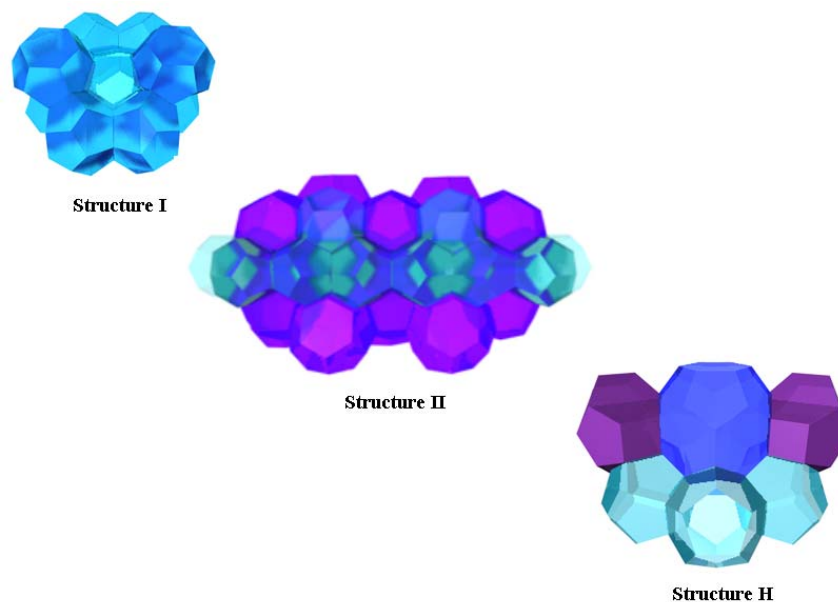


Figure 2.2. Structures of clathrate hydrates.

2.1.5 Semi-clathrate hydrates

Semi-clathrate hydrates or semi hydrates are another class of crystalline inclusion compounds. Similarly to clathrate hydrates, semi-hydrates also consist of networks of cavities formed by H₂O molecules. However, semi-hydrates are formed in mixtures of water and quaternary ammonium salts. Therefore, in this case, the cation of the quaternary ammonium salt plays the

role of guest molecule being placed inside a supercage that is the result of the combination of four large (T, P or H) cavities [15]. Such cavity forms when a water molecule is pushed out of a vertex shared by some of the large cavities, which is then occupied by the cationic central atom. Additionally, the anion of the salt is thus incorporated in the water lattice. This feature provides higher stability to semi-clathrate hydrates compared to clathrate hydrates. Semi-hydrates also contain D cages; therefore, they can host the molecules characteristic of such cavity like: CO₂, H₂, nitrogen, methane, etc. Figure 2.3 shows an example of semi-clathrate hydrate structure.

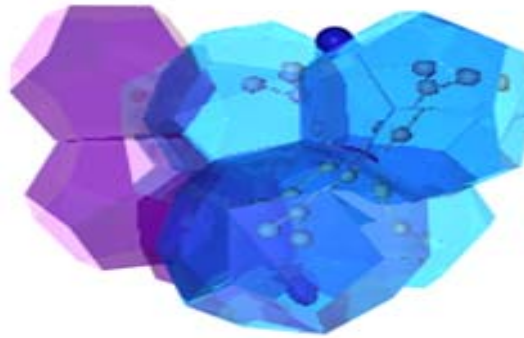


Figure 2.3. Semi-clathrate hydrate structure.

2.2 Stability of clathrate hydrates

For a better understanding of the properties of clathrate hydrates, in the following section fundamentals of phase equilibrium are presented.

2.2.1 Phase equilibrium and phase diagrams

In thermodynamics the equilibrium of a system is the absence of change or of any tendency toward change [16]. This means the absence of any driving force at certain conditions of pressure (p) temperature (T) and composition (x_i). Under this condition the chemical potential of each component in a system is equal in all the phases present, i.e.:

$$\mu_i^\alpha = \mu_i^\beta = \dots = \mu_i^\pi, i = 1, 2, \dots, N \quad (2.1)$$

where μ_i^α is the chemical potential of component i in the phase α and N is the number of chemical species.

2.2.2 The Gibbs' phase rule

The Gibbs' phase rule is used to classify the different types of systems and equilibria [17]. For instance, in any system at equilibrium, the number of independent variables that must be arbitrarily fixed to establish its intensive state is given by:

$$F = 2 - \pi + N \quad (2.2)$$

where π is the number of phases, and F is the number of degrees of freedom of the system. In special cases φ is introduced to account for extra relations between variables, therefore Equation 2.2 is rewritten as:

$$F = 2 - \pi + N - \varphi \quad (2.3)$$

examples of these extra relations occur, for example, at the critical state. Where two phases become identical and can be counted as one phase with $\varphi=2$ [18], or in the case of a binary azeotrope ($y_i=x_i$) with $\varphi=1$.

The minimum number of phases that can be present in a system is $\pi = 1$ and $\varphi=0$, the maximum value of F is given by:

$$F_{max} = N + 1 \quad (2.4)$$

For a unary system (one component system) such as pure water (H_2O) the maximum degree of freedom is equal to, $F_{max} = 2$. Consequently the phase behavior can be completely represented in a two dimensional p - T plane. Figure 2.4 shows a p - T diagram of H_2O phase behavior [19]. The phases that can take place in the unary system of H_2O are: ice/solid (I), liquid (L_w) and vapor (V). It is important to mention that ice can form fifteen separate phases, which differ from each other by their crystal structure. As it is observed in Figure 2.4, the regions where one phase is stable are bound by the equilibrium lines of two stable phases: I- L_w , L_w -V and I-V. These equilibrium lines intersect at the triple point I- L_w -V, which is the point where the three phases can coexist stable. The L_w -V equilibrium ends at the critical point $L_w=V$ where all the properties of the liquid (L_w) and vapor (V) phases are equal and therefore both phases are indistinguishable. Table 2.2

shows the result of applying the Gibbs' phase rule to the unary system of H_2O .

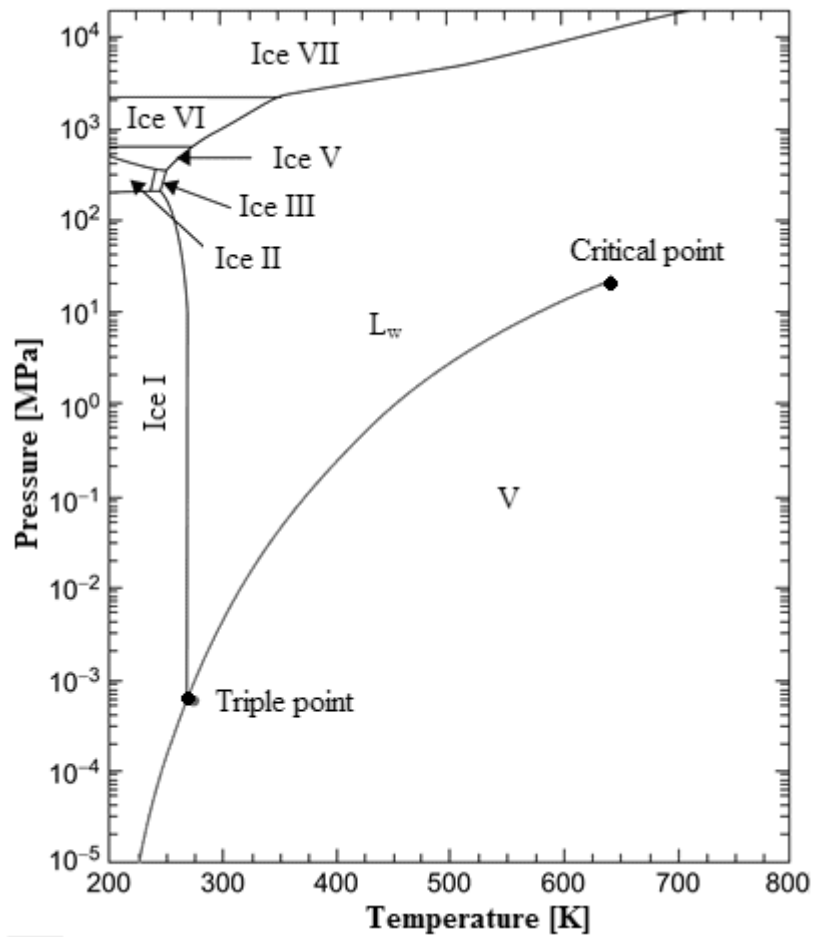


Figure 2.4. p - T diagram of H_2O phase behavior [19].

Table 2.2. Degrees of freedom in the unary system of H₂O.

π	ϕ	F	Example
1	0	2	L _w (single phase region)
2	0	1	L _w -V (equilibrium curve)
1	2	0	L _w =V (critical point)
3	0	0	I-L _w -V (triple point)

2.2.3 Clathrate hydrates phase behavior

Clathrate hydrates are commonly formed by binary, ternary or multi-component systems. In the case of the binary system the maximum number of degrees of freedom F_{max} is equal to 3. Consequently, a complete representation of the phase behavior can only be achieved in a three-dimensional diagram. Nevertheless a p - T , T - x_i or p - x_i diagram can be used to get insights in to the equilibrium conditions of coexisting phases.

In a binary system the number of coexisting phases increases as well as the types of phases than can be formed. For instance, in addition to the existing phases in the unary system, the following phases are also present: solid phase of the guest component (S), liquid phase other than H₂O (L_a) and the hydrate phase (H). The application of the Gibbs' phase rule to the binary system is shown in Table 2.3.

Two types of schematic phase diagrams can be encountered in binary systems of H₂O and gas. The distinction between the two phase diagrams is related to the critical temperature (T_c) of the gas. The phase diagram of gases with a T_c close or below the triple point of H₂O (T_{tr,H_2O}) differs from that of gases with a T_c higher than T_{tr,H_2O} . Components in the liquid state such as cyclic ethers can also form clathrate hydrates in binary systems with H₂O. Because the T_c of cyclic ethers is relatively high, the phase diagram will be similar to that of gases with a high T_c . Figure 2.5 shows a representation of the phase behavior of a binary system H₂O-gas in a p - T projection, the gas has lower T_c than the T_{tr,H_2O} . Figure 2.6 shows the representation in a p - x_i and T - x_i cross

section diagrams, the respective temperature and pressure are indicated in Figure 2.5.

Table 2.3. Degrees of freedom in the binary system of H₂O and clathrate hydrate forming component.

π	ϕ	F	Example
2	0	2	L _w -H (two phases)
3	0	1	H-L _w -V (three phase equilibrium)
1	0	3	L _a , V, H (one phase)
4	0	0	I-H-L _w -V (quadruple point)

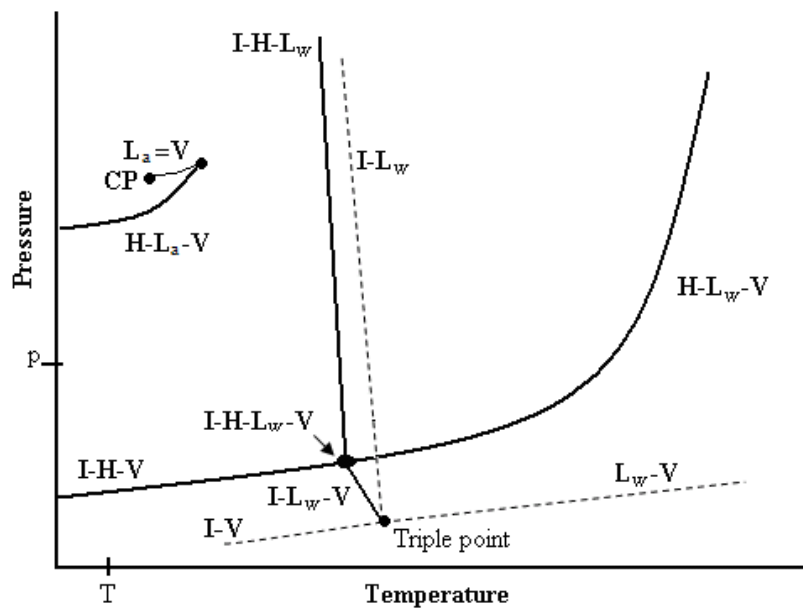


Figure 2.5. Representation of the phase behavior of a binary system H₂O-gas in a p - T projection, the gas has lower T_c than the T_{tr,H_2O} . The phase behavior of the unary system of H₂O is included as reference and is depicted by the dashed line. An example of such system is H₂O-CH₄.

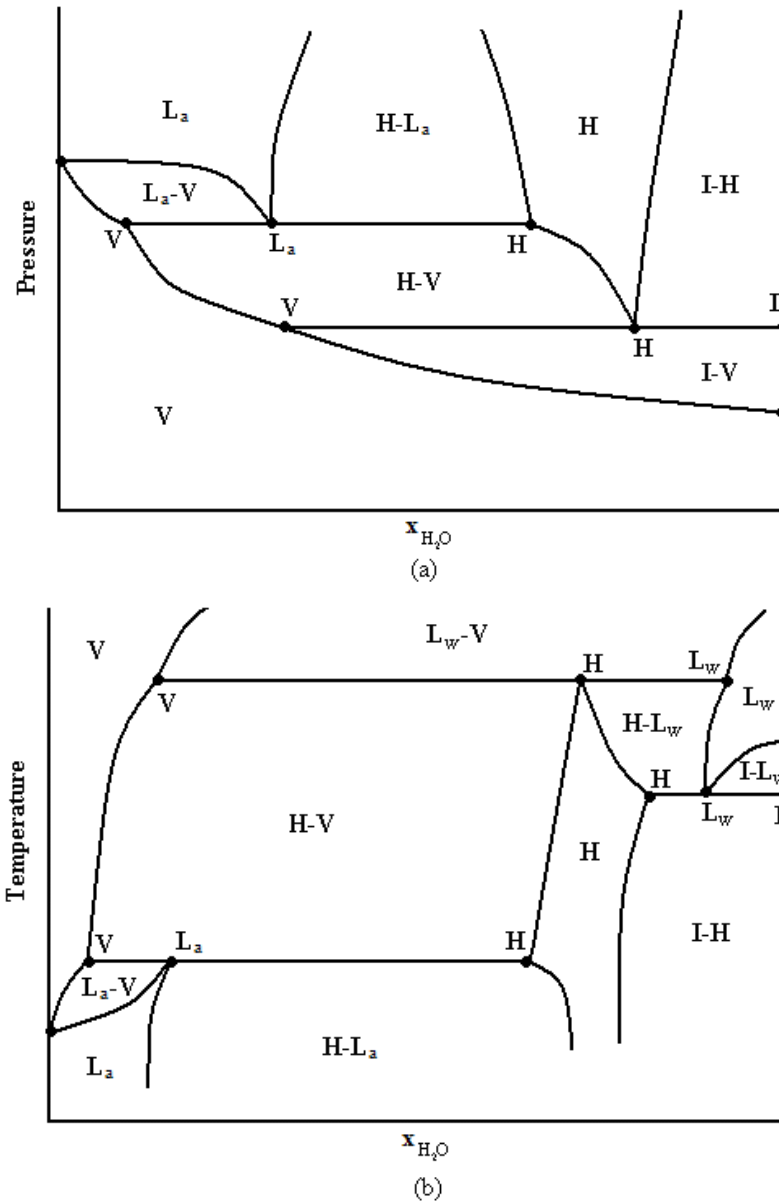


Figure 2.6. Representation of the phase behavior of a binary system H₂O-gas in (a) $p-x_i$ and (b) $T-x_i$ projection for p and T as indicated in Figure 2.4.

As it is expected the phase behavior of the binary systems is more complex than that of a unary system. In the $p-T$ diagram of a binary system, three phase equilibrium ($F=1$) is depicted by curves, i.e. $I-H-L_w$, $I-H-V$, $H-L_w-V$, $H-L-V$, $I-L_w-V$, these equilibrium curves intersect at the quadruple point

($F=0$): I-H- L_w -V. Cross section diagrams are necessary to achieve a complete understanding of the phase behavior. In the cross section diagrams, three phase equilibria are represented by horizontal lines. The lines are connected by points; which represent the composition of the corresponding phase in equilibrium. The quadruple point is also represented in a horizontal line. The surfaces between the equilibrium lines show the regions where two phases ($F=2$) or one phase are stable ($F=3$), this depends on the composition and on the pressure or temperature at which the representation is made [20]. For example, Figure 2.6 (b) shows a one phase region for the hydrate phase (H) in a very narrow range of compositions while in Figure 2.6 (a) the range of compositions is broader.

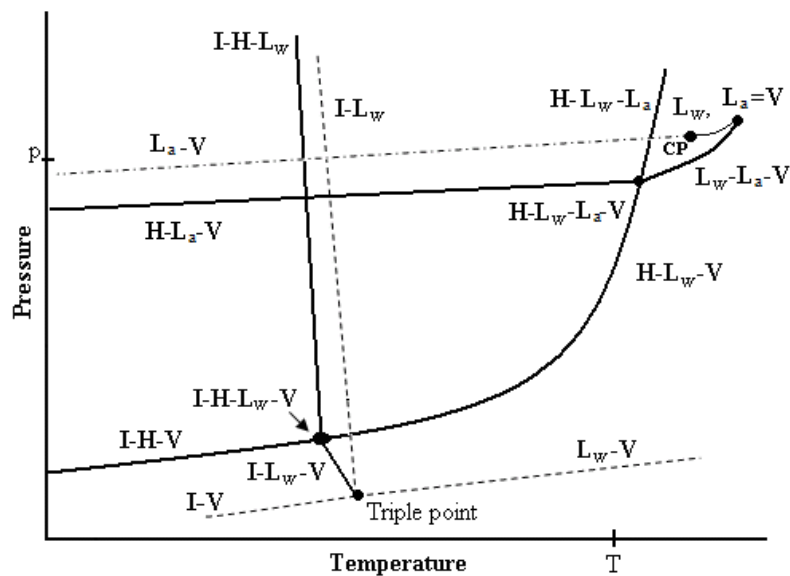


Figure 2.7. Representation of the phase behavior of a binary system H_2O -gas in a p - T projection with a gaseous component that has a T_c higher than T_{tr,H_2O} . The phase behavior of the unary system of H_2O is included as reference and is depicted by the dashed line (- - -) as well as the phase behavior of the gas component depicted as (-·-·-). An example of such system is H_2O - CO_2 .

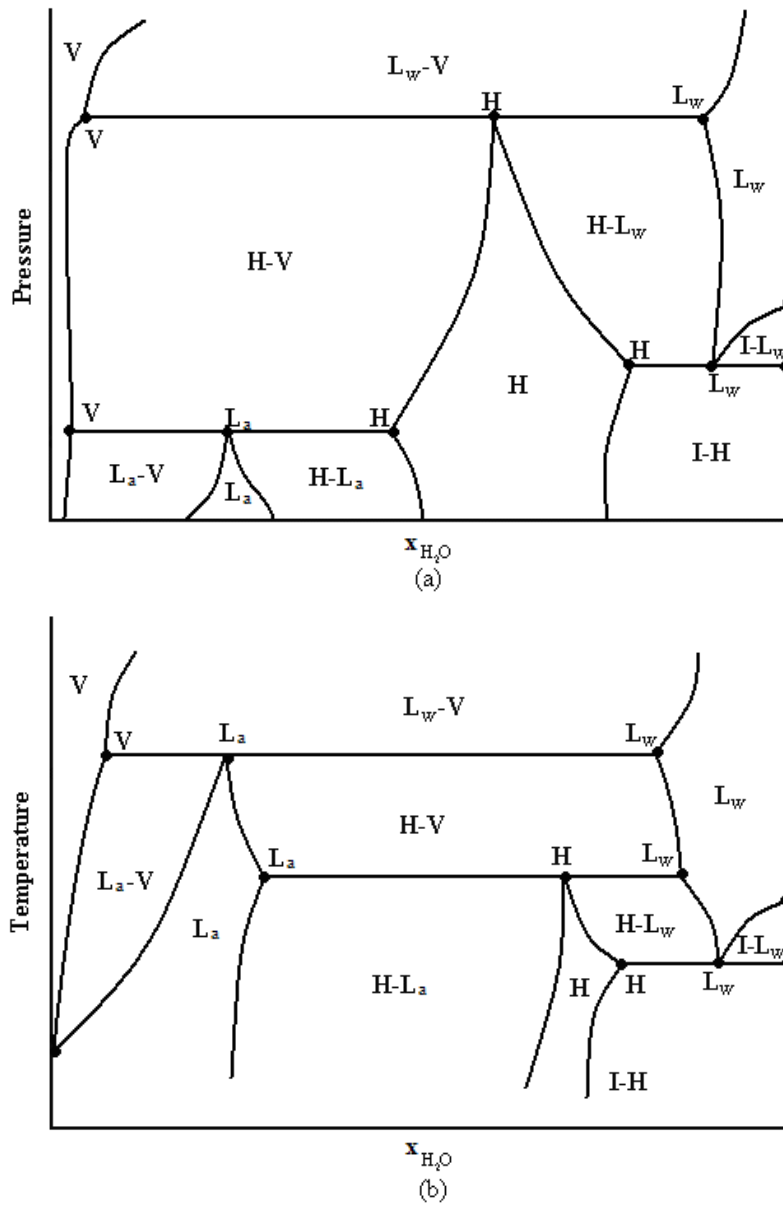


Figure 2.8. Representation of the phase behavior of a binary system H_2O -gas in (a) $p-x_i$ and (b) $T-x_i$ projection for p and T as indicated in Figure 2.6.

Figure 2.7 show a $p-T$ representation of a binary system with a gaseous component that has a T_c higher than T_{tr,H_2O} . Examples of $p-x_i$ and $T-x_i$ diagrams are given in Figure 2.8, the corresponding pressure and temperature

are indicated in Figure 2.7. Examples of such systems are $\text{H}_2\text{O}-\text{CO}_2$ and $\text{H}_2\text{O}-\text{SF}_6$. Since the gaseous component presents a T_c higher than $T_{tr,\text{H}_2\text{O}}$, the L_a phase is present at higher temperatures. Therefore, the $\text{H}-L_a-\text{V}$ curve intersects with the $\text{H}-L_w-\text{V}$ line at the quadruple point $\text{H}-L_w-L_a-\text{V}$. In addition two others three phase equilibria are also present: $\text{H}-L_w-L_a$ and $L_w-L_a-\text{V}$. The hydrate phase (H) is stable in the low-temperature and high pressure region bounded by the $\text{I}-\text{H}-\text{V}$, $\text{H}-L_w-\text{V}$ and $\text{H}-L_w-L_a$ phase equilibrium lines. When the guest has a T_c higher than $T_{tr,\text{H}_2\text{O}}$ but it is soluble in water, there is only one liquid phase, and the quadruple point $\text{H}-L_w-L_a-\text{V}$ is absent. These kind of guests (i.e. THF) are generally liquid at atmospheric pressure therefore is more convenient to display their hydrate phase behavior in a $T-x_i$ cross section diagram.

Triple or multicomponent systems of clathrate hydrates normally consist of H_2O , cyclic organic component and a gas or gas mixture. Because the number of degrees of freedom is $F_{max} \geq 4$, a complete representation of the phase behavior would require of four or more dimensions. Therefore, one or more variables are kept constant in order to elucidate the phase behavior of the system. A complete discussion on the types of phase diagrams and phase behavior of ternary and multicomponent clathrate hydrate systems can be found in Mooijer-van den Hevel [20].

2.3 Hydrate formation

Hydrate formation is a stochastic phase change considered a crystallization process, which requires a supersaturated environment to take place [9]. Usually the crystallization process can be divided into two separated phases. The first phase also known as “nucleation” involves the formation of hydrate nuclei. The second phase is the hydrate growth, which starts after stable nuclei have been formed. In the following section the two phases are described in detail.

2.3.1 Hydrate nucleation

Hydrate nucleation is a phenomenon of formation and growth of small clusters of water and gas or of any other guest molecule. These clusters also known as hydrate nuclei, grow until they reach a critical size (around 25-170 Å) forming stable nuclei that are the precursors of hydrate crystals. When the hydrate clusters are smaller than the critical size, the nuclei are unstable and may either grow or shrink as a result of density fluctuations [21]. The formation of hydrate nuclei usually occurs at the interface (fluid-solid / gas-liquid / liquid-liquid), not only due to the higher concentration of water and guest molecules but also because the interface lowers the Gibbs' free energy of nucleation.

The main component of hydrate nucleation is the driving force, defined as the chemical potential difference between the initial phase and the new phase [22]. The magnitude of the driving force or supersaturation is dependent on the pressure, temperature and concentration difference between the equilibrium conditions and the operation conditions [23].

Several experiments have been performed in order to understand the hydrate nucleation mechanism; as a result two hypotheses have emerged. One is the labile cluster nucleation hypothesis, proposed by Christiansen and Sloan [24]. This hypothesis proposes that the water molecules form labile clusters around dissolved gas molecules. These clusters combine until they achieve a critical radius. The other hypothesis is the local structuring. This hypothesis suggests that thermal fluctuation cause a group of guest molecules to be arranged in a configuration similar to that in the hydrate phase. The number of guest in a locally ordered arrangement exceed that in the critical nucleus and the order parameters in the arrangement are close to those of the hydrate phase resulting in the formation of a critical size nucleus. However, most of the evidence from hydrate nucleation simulations [25] and experimental studies [26] support the local structuring theory rather than the labile cluster.

Another important parameter to characterize hydrate nucleation is the induction time. The induction time is the time elapsed during the formation of the clusters and their growth to stable nuclei with a critical size. During the induction time, the pressure and temperature conditions are within the boundaries of hydrate stability. However hydrate growth does not take place due to metastability. The induction time is stochastic and apparatus dependent, parameters like degree of agitation, impurities, surface area of the system and rate of mass and heat transfer have a significant influence. It is important to notice that the history of the water has also an influence on the induction period; due to a phenomenon known as the memory effect. The memory effect refers to the phenomena of faster hydrate formation from gas and water obtained by hydrate dissociation than from fresh water with no previous hydrate history. The memory effect disappears when the system is heated sufficiently above the hydrate formation temperature at a given pressure.

2.3.2 Hydrate growth

Hydrate growth is the phase of hydrate formation where stable hydrate nuclei grow as solid hydrates [27]. During this period a significant amount of gas is incorporated in the hydrate phase. Therefore, mass and heat transfer play a significant role in this process. Other factors affecting hydrate nucleation such as driving force, surface area, agitation, etc. also play an important role in hydrate growth.

The first attempt to describe quantitatively and to model the hydrate formation kinetics was made by Vysniauskas and Bishnoi [28, 29]. They developed a semi-empirical model to correlate experimental kinetic data obtained by contacting gas and water at temperatures above the freezing point of water. Their results showed that the mechanism of hydrate formation consists of the appearance of nuclei and their subsequent growth. They also observed that factors like: contact area between the phases, pressure, temperature and degree of subcooling influence hydrate growth.

However, unlike hydrate nucleation, the history of water seemed to not have a significant effect on hydrate growth.

Later on, Englezos and co-workers [30] formulated an intrinsic kinetic model for hydrate growth with only one adjustable parameter. This model is based on crystallization and mass transfer theories. The model supposes that a solid hydrate particle is surrounded by an adsorption layer followed by a stagnant liquid diffusion layer. The hydrate particle growth, takes place by the diffusion of the dissolved gas from the bulk of the solution to the crystal-liquid interface through the laminar diffusion layer around the particle. At the interface an adsorption process takes place where the gas molecules are incorporated into the structured water framework. Since accumulation is not allowed in the diffusion layer, the two rates are equal; consequently the rate of growth per particle is given by:

$$\left(\frac{dn_i}{dt} \right)_p = K^* A_p (f_i^b - f_i^{eq}) \quad (2.5)$$

with

$$\frac{1}{K^*} = \frac{1}{k_r} + \frac{1}{k_d} \quad (2.6)$$

where $\left(\frac{dn_i}{dt} \right)_p$ is the number of gas moles consumed per second by the hydrate, A_p is the surface area of each particle, f_i^b is the fugacity of component i in the bulk liquid, f_i^{eq} is the equilibrium fugacity of component i in the liquid at the hydrate interface, K^* is the hydrate formation growth rate constant, representing a combined rate constant for diffusion and adsorption processes, k_r is the reaction rate constant, k_d is the mass transfer coefficient through the film around the particle and $f_i^b - f_i^{eq}$ defines the overall driving force.

Modifications to the model Englezos-Bishnoi were later made by Malegaonkar et al. [31] and by Skovborg and Radmusen [22] which significantly increased the accuracy of the model. However, Moundrakovski et al. [32] recently studied hydrate formation in water droplets by H^1 magnetic resonance microimaging. Their results showed that hydrate growth

is inhomogeneous and that actually the observation of gradual conversion is only the result of averaging over several local environments. Based on their observation in quiescent systems, they concluded that the definition of intrinsic kinetic parameters is difficult, if possible at all, due to the stochastic component that competes with more gradual conversion processes.

2.4 Characterization techniques for clathrate hydrate systems

A detailed study of clathrate hydrate systems requires the application of diverse physical techniques. The most used techniques for the study of hydrates are Powder and single crystal X-ray diffraction, Raman spectroscopy and Nuclear Magnetic Resonance Spectroscopy. Both, spectroscopy and diffraction provide important information of the properties and characteristics of clathrate hydrates. In the following sections a general overview of the methods is presented.

2.4.1 Powder X-ray diffraction

The structural features of clathrate hydrates have emerged from X-ray diffraction techniques. The first studies on this area date back on the early 50's, with the works of von Stackelberg and Muller [33], Claussen [34] and Pauling and Marsh [35]. In the 60's and 70's, X-ray diffraction was extensively employed by Jeffrey and his colleagues, from these studies, sI and sII were confirmed and refined [36, 37]. From the 70's to the date, X-ray diffraction has been used to determine sH [38], to provide the complete solution of bromine hydrate [39] and to identify and define new hydrate structures [11, 40-42]. Many of this works were performed by single crystal X-ray diffraction techniques. However, recent advances allow the determination of crystal structures directly from powder X-ray diffraction (PXRD) [43].

X-ray diffraction is a characterization technique which consists on the diffraction of an X-ray beam by the lattice planes in a crystal. A three-

dimensional picture of the density of electrons within the crystal is reproduced by the measure of the intensity and angles of the diffracted beams. The diffracted beams are governed by Bragg's law (see eq. 2.7), where d is the space between diffracted planes, θ is the incident angle, n is any integer and λ is the wave length of the beam.

$$n \lambda = 2 d_{hkl} \sin \theta \quad (2.7)$$

Bragg's model proposes that the X-ray are scattered specularly (mirror-like) from each plane of the regular arrays of atoms. Therefore, the diffraction from adjacent planes will combine constructively when the angle θ between the plane and the X-ray results in a path-length difference that is an integer multiple n of the wavelength λ . Figure 2.9 illustrates Bragg's law. A unit cell determination (or indexing) requires the identification of the reciprocal lattice vector components (or Miller indices) of a reflection from the known wavelength and the scattering angle 2θ . The indexing provides the unit cell parameters, the length and angles of the unit cell, as well as its space group.

X-ray diffraction techniques are appropriate for clathrate hydrate identification because they provide insights into the geometry of the cavities. The H₂O molecules in the lattice generate diffraction of the incident X-ray radiation revealing their location in the unit cell and their unit cell parameters. X-ray diffraction is thus conclusive on the clathrate hydrate structure.

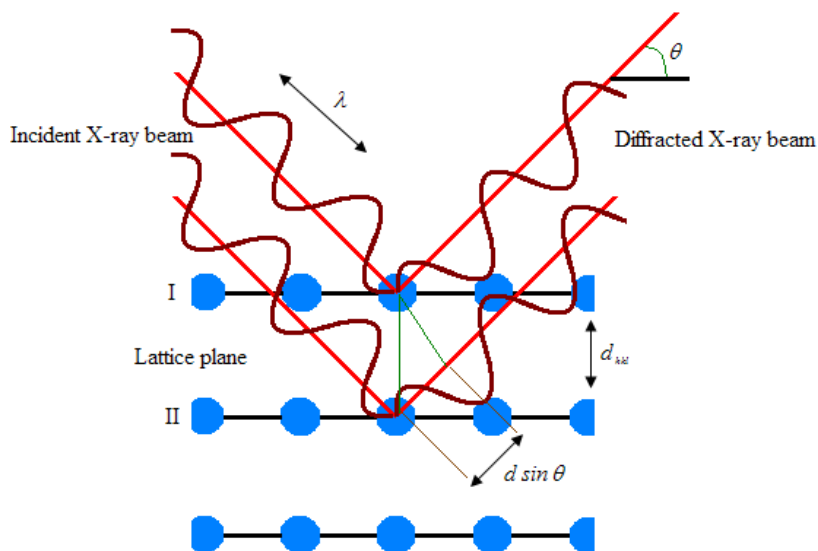


Figure 2.9. Bragg's law illustration.

2.4.2 Raman spectroscopy

Raman spectroscopy is an inelastic scattering technique in which an energy exchange between incident electromagnetic radiation and molecules in a sample induce molecular vibrations. When electromagnetic radiation impinges on molecules, the associated electric field of the radiation induces an oscillating dipole moment in the molecule by displacing electron density at the frequency of the incident wave. The interaction of a molecule with electromagnetic radiation can be examined using classical wave model or a quantum mechanical model. From the quantum mechanical point of view, the energy of an incident photon of radiation is $h\nu_{inc}$ where h is Planck's constant and ν_{inc} is the frequency of the incident radiation. The induced dipole moment oscillates at the incident frequency. The energy coupled into the oscillation of the induced dipole moment can result in vibratory quantum transitions in the molecule [44].

Initially, the most populated vibrational level is the ground state. After the excitation, electrons from the lower vibrational state are excited to the higher vibrational level. If the excitation energy matches the difference energy between the two quantum levels the energy is absorbed. This process is used

in infrared absorption spectroscopy (IR). If the energy increase does not match a specific electronic transition, electrons are promoted to a virtual vibrational state. This virtual state is unstable and subsequent release of energy takes place in the form of a photon in a process known as scattering. Elastic scattering occurs when the emitted or scattered photon contains the same quanta of energy as the incident exciting photon. Inelastic scattering occurs when a portion of the imparted energy from the incident photon is retained by the molecule, as a result the scattered photon exhibits a shift in frequency from the incident photon. If the retained energy is linked to a vibrational or vibrational-rotational mode of the molecule, the inelastic scattering is entitled Raman scattering. The magnitude of the shift in frequency of the scattered light is unique for a molecule and a given vibrational state is constant and independent of the excitation source frequency. If the shift occurs to a lower photon frequency, it is named Stokes shift. Stokes shifts take place when the final vibrational state of the molecule is greater than the initial vibrational state. A shift to higher photon frequency is called Anti-Stokes shift. Anti-Stokes shifts occur when the relaxation of the molecule during the scattering interaction allows the molecule to return to a lower vibration energy than the molecule was before the excitation. At room temperature, Stokes Raman scattering predominates because most molecules are in the ground vibrational state. The Raman shift observed in the frequency of the scattered photon is usually quantified by wave number expressed in dimensions of cm^{-1} .

The difference in energy between the excitation photon and scattered photon corresponds to a vibrational frequency of the molecule. For a shift to be displayed in the Raman spectrum there must be a change in the polarizability of a bond when the radiation is incident on a molecule. Polarizability is a measure of the ease of distortion of the electron cloud of a chemical bond in an external electric field. In general, this means that the vibrations of non-polar bonds produce stronger Raman intensities than polar bonds because their electron cloud is delocalized, therefore is more easily distorted by the incoming radiation. Symmetric stretches are typically more intense in Raman spectra whereas asymmetric stretches are stronger in IR.

Raman spectroscopy is a powerful tool to study hydrates. Since the environment of a molecule affects its vibrational activity, the Raman spectrum allows the distinction between guest molecules in different phases and cavities and as a result the identification of clathrate structures. Furthermore, the intensity of the Raman shifts is proportional to the number of molecules therefore it can be used for quantitative analysis [45-48]. Raman spectroscopy also allows kinetic studies during hydrate formation and decomposition by identifying changes in the hydrate structure and on the relative cage occupancy [10, 18].

2.4.3 Nuclear magnetic resonance

Nuclear Magnetic Resonance Spectroscopy is based on the magnetic properties of nuclei atoms and the information they display about their chemical environment. Nuclei possessing angular momentum "I" (also called overall spin) has an associated magnetic moment μ . Examples of such magnetic isotopes are ^{13}C , ^1H and ^{19}F . When a population of magnetic nuclei is placed under the influence of an external magnetic field " \mathbf{B}_0 " the nuclei will align in a predictable and finite number of orientations given by $2I+1$. For instance, ^1H has an overall spin $I=1/2$, therefore there are two possible orientations since $2I+1=2$. In one orientation the protons are aligned with the external magnetic field and in the other the nuclei are aligned against the field. The alignment with the field is also called " α " orientation and the alignment against the field is called " β " orientation. The preferred orientation is the α , since it possesses the lower energy. As a result, more nuclei are aligned with the field than against the field. The separation of energy levels is called the resonance energy ΔE and depends on the magnitude of the nuclear magnetic moment, which is specific for the nucleus studied. Furthermore, the rotational axis of the spinning nucleus is not orientated exactly parallel (or anti-parallel) with the direction of the applied field but precess about this field at an angle with an angular velocity given by the expression:

$$\omega_0 = \gamma \mathbf{B}_0 \quad (2.8)$$

also known as “Larmor frequency”. The constant γ is called the magnetogyric ratio and relates the magnetic moment μ and the spin number I for any specific nucleus:

$$\gamma = 2\pi\mu/hI \quad (2.9)$$

where h is Planck's constant. The resonance energy can be found from:

$$\Delta E = \frac{\gamma h \mathbf{B}_0}{2\pi} \quad (2.10)$$

The nuclear magnetic resonance (NMR) spectroscopy experiment involves using energy in the form of electromagnetic radiation to take the excess α oriented nuclei into the β state. Once the energy is removed, the energized nuclei relax back to the α state. The fluctuation of the magnetic field associated with this relaxation process is called resonance and this resonance can be detected and converted into the NMR spectrum. The exact resonance frequency depends on the chemical environment of the nucleus in a molecule, providing a medium to determine the structure of the molecules. This effect is called chemical shift and is defined as: nuclear shielding / applied magnetic field. Nuclear shielding is the difference between the applied magnetic field and the field at the nucleus. The chemical shift is measured relative to a reference compound. For ^{13}C NMR, the reference is usually adamantane. As there is a one-to-one correspondence between chemically distinct nuclei and the resonance lines in a spectrum, the resolved shifts can be integrated providing a ratio that reflects the population of nuclei of each type. The nucleus magnetic field is also affected by the orientation of the neighboring nuclei. This effect is known as spin-spin coupling which can cause splitting of the signal for each type of nucleus into two or more lines.

It is important to notice that the NMR spectra of solids show signals wider than their chemical shift range and too broad to be observed with a regular-resolution NMR. This is because of the reduced rotational and diffusion motion of solids. Since averaging of their isotropic values of the nuclear magnetic dipole-dipole and chemical shift interactions is not possible. The

effects of chemical shift anisotropy and homonuclear coupling can be removed by spinning the sample very fast about the magic angle (54.726° to the vertical). However, such speeds are not always reached and a combination of high-power multiple pulse decoupling (HPDEC) and fast spinning around the magic angle might be required. When there are protons in the vicinity the sensibility can be increased by exciting the ^1H and ^{13}C together with matching spin-lock pulses in a process called cross-polarization (CP) that works via dipolar coupling. When CP is combined with magic angle spinning the technique is called cross polarized magic angle spinning (CP-MAS)

Nuclear Magnetic Resonance Spectroscopy (NMR) is one of the most important techniques for characterization of clathrate hydrates. For instance, ^1H and ^{13}C NMR have been employed for structure identification, determination of the chemical composition and cage occupancy of several clathrate hydrates i.e. ethane, propane, isobutene, H_2S , etc. [49-51]. Similarly, ^{129}Xe has helped to identify and determine hydrate structures [12, 38, 52, 53] and to quantify the occupancy of the cavities. NMR spectroscopy has also been employed to study hydrate formation, dissociation dynamics and inter-hydrate structure transformations [32, 54]. It bears mentioning that most of the work done on the study of hydrates with NMR has been performed by John A. Ripmeester and his group at the National Research Council of Canada.

2.5 References

- [1] Davy H. On a Combination of Oxymuriatic Gas and Oxygene Gas. *Philosophical Transactions of the Royal Society*. 1811;101.
- [2] Hammerschmidt E. G. Formation of gas hydrates in natural gas transmission lines. *Industrial and Engineering Chemistry*. 1934;26:851-5.
- [3] Koh C. A., Sum A. K., Sloan E. D. Gas hydrates: Unlocking the energy from icy cages. *Journal of Applied Physics*. 2009;106.
- [4] Jeffrey G. A. Hydrate Inclusion Compounds *Journal of Inclusion Phenomena*. 1984;1:211-22.

- [5] Alavi S., Udachin K., Ratcliffe C. I., Ripmeester J. A. Clathrate Hydrates. Supramolecular Chemistry: John Wiley & Sons, Ltd.
- [6] Shin K., Kumar R., Udachin K. A., Alavi S., Ripmeester J. A. Ammonia clathrate hydrates as new solid phases for Titan, Enceladus, and other planetary systems. Proceedings of the National Academy of Sciences of the United States of America. 2012;109:14785-90.
- [7] Sabil K. M. Phase Behaviour, Thermodynamics and Kinetics of Clathrate Hydrates Systems of Carbon Dioxide in Presence of Tetrahydrofuran and Electrolytes: Delft University of Technology; 2009.
- [8] Davison D. W. Water: A Comprehensive Treatise. New York: Plenum Press; 1973.
- [9] Natarajan V., Bishnoi P. R., Kalogerakis N. Induction phenomena in gas hydrate nucleation. Chemical Engineering Science. 1994;49:2075-87.
- [10] Sloan E. D., Koh C. A. Clathrate Hydrates of Natural Gases. 3rd ed. Florida: CRC Press; 2008.
- [11] Dyadin Y. A., Bondaryuk, I. V., Zhurko, F. V. Clathrate hydrates at high pressure. In: Atwood J. L., Davies, J. E. D., MacNicol D. D., editor. Inclusion Compounds: Inorganic and physical aspects of inclusion. Oxford, New York, Tokyo: Oxford Science Publications; 1991.
- [12] Ripmeester J. A., Ratcliffe C. I. Xe-129 NMR-Studies of clathrate hydrates - new guests for structure-II and structure-H. Journal of Physical Chemistry. 1990;94:8773-6.
- [13] McMullan R. K., Jeffrey G. A. Polyhedral clathrate hydrates .9. Structure of ethylene oxide hydrate. Journal of Chemical Physics. 1965;42:2725-&.
- [14] Mak T. C. W., McMullan R. K. Polyhedral clathrate hydrates .X. Structure of double hydrate of tetrahydrofuran and hydrogen sulfide. Journal of Chemical Physics. 1965;42:2732-&.
- [15] Strobel T. A., Koh C. A., Sloan E. D. Hydrogen storage properties of clathrate hydrate materials. Fluid Phase Equilibria. 2007;261:382-9.
- [16] Smith J. M., Van Ness H. C., Abbott M. M. Chemical engineering Thermodynamics 2001.

- [17] de Loos T. W., van der Kooi H. J., Ott P. L. Vapor liquid critical curve of the system ethane + 2-methylpropane. *Journal of Chemical & Engineering Data*. 1986;31:166-8.
- [18] Mooijer van den Heuvel M. M. Phase Behaviour and Structural Aspects of ternary Clathrate Hydrate Systems. Delft: TU Delft University; 2004.
- [19] Sonntag R. E. B. C., van Wylen G. J. Fundamentals of Thermodynamics 6th ed. New York: Wiley; 2003.
- [20] Mooijer-van den Heuvel M. M. Phase Behaviour and Structural Aspects of Ternary Clathrate Hydrates Systems; The Role of Additives: Delft University of Technology; 2004.
- [21] Bishnoi P. R., Natarajan V., Kalogerakis N. A unified description of the kinetics of hydrate nucleation, growth and decomposition. In: Sloan E. D., Happel J., Hnatow M. A., editors. *International Conference on Natural Gas Hydrates*. New York: New York Acad Sciences; 1994. p. 311-22.
- [22] Skovborg P., Rasmussen P. A mass transport limited model for the growth of methane and ethane gas hydrates. *Chemical Engineering Science*. 1994;49:1131-43.
- [23] Groen C. B. CO₂ hydrate formation in coil heat exchangers. Delft: Delft University of Technology; 2012.
- [24] Christiansen R. L., Sloan E. D. Mechanisms and kinetics of hydrate formation. In: Sloan E. D., Happel J., Hnatow M. A., editors. *International Conference on Natural Gas Hydrates*. 1994. p. 283-305.
- [25] Moon C., Taylor P. C., Rodger P. M. Molecular dynamics study of gas hydrate formation. *Journal of the American Chemical Society*. 2003;125:4706-7.
- [26] Staykova D. K., Kuhs W. F., Salamatin A. N., Hansen T. Formation of porous gas hydrates from ice powders: Diffraction experiments and multistage model. *Journal of Physical Chemistry B*. 2003;107:10299-311.
- [27] Bishnoi P. R., Natarajan V. Formation and decomposition of gas hydrates. *Fluid Phase Equilibria*. 1996;117:168-77.
- [28] Vysniauskas A., Bishnoi P. R. Kinetics of ethane hydrate formation. *Chemical Engineering Science*. 1985;40:299-303.
- [29] Vysniauskas A., Bishnoi P. R. A Kinetic-study of Methane Hydrate Formation. *Chemical Engineering Science*. 1983;38:1061-72.

- [30] Englezos P., Kalogerakis N., Dholabhai P. D., Bishnoi P. R. Kinetics of gas hydrate formation from mixtures of methane and ethane. *Chemical Engineering Science* 1987;42:2659-66.
- [31] Malegaonkar M. B., Dholabhai P. D., Bishnoi P. R. Kinetics of carbon dioxide and methane hydrate formation. *Canadian Journal of Chemical Engineering*. 1997;75:1090-9.
- [32] Moudrakovski I. L., McLaurin G. E., Ratcliffe C. I., Ripmeester J. A. Methane and carbon dioxide hydrate formation in water droplets: Spatially resolved measurements from magnetic resonance microimaging. *Journal of Physical Chemistry B*. 2004;108:17591-5.
- [33] Stackelberg M. v., Muller H. R. On the Structure of Gas Hydrates. *The Journal of Chemical Physics*. 1951;19:1319-20.
- [34] Claussen W. F. Suggested Structures of Water in Inert Gas Hydrates. *The Journal of Chemical Physics*. 1951;19:259-60.
- [35] Pauling L., Marsh R. E. The Structure of Chlorine Hydrate. *Proceedings of the National Academy of Sciences*. 1952;38:112-8.
- [36] McMullan R. K., Jeffrey G. A., Bonamico M. Polyhedral Clathrate Hydrates. 5. Structure of Tetra-n-butyl ammonium fluoride hydrate *Journal of Chemical Physics*. 1963;39:3295-&.
- [37] McMullan R., Jeffrey G. A. Hydrates of the tetra n-butyl and tetra I-amil quaternary ammonium salts. *Journal of Chemical Physics*. 1959;31:1231-4.
- [38] Ripmeester J. A., Tse J. S., Ratcliffe C. I., Powell B. M. A new clathrate hydrate structure. *Nature*. 1987;325:135-6.
- [39] Udachin K. A., Enright G. D., Ratcliffe C. I., Ripmeester J. A. Structure, stoichiometry, and morphology of bromine hydrate. *Journal of the American Chemical Society*. 1997;119:11481-6.
- [40] Ripmeester J. A., Davidson D. W. Some New Clathrate Hydrates. *Molecular Crystals and Liquid Crystals*. 1977;43:189-95.
- [41] Davidson D. W., Handa Y. P., Ratcliffe C. I., Ripmeester J. A., Tse J. S., Dahn J. R., et al. Crystallographic Studies of Clathrate Hydrates. Part I. *Molecular Crystals and Liquid Crystals*. 1986;141:141-9.

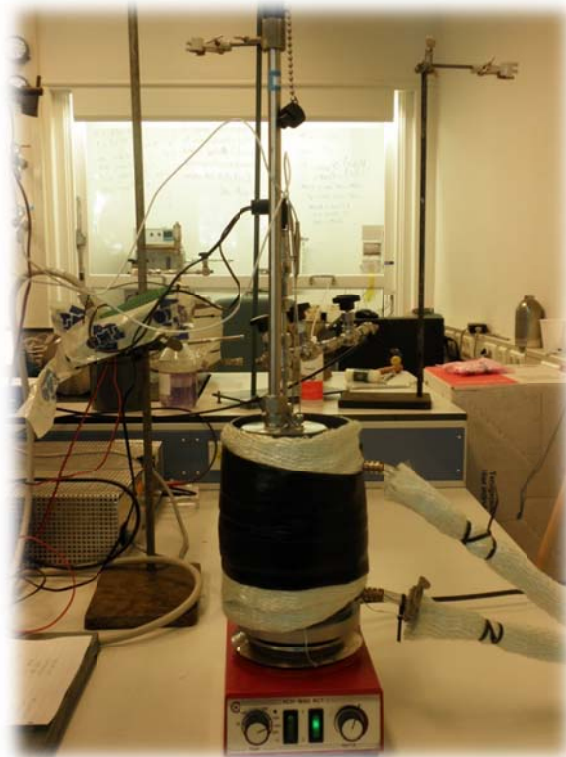
- [42] Udachin K. A., Lipkowski J., Progep N. G. H. New structures of clathrate hydrates. Ngh '96 - 2nd International Conference on Natural Gas Hydrates, Proceedings. 1996:25-32.
- [43] Harris K. D. M. Powder Diffraction Crystallography of Molecular Solids. In: Rissanen K., editor. Advanced X-Ray Crystallography. 2012. p. 133-77.
- [44] Ball A. J. Investigation of gaseous hydrogen leak detection using raman scattering and laser-induced breakdown spectroscopy. Florida: University of Florida; 2005.
- [45] Sum A. K., Burruss R. C., Sloan E. D. Measurement of clathrate hydrates via Raman spectroscopy. Journal of Physical Chemistry B. 1997;101:7371-7.
- [46] Uchida T., Okabe R., Mae S., Ebinuma T., Narita H. In situ observations of methane hydrate formation mechanisms by Raman spectroscopy. In: Holder G. D., Bishnoi P. R., editors. Gas Hydrates: Challenges for the Future. 2000. p. 593-601.
- [47] Uchida T., Ohmura R., Hori A. Raman Peak Frequencies of Fluoromethane Molecules Measured in Clathrate Hydrate Crystals: Experimental Investigations and Density Functional Theory Calculations. Journal of Physical Chemistry A. 2010;114:317-23.
- [48] Nakano S., Moritoki M., Ohgaki K. High-pressure phase equilibrium and Raman microprobe spectroscopic studies on the CO₂ hydrate system. Journal of Chemical Engineering Data. 1998;43:807-10.
- [49] Garg S. K., Majid Y. A., Ripmeester J. A., Davidson D. W. Reorientation and diffusion of water-molecules in xenon hydrate and other structure .1. Clathrate hydrates. Molecular Physics. 1977;33:729-34.
- [50] Davidson D. W., Garg S. K., Gough S. R., Hawkins R. E., A. R. J. Characterization of natural gas hydrates by nuclear magnetic resonance and dielectric relaxation. Canadian Journal of Chemistry-Revue Canadienne De Chimie. 1977;55:3641-50.
- [51] Ripmeester J. A., Ratcliffe C. I. Low-temperature cross-polarization magic angle spinning c-13 nmr of solid methane hydrates - structure, cage occupancy, and hydration number. Journal of Physical Chemistry. 1988;92:337-9.

- [52] Ripmeester J. A., Davidson D. W. Xe-129 nuclear magnetic-resonance in the clathrate hydrate of xenon. *Journal of Molecular Structure*. 1981;75:67-72.
- [53] Ripmeester J. A., Ratcliffe C. I. On the contributions of NMR spectroscopy to clathrate science. *Journal of Structural Chemistry*. 1999;40:654-62.
- [54] Susilo R., Moudrakovski I. L., Ripmeester J. A., Englezos P. Hydrate kinetics study in the presence of nonaqueous liquid by nuclear magnetic resonance spectroscopy and imaging. *Journal of Physical Chemistry B*. 2006;110:25803-9.

Chapter 3

Experimental

Methodology



3.1 Introduction

This chapter presents a description of the experimental apparatus and procedures used in the present work. Section 3.2 provides the methodology used to perform phase equilibrium measurements with the Cailletet apparatus together with a description of the experimental set-up. Section 3.3 presents the procedure for kinetic measurements and a description of the experimental set-up. Finally, section 3.4 describes the procedures and equipment used for Powder X-ray diffraction, Raman spectroscopy and Nuclear Magnetic Resonance spectroscopy measurements.

3.2 Phase behavior measurements

3.2.1 Sample preparation

The phase equilibrium measurements were carried out in a high pressure tube also known as a Cailletet tube which serves as an equilibrium cell. The Cailletet tube is about 50 cm in length and has an open lower and a closed upper end. Water and the corresponding organic compounds are dosed gravimetrically into the Cailletet tube using a micrometer syringe. Before dosing the liquid compounds, a stainless ball which has the function to magnetically stir the sample is placed into the Cailletet tube.

Subsequently, the Cailletet tube is connected to the gas-rack apparatus. The gas-rack apparatus is operated based on the principle of communicating vessels. The apparatus allows: liquid sample degassing, measurement of the amount of gaseous sample, filling the gaseous sample in the Cailletet tube and confining the global sample with mercury. A schematic representation of the gas-rack apparatus is shown in Figure 3.1. Once the sample is in the gas-rack, the air dissolved in the H₂O + organic compound mixture is removed by freezing and melting the sample several times and degassing under high vacuum.

When de-gassing has been completed, in the case of the mixed clathrate hydrate measurements, H₂ is dosed volumetrically into the Cailletet tube at known temperature and pressure via the gas rack apparatus. This is performed by filling the volumetric calibrated vessel (57.43 cm³) on the gas-rack with H₂. Then, the valve connecting the vessel to the H₂ tank is closed and the mercury level is raised by pressurizing the mercury with nitrogen. The H₂ is then confined in the vessel by sealing the vessel with mercury. Then the temperature and pressure readings are taken. Next, the H₂ is allowed to flow in the tube and the tube is sealed with mercury. As the pressure, temperature and volume of the H₂ sample are known the number of moles is calculated by applying the virial equation of state (see Eqn. 3.1). The second virial coefficient (*B*) is determined from data collected in Dyamond and Smith [1]. In the case of the non-gaseous samples, following the de-gassing they are sealed with mercury.

$$\frac{pV}{nRT} = 1 + \frac{B}{V} \quad (3.1)$$

3.2.2. Experimental set-up

The experiments were carried out in a Cailletet apparatus, which is suitable for phase equilibrium measurements within a temperature range of 255 K to 455 K and a pressure range of 0.1 MPa to 15 MPa. This equipment allows visual observation of the phase transitions and operates according to the synthetic method. Details of the Cailletet apparatus can be found elsewhere [2]. Figure 3.2 depicts the schematic diagram of the Cailletet apparatus.

After the sample of known fixed composition is sealed into the closed top of the Cailletet tube with mercury, the open bottom-end of the tube is immersed in mercury contained in an autoclave. The autoclave is connected to a high-pressure hydraulic system applying oil as pressure medium. The pressure is measured with a dead weight pressure balance with an accuracy of 0.03% of the reading. The Cailletet tube is jacketed and ethanol is used as coolant fluid. The temperature of the sample is kept constant by circulating the coolant fluid with the help of a thermostatic bath (Lauda), which is

capable to maintain the coolant fluid at the desired temperature with an accuracy better than ± 0.01 K. A platinum resistance thermometer (Pt-100) located as close as possible to the sample, recorded the temperature of the coolant fluid with a maximum error of 0.02 K. The sample inside the tube is stirred by the stainless steel ball which is moved up and down by two button magnets activated by a rotating disc mounted on a stirring motor.

3.2.3 Experimental procedure

The hydrate phase equilibrium measurements are carried out by fixing the pressure and cooling down the sample until the hydrate phase was present. Then the temperature was elevated in small steps at a rate of 0.1 K per 10 min until the dissociation of the hydrate phase could be observed. Then, the temperature is increased stepwise (every step took much longer than 10 min) until no hydrate crystals were observed. The temperature where the hydrate phase disappeared was taken as the phase transition temperature. The measurements are repeated at lower temperature ramp rates in order to confirm the reliability of the experimental data [4]. It was determined that the temperature difference between appearance and disappearance of the solid phase was ± 0.2 K.

This procedure is performed for different pressures, obtaining the clathrate hydrate phase transition conditions at every pressure.

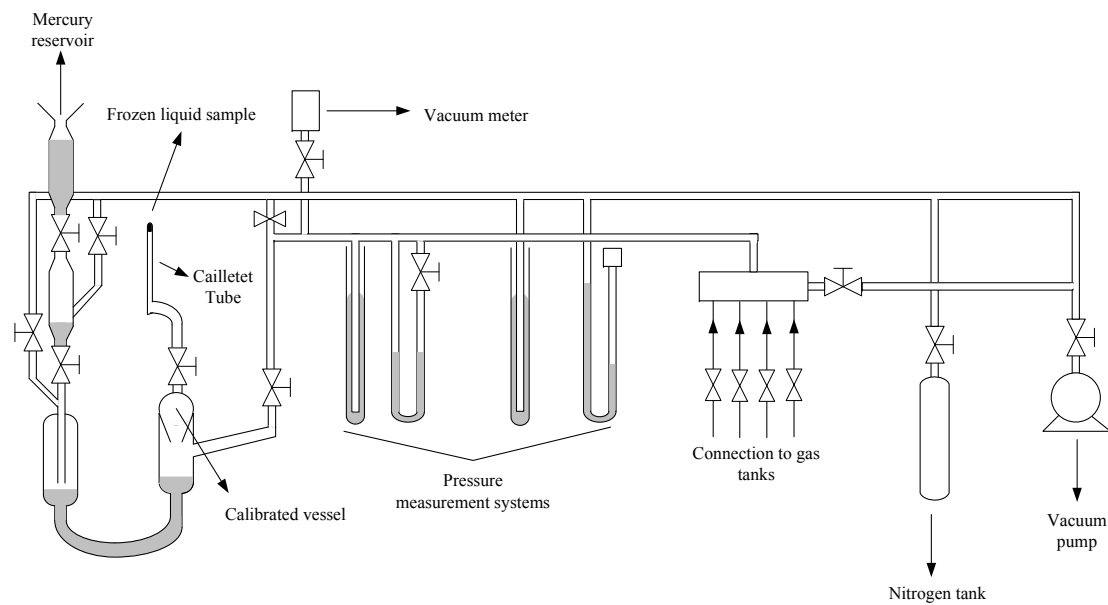


Figure 3.1. Schematic representation of the gas-rack.

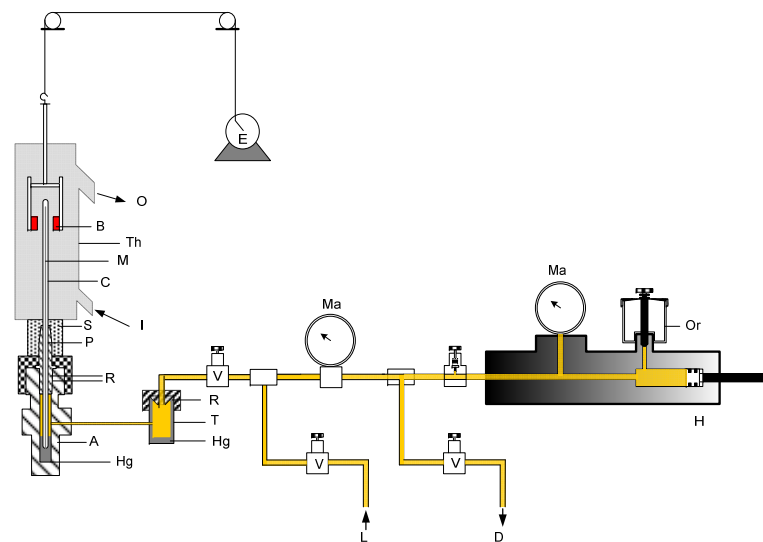


Figure 3.2. Schematic representation of the Cailletet apparatus: A, autoclave; B, magnets; C, Cailletet tube; D, drain; E, stirring motor; H, hydraulic pump; Hg, mercury; I, inlet thermostat liquid; L, connection with dead-weight pressure gauge; M, sample of mercury; Ma, manometers; O, outlet thermostat liquid; Or, oil reservoir; P, closing plug; R, O-rings; S, silicone rubber stopper; T, mercury trap; Th, glass thermostat; V, valve. (Adapted from Sabil 2009 [3]).

3.3. Kinetics of formation of clathrate and semi-clathrate hydrates

3.3.1 Experimental set-up

The kinetics experiments were performed in a high-pressure stainless steel vessel with an internal volume of 150 cm³ and a maximum pressure of 100 MPa. The experimental apparatus is illustrated in Figure 3.3. The vessel is immersed in a thermostatic bath to regulate the temperature. The temperature of the thermostatic bath is controlled by circulating ethylene glycol by means of a thermocontroller, which has an operating temperature range of 263 K to 373 K. The thermocontroller can maintain the circulating fluid at the desired temperature with an accuracy of ± 0.01 K. The temperature inside the vessel is monitored both in the gas and liquid phases by two platinum resistance temperature detectors (Pt100) Newport Omega with an accuracy of ± 0.01 K. In order to achieve proper mixing of the liquid phase, a magnetic stirrer is placed into the vessel. The pressure inside the vessel is measured by a pressure transducer (a piezo-resistive AESML series pressure sensor) with a reading range between 0 and 25 MPa and a reading accuracy of ± 0.025 MPa. The pressure and temperature readings are recorded and stored in a data acquisition system.

The Raman spectrum was collected by using a Kaiser MR immersion probe with a half-inch diameter and a focal distance of 3 mm, which is directly immersed into the sample. The Kaiser MR immersion probe is capable of operating up to 25 MPa. The position of the probe can be adjusted in order to obtain measurements at the surface (~ 1 mm under the surface) and at the bottom (~ 3 cm under the surface) of the set up. The probe is connected via optical fibers to the Raman spectrometer RXN1-TM Analyzer System (Kaiser Optical Systems), equipped with a 2400 grooves/mm grating and an external thermoelectrically (TE) cooled Charge Coupled Device (CCD) detector. The Raman system is equipped with an InvictusTM 532-nm Visible (VIS) solid-state diode pumped laser. The dispersion is 2.05 cm⁻¹/pixel and the spectral resolution is 5 cm⁻¹. The

spectral data are analyzed using HOLOREACT™ data treatment software.

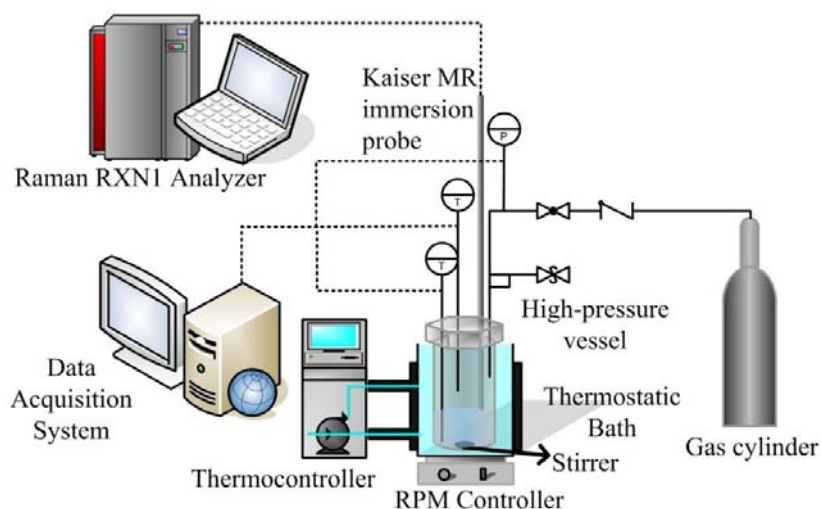


Figure 3.3. Diagram of the high-pressure apparatus for kinetic measurements with *in situ* Raman spectroscopy.

3.3.2 Experimental procedure

The kinetics experiments were performed by loading a known volume of aqueous solution with a known concentration in the high pressure vessel. All the solutions were prepared gravimetrically with a scale having an accuracy of ± 0.001 g. After the liquid solution was loaded the high pressure vessel was flushed five times with the help gas (H_2 or CO_2) in order to remove other gases (air). During flushing, the stirrer was switched off to prevent mixing of the gas and liquid phases. After flushing, the system was ready to start the experiments.

Hydrate formation was performed by two methods: (i) the T-cycle and (ii) the T-constant. For the T-cycle method, the temperature was first stabilized at a temperature higher than the equilibrium temperature, denoted as T_1 . After that, the high pressure vessel was pressurized with the help gas to the desired pressure. When the pressure and temperature

inside the high pressure vessel were constant, the system was cooled to a temperature below the equilibrium temperature, denoted as T_2 , at a constant cooling rate of 0.1 K/min. For the T-constant method, the temperature was first stabilized at T_2 and then the high pressure vessel was pressurized with the help gas to the desired pressure. The temperature conditions (T_1 and T_2) were chosen on the basis of the hydrate phase equilibrium temperatures of the system at the concentrations tested. In both approaches the stirrer was switched on after pressurization. In order to remove the hydrate phase from the gas–liquid interface and to keep the semi-hydrate particles as small crystals in slurry, the rate of stirring was kept at 500 rpm [5, 6]. For both formation methods, the stirring was switched off when the pressure was stabilized at T_2 . The system remained in this state for at least 24 h to ensure hydrate phase formation and maximum gas consumption. The dissociation of the hydrate phase was performed by heating up the system to T_1 with a constant heating rate of 0.5 K/h. Pressure and temperature changes were monitored throughout the process and recorded every second by the data acquisition system. The number of moles in the gas phase was calculated from the measured (p-T) data by applying the Peng–Robinson equation of state [7]. In order to ensure the reproducibility of the results, the experiments were repeated at least three times. Additionally, the Raman spectra were monitored every minute throughout the process and recorded by the Raman analyzer, the exposure time was set to 30 s.

3.4 Characterization techniques to determine structural aspects of clathrate hydrates

3.4.1 Sample preparation

Clathrate hydrates with one gas component were prepared in a Pyrex tube attached to a vacuum system by means of a flexible stainless steel tube. sI clathrate hydrates were formed by placing in contact finely powdered ice and the guest gas at a pressure of 500 torr. sII and sH clathrate hydrates

are formed by placing in contact with the guest gas (500 torr) finely powdered ice and sufficient quantities of guest liquid to give a water/large molecule mole ratio of 1:20. Afterwards, the sample tubes were sealed and then alternately cooled and shaken on a Vortex mixer. The samples were conditioned at -3°C for seven days. Some helium gas at low pressure was admitted to provide good thermal contact between the sample and the tube walls.

Clathrate hydrates of gas mixtures were synthesized from a mixture of solid particles of large guest molecule and water. The solid particles were formed by preparing gravimetrically a liquid solution of the large guest molecule and water. The solution was then frozen *eeze* and crushed under liquid nitrogen (LN). The crushed particles were poured by gravity into a chilled 50 cm^3 pressure vessel; approximately $\sim 4.7\text{g}$ of solid particles were used. In order to prevent the melting of the solid material the loading was performed in a freezer at 253K . After the loading, the vessel was sealed and immersed in a constant temperature bath containing a water-methanol mixture and connected to a valve and pressure transducer. The cell was slowly purged with the gas mixture three times, and then pressurized slowly to 50 bar. The sample was kept at 253 K and 50 bar for about 5-6 days. At the end of the formation period the gas was released and the hydrate sample was collected at LN temperature (77 K) and kept in LN for subsequent analysis.

3.4.2 Powder X-ray diffraction measurements

Powder X-Ray Diffraction (PXRD) patterns were recorded on a BRUKER AXS model D8 Advance diffractometer in the $\theta\theta$ scan mode using Cu $K\alpha$ radiation ($\lambda_1 = 1.5406\text{ \AA}$, $\lambda_2 = 1.5444\text{ \AA}$, and $I_2/I_1 = 0.5$). The samples stored in LN were groundrained and mounted on the X-ray stage which was cooled down to approximately 183.15 K in air. The diffraction patterns were measured with increasing temperature. The experiment was performed in the step mode with a fixed time of 2s and a step size of 0.0197° for $2\theta = 6-50^{\circ}$ with a total acquisition time of $\sim 75\text{ min}$. The

powder pattern was refined by the Le Bail method using the profile matching method within FULLPROF [8].

3.4.3 Nuclear magnetic resonance spectroscopy measurements

^{13}C NMR spectra were collected on a Bruker Avance III 400 MHz instrument at ^{13}C Larmor frequency of 100.6 MHz. The spinning speed and the temperature inside the probe were controlled using standard Bruker equipment. Prior to the NMR experiments the hydrate samples were groundrained under LN and packed in 7-mm zirconia rotors. The measurements were performed at temperatures from 183 K to 253 K and 3-kHz spinning speed. Both Bloch decay (single-pulse excitation) and cross polarization (CP) experiments were performed in order to differentiate the signals from the solid and liquid phases. Bloch decay experiments used a 90° pulse of 5 μs and composite pulse proton high power decoupling (HPDEC). The high frequency ^{13}C NMR resonance peak of adamantane (38.56 ppm from Tetramethylsilane (TMS), $\delta=0.0$ ppm) at 298 K and was used as the secondary external chemical shift reference. Static solid state ^2H NMR spectra were obtained at 46.05 MHz on a Bruker AMX-300 spectrometer, using a quadrupole echo pulse sequence [9] with echo delay times of 35 μs . The various temperatures were obtained using a modified Bruker probe and a Eurotherm controller using cold flowing nitrogen gas. Between 200 and 480 accumulations were obtained with delays of 1 second.

3.4 References

- [1] Dyamond J. H., Smith, E. B. The virial coefficients of pure gases and mixtures. Amsterdam 1980.
- [2] de Loos T. W., van der Kooi H. J., Ott P. L. Vapor liquid critical curve of the system ethane + 2-methylpropane. Journal of Chemical Engineering Data. 1986;31:166-8.

- [3] Sabil K. M. Phase Behaviour, Thermodynamics and Kinetics of Clathrate Hydrates Systems of Carbon Dioxide in Presence of Tetrahydrofuran and Electrolytes: Delft University of Technology; 2009.
- [4] Tohidi B., Burgass R. W., Danesh A., Ostergaard K. K., Todd A. C. Improving the Accuracy of Gas Hydrate Dissociation Point Measurements. *Annals of the New York Academy of Sciences*. 2000;912:924-31.
- [5] Sabil K. M., Duarte A. R. C., Zevenbergen J., Ahmad M. M., Yusup S., Omar A. A., et al. Kinetic of formation for single carbon dioxide and mixed carbon dioxide and tetrahydrofuran hydrates in water and sodium chloride aqueous solution. *International Journal of Greenhouse Gas Control*. 2010;4:798-805.
- [6] Vysniauskas A., Bishnoi P. R. A Kinetic-study of Methane Hydrate Formation. *Chemical Engineering Science*. 1983;38:1061-72.
- [7] Peng D., Robinson D. B. New 2-Constant Equation of State. *Industrial and Engineering Chemistry Fundamentals*. 1976;15:59-64.
- [8] Rodriguez-Carvajal J. FULLPROF: A program for rietveld refinement and pattern matching analysis. *Abstracts of the Satellite Meeting on Powder Diffraction of the XV Congress of the IUCr (International Union of Crystallography, Toulouse, France)* p 127. 1990.
- [9] Davis J. H., Jeffrey K. R., Bloom M., Valic M. I., Higgs T. P. Quadrupolar echo deuteron magnetic-resonance spectroscopy in ordered hydrocarbon chains. *Chemical Physics Letters*. 1976;42:390-4.

Chapter 4

Phase Equilibrium of Structure II Clathrate Hydrates of Hydrogen with Various Promoters

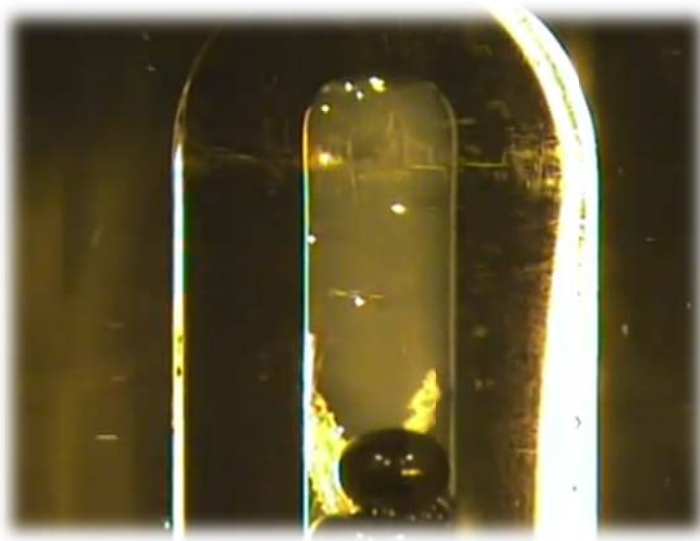


Photo courtesy of Eugene Straver

4.1. Introduction

In the present chapter phase equilibrium measurements of single and mixed organic clathrate hydrates with hydrogen are presented. Section 4.2 provides a background and justification of the current study. Section 4.3 describes the materials and methods. Section 4.4 presents the results together with a discussion. Finally section 4.5 provides the conclusions of the study. The present chapter is a modified version of the original article published in *Fluid Phase Equilibria*, volume 307, issue 1, page 6.

4.2 Background

In 1999, the first experimental reports of clathrate hydrates with hydrogen (H_2) as guest molecules stored within the cavities were published [1, 2]. Since then, these materials have been attracting particular interest due to their potential for H_2 storage. The major scientific and technological challenge is therefore to increase the storage capacity and to stabilize the material at more practical conditions (close to ambient conditions).

Single H_2 clathrate hydrates show a sII configuration, where 136 H_2O molecules form sixteen small cavities (5^{12}) and eight large cavities ($5^{12}6^4$) [3]. With a double H_2 occupancy of all sixteen small cavities, and quadruple occupancy of the large cavities, the maximum H_2 storage capacity of this sII clathrate hydrate is 5.0 wt%. However this maximum capacity has only been reported at extremely high pressures in excess of 200 MPa [4].

The addition of a second type of guest molecule, a so-called promoter, was found to reduce the formation pressure by two orders of magnitude. For example, the addition of tetrahydrofuran (THF) to form sII H_2 clathrate hydrate resulted in the formation of a mixed sII THF- H_2 clathrate hydrate that was stable at pressures as low as 5 MPa at 280 K [5]. However, the addition of a promoter significantly reduces the H_2 storage

capacity of the clathrate hydrate. The addition of THF, for example, reduces the maximum H₂ storage capacity to only 1.1 wt% [6]. Lee *et al.* [7] reported that the H₂ storage capacity of the mixed THF-H₂ clathrate hydrate could be increased up to 4.0 wt% at 12 MPa and 270 K by tuning its composition. Nevertheless, further studies suggested the unfeasibility of reproducing the results at the conditions tested [6, 8]. Recently, Sugahara *et al.* [9] reported the possibility of reproducing the tuning effect by a new method of hydrate formation from ice and solid THF. Using this method the H₂ storage capacity of the mixed THF-H₂ clathrate hydrate can be increased to 3.4 wt% at 70 MPa and 255 K [9]. Although the pressure and temperature conditions reported by Sugahara *et al.* [9] to stabilize these materials are still far from practical, the results highlight the importance of the promoter on the stability of the hydrate phase.

Several studies have been performed in order to determine the role of the promoter molecule on the stability conditions of clathrate hydrates of methane (CH₄) [10-13], carbon dioxide (CO₂) [14-16] and propane (C₃H₈) [17-19], among others. However, the role of the promoter in systems involving H₂ is still not clearly understood. Phase equilibrium measurements of mixed organic sII clathrate hydrates with H₂ are scarce [20, 21] because most of the research has been focused on THF-H₂ clathrate hydrates. Consequently, from the practical and scientific point of view the search for H₂ clathrate hydrates with increased storage capacity at more practical conditions is a priority, and a suitable promoter molecule could play an important role in the development of such material.

In the present work the effect of five organic compounds on the stability of mixed sII (promoter-H₂) clathrate hydrates was studied. The additives studied are: furan, 2,5-dihydrofuran, tetrahydropyran, 1,3-dioxolane and cyclopentane. These organic compounds are known to form single sII clathrate hydrates [22, 23] and consequently are suitable to form mixed sII (promoter-H₂) clathrate hydrates. The hydrate phase equilibrium conditions (p , T data) of the ternary systems H₂O + H₂ + furan, H₂O + H₂ + 2,5-dihydrofuran, H₂O + H₂ + tetrahydropyran, H₂O + H₂ + 1,3-

dioxolane, $\text{H}_2\text{O} + \text{H}_2 + \text{cyclopentane}$, and of the binary systems $\text{H}_2\text{O} + \text{furan}$, $\text{H}_2\text{O} + 2,5\text{-dihydrofuran}$, $\text{H}_2\text{O} + \text{tetrahydropyran}$, $\text{H}_2\text{O} + 1,3\text{-dioxolane}$ and $\text{H}_2\text{O} + \text{cyclopentane}$ up to pressures of 14.0 MPa, have never been measured before and they may help to elucidate the factors dictating the stability trend of the mixed sII H_2 clathrate hydrates.

4.3 Experimental Methodology

4.3.1 Materials

Table 4.1 lists the different hydrocarbons studied as promoter materials for sII clathrate hydrates and shows the molecular structures. For the liquid phase, double distilled and de-ionized H_2O was used. H_2 was supplied by Hoek Loos with a purity of 99.999 mol%. All the chemicals were used without any further purification.

4.3.2 Experimental procedure

The sample was prepared as described in Chapter 3. The liquid samples were prepared in such way that the concentration in the clathrate hydrate lattice was as close as possible to the stoichiometric concentration (5.6 mol%). The maximum error in the mole fraction x in $\{(1 - x) \text{ organic compound} + x\text{H}_2\text{O}\}$ was estimated to be 0.002. The experimental data for the phase equilibrium were determined with the Caillitet equipment as described in the previous chapter.

4.4 Results and discussion

The phase equilibrium measurements of the single sII clathrate hydrates of furan, 2,5-dihydrofuran, tetrahydropyran, 1,3-dioxolane and cyclopentane are reported in Table 4.2. The data presented in this work correspond to the dissociation curve of the clathrate hydrates i.e., the maximum temperature at which the clathrate hydrate is stable for a given pressure.

The systems consisting of H₂O and a water-insoluble organic compound (furan, 2,5-dihydrofuran, tetrahydropyran and cyclopentane) showed a three-phase equilibrium of the nature: aqueous (water-rich) phase (L₁) – organic-rich phase (L₂) - hydrate phase (H). The system consisting of H₂O and water-soluble organic compound (1,3-dioxolane) displayed a two-phase equilibrium of the nature: aqueous phase (L₁) - hydrate phase (H). Figure 4.1 shows graphically the hydrate phase equilibrium of the binary systems.

Table 4.1. List of promoter materials studied in this work



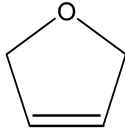
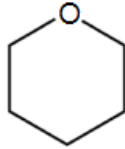
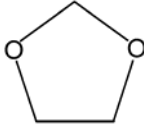
Promoter material	Molecular Structure
Cyclopentane	
C ₅ H ₁₀	
CAS [287-92-3]	
Fluka	
Furan	
C ₄ H ₄ O	
CAS [110-00-9]	
Fluka	
2,5-Dihydrofuran	
C ₄ H ₆ O	
CAS [1708-29-8]	
Sigma-Aldrich	
Tetrahydropyran	
C ₅ H ₁₀ O	
CAS [142-68-7]	
Sigma-Aldrich	
1,3-Dioxolane	
C ₃ H ₆ O ₂	
CAS [646-06-0]	
Sigma-Aldrich	

Table 4.2. Phase equilibrium data (temperature, T , pressure, p and type of phase transition) for single sII organic clathrate hydrates (without help gas). L_1 is the aqueous (water-rich) phase, L_2 is the organic-rich phase and H is the solid (hydrate) phase

System	T (K)	p (MPa)	Phase Transition
H₂O + Furan	277.37	2.00	H-L ₁ -L ₂ → L ₁ -L ₂
5.79 mol% Furan	277.33	4.00	
	277.21	8.00	
	277.10	12.01	
	276.95	14.01	
H₂O + 2,5-Dihydrofuran	272.00	2.00	H-L ₁ -L ₂ → L ₁ -L ₂
5.96 mol% 2,5-Dihydrofuran	271.88	4.00	
	271.73	8.00	
	271.55	12.01	
	271.44	14.00	
H₂O + Tetrahydropyran	272.36	1.91	H-L ₁ -L ₂ → L ₁ -L ₂
5.44 mol% Tetrahydropyran	272.29	6.00	
	272.26	10.00	
	272.26	12.00	
	272.24	14.00	
H₂O + 1,3-Dioxolane	270.47	1.99	H-L ₁ → L ₁
6.39 mol% 1,3-Dioxolane	270.45	2.49	
	270.29	5.99	
	270.08	10.49	
	269.94	13.50	
H₂O + Cyclopentane	279.90	2.55	H-L ₁ -L ₂ → L ₁ -L ₂
5.60 mol% Cyclopentane	279.94	5.05	
	280.02	7.55	
	280.00	10.03	
	280.03	12.55	

From Figure 4.1 it can be noticed that furan and cyclopentane form the most stable hydrate phases at temperatures above the melting point of H₂O. The other three hydrate phases are less stable than ice. Another

interesting fact is that the influence of the pressure on the hydrate dissociation temperature is negligible, as can be observed from the very steep slopes in Figure 4.1. This can be explained by the absence of any gaseous compound, due to the incompressibility of the phases under this pressure range, the pressure increases steeply with increasing temperature according to Clapeyron's equation [24]. In Figure 4.1, it can be observed that the slopes (dp/dT) of the systems H_2O -1,3-dioxolane, H_2O -2,5-dihydrofuran and H_2O -furan are negative. The reason for this might be that the hydrate phase was decomposed to the organic liquid phase and ice before the ice was melted.

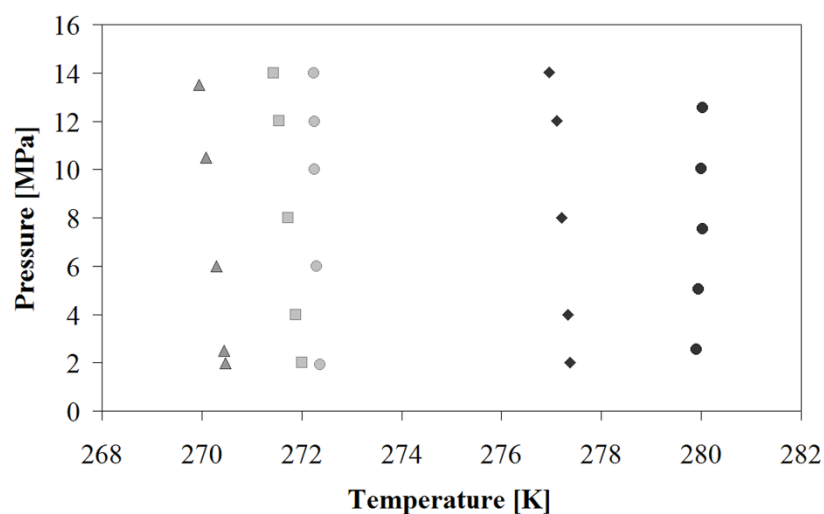


Figure 4.1. Phase equilibrium data for the binary systems: H_2O -furan (◆), H_2O -2,5-dihydrofuran (■), H_2O -tetrahydropyran (●), H_2O -1,3-dioxolane (▲) and H_2O -cyclopentane (✱).

The phase equilibrium measurements of the mixed sII clathrate hydrates of H_2 and organic compounds are reported in Table 4.3. The systems consisting of H_2O , H_2 and a water-insoluble organic compound exhibit a four-phase equilibrium of the nature: hydrate phase (H) - aqueous (water-rich) phase (L_1) - organic-rich phase (L_2) - vapor phase (V). The system consisting of H_2O , H_2 and water-soluble organic compound shows a three-phase equilibrium of the nature: hydrate phase (H) - aqueous phase

(L₁) - vapor phase (V). The results are graphically depicted in Figure 4.2. For comparison, the previously reported thermodynamic equilibrium conditions of the mixed sII clathrate hydrates of H₂-cyclopentane [20] and H₂-furan [21] were included in Figure 4.2, and show good agreement with our data. For illustrative purposes, the thermodynamic equilibrium conditions of the mixed H₂-THF clathrate hydrates at the stoichiometric concentration [25] are also included in Figure 4.2.

From the slopes (dp/dT) in Figure 4.2 it can be noticed that the influence of pressure on the hydrate stability is large, which can be explained by the involvement of a gaseous guest molecule (H₂). It is expected that the H₂ molecules occupy the small cavities, while the organic compound occupies the larger cavities. Moreover, Figure 4.2 shows that all mixed hydrate phases are more stable than ice at higher pressures. All mixed hydrate phases are also more stable than the corresponding single clathrate hydrates. Thus, the inclusion of H₂ to form a mixed clathrate hydrate increases the stability compared to the single organic clathrate hydrates. The mixed clathrate hydrate also has a much higher stability compared to a pure H₂ sII clathrate hydrate (stable at pressures > 200 MPa). Therefore, the organic compounds act as promoter materials.

Table 4.3. Phase equilibrium data (temperature, T , pressure, p and type of phase transition) for mixed sII (H_2 - organic compound) clathrate hydrates. L_1 is the aqueous (water-rich) phase, L_2 is the organic-rich phase, H is the solid (hydrate) phase and V is the vapor phase

System	T (K)	p (MPa)	Phase Transition
H ₂ O + H ₂ + Furan 5.61 mol% Furan	278.44	2.55	H-L ₁ -L ₂ -V → L ₁ -L ₂ -V
	279.10	5.05	
	279.95	7.55	
	280.75	10.05	
	281.38	12.55	
H ₂ O + H ₂ + 2,5-Dihydrofuran 5.90 mol% 2,5-Dihydrofuran	273.65	2.55	H-L ₁ -L ₂ -V → L ₁ -L ₂ -V
	274.64	5.05	
	275.58	7.55	
	276.40	10.05	
	277.18	12.55	
H ₂ O + H ₂ + 1,3-Dioxolane 5.62 mol% 1,3-Dioxolane	271.75	2.55	H-L ₁ -V → L ₁ -V
	272.71	5.05	
	273.63	7.55	
	274.37	10.05	
	275.07	12.55	
H ₂ O + H ₂ + Tetrahydropyran 6.02 mol% Tetrahydropyran	273.76	2.55	H-L ₁ -L ₂ -V → L ₁ -L ₂ -V
	275.03	5.05	
	275.95	7.55	
	276.88	10.05	
	277.71	12.55	
H ₂ O + H ₂ + Cyclopentane 5.60 mol% Cyclopentane	280.83	2.50	H-L ₁ -L ₂ -V → L ₁ -L ₂ -V
	281.65	5.00	
	282.64	7.55	
	283.43	10.00	
	284.01	12.50	

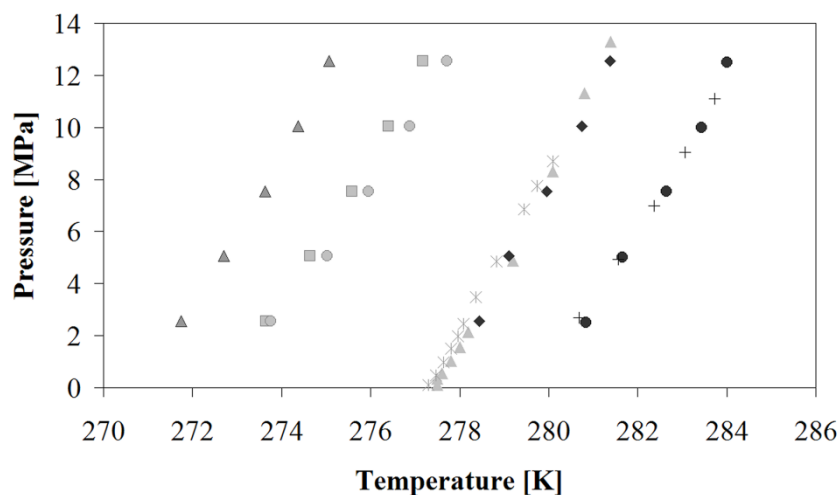
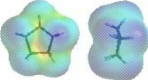
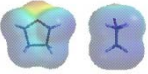
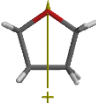
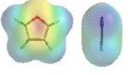
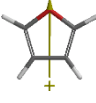
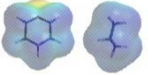
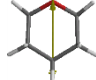
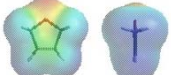
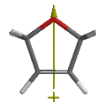
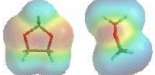
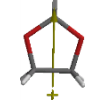


Figure 4.2. Phase equilibrium data for the ternary systems in this work: $\text{H}_2\text{O}-\text{H}_2$ -furan (◆), $\text{H}_2\text{O}-\text{H}_2$ -2,5-dihydrofuran (◻), $\text{H}_2\text{O}-\text{H}_2$ -tetrahydropyran (●), $\text{H}_2\text{O}-\text{H}_2$ -1,3-dioxolane (▲) and $\text{H}_2\text{O}-\text{H}_2$ -cyclopentane (●). For comparison, also the existing data for $\text{H}_2\text{O}-\text{H}_2$ -furan (✕) [21], $\text{H}_2\text{O}-\text{H}_2$ -cyclopentane (+) [20] and $\text{H}_2\text{O}-\text{H}_2$ -THF [25] (▲) are presented.

When comparing Figures 4.1 and 4.2, one can observe the same trend with respect to stability of the hydrate phase for the single and mixed clathrate hydrates. This stability increases in the order: 1,3-dioxolane < 2,5-dihydrofuran < tetrahydropyran < furan, THF < cyclopentane. The stability of a clathrate hydrate is influenced by the interactions between the guest and the H_2O molecules. For a better understanding, the magnitude and direction of the dipole moment, the molecular weight and the van der Waals volume of the additives are presented in Table 4.4. All the organic compounds studied fulfilled the size requirement to fit into the larger cavity of the sII clathrate hydrate [3, 11, 23, 26], although tetrahydropyran is rather large for optimal fit. From the data in Table 4.4 it is also possible to notice that there is not a clear trend on the stability related to the magnitude of the dipole moment. Alavi *et al.* [27] reported that tetrahydropyran and THF form hydrogen bonds with the large cage water molecules of sII clathrate hydrates. The hydrogen bonds between the host and the guest lead to the formation of L-Bjerrum defects which

may have an influence on the stability of the hydrate phase. According to Alavi *et al.* [27] three criteria are necessary for the formation of hydrogen bonds: i) the guest must have an electronegative hydrogen bond accepting atom, ii) the guest must have relatively large molar volume such that the electronegative atom is in close proximity to the large cage water molecule and iii) the guest must have a large dipole vector that is oriented in the direction of an electronegative atom. Therefore, furan and 2,5-dihydrofuran may also form hydrogen bonds with the cage water molecules, while these are absent in cyclopentane and 1,3-dioxolane. Although this might have some influence it seems that stability is mainly dominated by other factors. For instance it was noticed that 1,3-dioxolane, 2,5-dihydrofuran and furan have similar molecular weight and van der Waals volumes, but their clathrate hydrate stabilities differ significantly from each other. This difference also does not seem to be related to the magnitude of the dipole moment. For example, compounds with similar dipole moments, such as THF and 2,5-dihydrofuran, show significant differences in hydrate stabilities. It can thus be suggested that the molecular geometry of the organic compound has the largest influence on the hydrate stability. The organic compounds with the symmetry that better fits the large cavity seem to be able to produce the most stable clathrate hydrates.

Table 4.4. Physical properties (molecular weight, MW , dipole moment, D , and van der Waals volume, V_{vdW}) of the promoters studied

Promoter	MW (g mol^{-1})	D (D) ^[28]	V_{vdW} ^a (Å^3)	Dipole vector ^a
 Cyclopentane	70.1	0.0	94.87	
 Tetrahydrofuran	72.1	1.75 ± 0.04	85.56	
 Furan	68.0	0.66 ± 0.01	77.12	
 Tetrahydropyran	86.1	1.58 ± 0.03	102.3	
 2,5-Dihydrofuran	70.0	1.63 ± 0.01	81.65	
 1,3 – Dioxolane	74.0	1.19 ± 0.06	76.27	

^aThe van der Waals volumes and the dipole vector were determined from Spartan[®] calculations at the Hartree-Fock level.

The Clausius-Clapeyron equation is used to determine the hydrate dissociation enthalpies ΔH_{diss} of the mixed H₂ clathrate hydrates from the phase equilibrium data obtained in this study [29]:

$$\frac{d \ln p}{d(1/T)} = -\frac{\Delta H_{diss}}{z R} \quad (4.2)$$

where p and T are the absolute pressures and temperatures of hydrate equilibrium, R is the universal gas constant, and z is the compressibility factor. The dissociation enthalpy ΔH_{diss} is the enthalpy change that takes place when hydrates are melted. According to van der Waals & Platteeuw [30] the application of the Clapeyron equation for the calculation of ΔH_{diss} is thermodynamically acceptable for clathrate hydrates as long as the system is univariant, irrespective of the number of components. In this work the compressibility factor and the stoichiometric ratios of H₂O to guest molecules are assumed to be constant. This may generate inaccuracies caused by volume changes, the non-ideality of the vapor phase and the solubility of the gas in the liquid phase [31, 32]. Therefore, the enthalpy data in this report should be only taken as an approximation. The estimated hydrate dissociation enthalpies can then be obtained from the slope of the straight line in a semi-logarithmic plot of the dissociation pressure versus the reciprocal temperature. Table 4.5 presents the hydrate dissociation enthalpies of the mixed clathrate hydrates of H₂ and water-insoluble organic compounds. The dissociation enthalpies calculated are in the range of values reported for other mixed sII organic clathrate hydrates [33].

Table 4.5. Hydrate dissociation enthalpies of the mixed clathrate hydrates of H₂ and water-insoluble organic compounds

System	ΔH (kJ mol ⁻¹)
H ₂ O-H ₂ -Furan	343.57
H ₂ O-H ₂ -2,5-Dihydrofuran	287.26
H ₂ O-H ₂ -Tetrahydropyran	343.62
H ₂ O-H ₂ -Cyclopentane	329.23

4.5 Conclusions

In this study the phase equilibrium data of several different single and mixed organic hydrate phases with H₂ were determined. It was shown that the addition of H₂ increases the stability of the mixed hydrate phase compared to the corresponding single organic hydrate phase. The mixed H₂ clathrate hydrates are also more stable than pure H₂ clathrate hydrate, indicating that the organic compounds act as promoter materials. The molecular size and geometry of the organic compound most likely determine the stability of the clathrate hydrates, while the dipole moment does not seem to have a strong influence.

4.6 References

- [1] Dyadin Y. A., Aladko E. Y., Manakov A. Y., Zhurko F. V., Mikina T. V., Komarov V. Y., Grachev E. V. Clathrate formation in water-noble gas (hydrogen) systems at high pressures. *Journal of Structural Chemistry*. 1999;40:790-5.
- [2] Dyadin Y. A., Larionov E. G., Manakov A. Y., Zhurko F. V., Aladko E. Y., Mikina T. V., Komarov V. Y. Clathrate hydrates of hydrogen and neon. *Mendeleev Communications*. 1999;9:209-10.
- [3] Sloan E. D., Koh C. A. *Clathrate Hydrates of Natural Gases*. 3rd ed. Florida: CRC Press; 2008.
- [4] Mao W. L., Mao H. K., Goncharov A. F., Struzhkin V. V., Guo Q. Z., Hu J. Z., Shu J. F., Hemley R. J., Somayazulu M., Zhao Y. S. Hydrogen clusters in clathrate hydrate. *Science*. 2002;297:2247-9.
- [5] Florusse L. J., Peters C. J., Schoonman J., Hester K. C., Koh C. A., Dec S. F., Marsh K. N., Sloan E. D. Stable low-pressure hydrogen clusters stored in a binary clathrate hydrate. *Science*. 2004;306:469-71.
- [6] Anderson R., Chapoy A., Tohidi B. Phase relations and binary clathrate hydrate formation in the system H₂-THF-H₂O. *Langmuir*. 2007;23:3440-4.

- [7] Lee H., Lee J. W., Kim D. Y., Park J., Seo Y. T., Zeng H., Moudrakovski I. L., Ratcliffe C. I., Ripmeester J. A. Tuning clathrate hydrates for hydrogen storage. *Nature*. 2005;434:743-6.
- [8] Strobel T. A., Taylor C. J., Hester K. C., Dec S. F., Koh C. A., Miller K. T., Sloan E. D. Molecular hydrogen storage in binary THF-H₂ clathrate hydrates. *Journal of Physical Chemistry B*. 2006;110:17121-5.
- [9] Sugahara T., Haag J. C., Prasad P. S. R., Warntjes A. A., Sloan E. D., Sum A. K., Koh C. A. Increasing Hydrogen Storage Capacity Using Tetrahydrofuran. *Journal of the American Chemical Society*. 2009;131:14616-7.
- [10] Mehta A. P, Sloan E. D. Structure-H hydrate phase-equilibria of methane plus liquid-hydrocarbon mixtures. *Journal of Chemical Engineering Data*. 1993;38:580-2.
- [11] Mooijer-van den Heuvel M. M., Peters C. J., Arons J. D. Influence of water-insoluble organic components on the gas hydrate equilibrium conditions of methane. *Fluid Phase Equilibria*. 2000;172:73-91.
- [12] Danesh A., Tohidi B., Burgass R. W., Todd A. C. Hydrate equilibrium data of methylcyclopentane with methane or nitrogen. *Chemical Engineering Research and Design*. 1994;72:197-200.
- [13] Mainusch S., Peters C. J., deSwaan A. J., Javanmardi J., Progep N. G. H. Experimental determination and modeling of methane hydrates in mixtures of acetone and water. *NGH '96 - 2nd International Conference on Natural Gas Hydrates, Proceedings*. Toulouse: Institut National Polytechnique; 1996. p. 71-6.
- [14] Mooijer-van den Heuvel M. M., Witteman R., Peters C. J. Phase behaviour of gas hydrates of carbon dioxide in the presence of tetrahydropyran, cyclobutanone, cyclohexane and methylcyclohexane. *Fluid Phase Equilibria*. 2001;182:97-110.
- [15] Sabil K. M., Witkamp G. J., Peters C. J. Phase equilibria of mixed carbon dioxide and tetrahydrofuran hydrates in sodium chloride aqueous solutions. *Fluid Phase Equilibria*. 2009;284:38-43.
- [16] Lin W., Delahaye A., Fournaison L. Phase equilibrium and dissociation enthalpy for semi-clathrate hydrate of CO₂ plus TBAB. *Fluid Phase Equilibria*. 2008;264:220-7.

- [17] Mooijer-van den Heuvel M. M., Peters C. J., Arons J. D. Gas hydrate phase equilibria for propane in the presence of additive components. *Fluid Phase Equilibria*. 2002;193:245-59.
- [18] Sun Z. G., Wang R. Z., Ma R. S., Guo K. H., Fan S. S. Natural gas storage in hydrates with the presence of promoters. *Energy Conversion and Management*. 2003;44:2733-42.
- [19] Gayet P., Dicharry C., Marion G., Graciaa A., Lachaise J., Nesterov A. Experimental determination of methane hydrate dissociation curve up to 55 MPa by using a small amount of surfactant as hydrate promoter. *Chemical Engineering Science*. 2005;60:5751-8.
- [20] Zhang J. S., Lee J. W. Equilibrium of Hydrogen plus Cyclopentane and Carbon Dioxide plus Cyclopentane Binary Hydrates. *Journal of Chemical Engineering Data*. 2009;54:659-61.
- [21] Tsuda T., Ogata K., Hashimoto S., Sugahara T., Moritoki M., Ohgaki K. Storage capacity of hydrogen in tetrahydrothiophene and furan clathrate hydrates. *Chemical Engineering Science*. 2009;64:4150-4.
- [22] Handa Y. P. Heat capacities in the range 95 to 260 K and enthalpies of fusion for structure-II clathrate hydrates of some cyclic ethers. *The Journal of Chemical Thermodynamics*. 1985;17:201-8.
- [23] Udachin K. A., Ratcliffe C. I., Ripmeester J. A. Single Crystal Diffraction Studies of Structure I, II and H Hydrates: Structure, Cage Occupancy and Composition. *Journal of Supramolecular Chemistry*. 2002;2:405-8.
- [24] Mooijer-van den Heuvel M. M. Phase Behaviour and Structural Aspects of Ternary Clathrate Hydrates Systems; The Role of Additives: Delft University of Technology; 2004.
- [25] Hashimoto S., Murayama S., Sugahara T., Sato H., Ohgaki K. Thermodynamic and Raman spectroscopic studies on H_2 +tetrahydrofuran+water and H_2 + tetra-n-butyl ammonium bromide+water mixtures containing gas hydrates. *Chemical Engineering Science*. 2006;61:7884-8.
- [26] Davison D. W. *Water: A Comprehensive Treatise*. New York: Plenum Press; 1973.

- [27] Alavi S., Susilo R., Ripmeester J. A. Linking microscopic guest properties to macroscopic observables in clathrate hydrates: Guest-host hydrogen bonding. *Journal of Chemical Physics*. 2009;130.
- [28] Lide D. R. *Handbook of Chemistry and Physics*. 90 th ed. Online Version 2010.
- [29] Sloan E. D., Fleyfel F. Hydrate dissociation enthalpy and guest size. *Fluid Phase Equilibria*. 1992;76:123-40.
- [30] Van Der Waals J. H., Platteeuw J. C. Validity of Clapeyron's Equation for Phase Equilibria involving Clathrates. *Nature*. 1959;183:462-.
- [31] Anderson G. K. Enthalpy of dissociation and hydration number of methane hydrate from the Clapeyron equation. *The Journal of Chemical Thermodynamics*. 2004;36:1119-27.
- [32] Anderson G. K. Enthalpy of dissociation and hydration number of carbon dioxide hydrate from the Clapeyron equation. *The Journal of Chemical Thermodynamics*. 2003;35:1171-83.
- [33] Rydzy M. B., Schicks J. M., Naumann R., Erzinger J. Dissociation enthalpies of synthesized multicomponent gas hydrates with respect to the guest composition and cage occupancy. *Journal of Physical Chemistry B*. 2007;111:9539-45.

Chapter 5

Kinetics Measurements

and *In situ* Raman

Spectroscopy of Formation

of Hydrogen-

Tetrabutylammonium

Bromide Semi-Hydrates



5.1 Introduction

In the present chapter the kinetics of formation of H₂-TBAB semi-clathrate hydrates was studied in order to elucidate their potential for H₂ storage. Section 5.2 provides a general background of the study, while section 5.3 presents the materials used and a brief description of the methodology. Section 5.4.1 presents an overview of the two methods used for hydrate formation from aqueous solutions. Sections 5.4.2 and 5.4.3 provide the results and respective discussions on induction time, rate of formation and amount of hydrogen stored. Sections 5.4.4 and 5.4.5 provide the Raman spectroscopic measurements of hydrate formation, together with the respective discussion. Finally, section 5.5 presents the conclusions of the study. The present chapter is a modified version of the article published in International Journal of Hydrogen Energy, volume 37, issue 7, page 5790.

5.2 Background

Recently, tetrabutylammonium bromide (TBAB) semi-clathrate hydrates, or TBAB semi-hydrates, have been proposed as potential H₂ storage materials [1]. TBAB semi-hydrates are another class of crystalline inclusion compounds formed by H₂O molecules and by TBAB salts. In the TBAB semi-hydrates however, the cage frame consists of H₂O molecules and bromide anions, unlike clathrate hydrates where the cages are formed exclusively by H₂O molecules. The tetrabutylammonium cations play the role of host molecules and are placed inside large cavities made of four smaller cages (T, H, P) [2]. Similar to clathrate hydrates, TBAB semi-hydrates also contain some small cages that can be filled by suitably sized 'guest' molecules, such as H₂ [3, 4]. Hashimoto *et al.* [1], Chapoy *et al.* [5] and Strobel *et al.* [2] have confirmed and reported the formation of H₂-TBAB semi-hydrates. The TBAB semi-hydrates present some advantages over mixed (gas-promoter) clathrate hydrates. Unlike common promoters (volatile organic compounds), TBAB salts are highly stable. This means that there is no contamination by TBAB when the H₂ is released after dissociation of the semi-hydrate.

Moreover, phase equilibrium measurements have shown that H₂-TBAB semi-hydrates are stable at more favorable conditions (~1 MPa at 285 K) [5] than mixed sII H₂-promoter clathrate hydrates.

The studies conducted on H₂-TBAB semi-hydrates have been mainly focused on phase equilibrium measurements [1, 5-7], and only few attempts have been made to determine the H₂ storage capacity [8]. To the best of our knowledge, there are no works studying the kinetics of H₂-TBAB semi-hydrates formation. In order to develop semi-hydrate based technology for H₂ storage, it is necessary to take into account the optimal kinetics of formation, which depends on the conditions applied. Therefore, time-dependent experiments were performed in this study in order to determine the optimal kinetics of formation as well as the H₂ storage potential of H₂-TBAB semi-hydrates. Two formation methods were tested: (i) the closed loop cycle method (Temperature-cycle method) [8], and (ii) the isothermal method (Temperature-constant method), in order to determine the influence of the formation method on the rate of hydrate formation and on the amount of H₂ consumed.

The existence of different types of crystal structures of TBAB semi-hydrates has already been reported before [9]. However, only two types of H₂-TBAB semi-hydrate crystal structures have been extensively studied [10]: (i) structure A (C₁₆H₃₆N⁺Br⁻·26H₂O), and (ii) structure B (C₁₆H₃₆N⁺Br⁻·38H₂O). In some studies, it has been reported that the H₂ storage capacity of H₂-TBAB semi-hydrates is affected by the concentration of TBAB [2]. In this study, the effect of concentration on the hydrate nucleation, hydrate growth and H₂ storage capacity was determined by testing two concentrations of TBAB in the aqueous solutions: (i) 2.6 mol%, and (ii) 3.7 mol%. The lower concentration (2.6 mol%) was reported by Strobel *et al.* [2] to present higher H₂ storage capacity. The higher concentration (3.7 mol%) was chosen because it corresponds to the stoichiometric concentration of structure A of TBAB semi-hydrates and because it is the concentration with the higher stability [11].

Additionally, an innovative approach was used to study the hydrate phase formation and dissociation *in situ* by using Raman spectroscopy. This approach allows the study of the Raman spectra *in situ* by immersing a pressure resistant probe directly in the bulk of the sample, which is closer to industrial conditions. To confirm the reliability of the applied approach, the Raman spectra of binary sII H₂-THF clathrate hydrates at stoichiometric concentration (~5.56 mol% of THF) were recorded, analyzed and compared to literature data. Coupled with the kinetic results, the Raman spectra during formation and dissociation of the H₂-TBAB semi-hydrates were recorded *in situ* by using this approach. To the best of our knowledge, this experimental procedure, using an immersion probe inside a high pressure cell (up to 20 MPa) of large volume (150 cm³) to study the Raman spectra, has never been used in kinetics studies of hydrate systems [1, 2, 7]. In order to analyze the influence of the H₂ mass transfer in the hydrate phase, the Raman probe was adjusted in two positions: (i) at the surface and (ii) at the bottom of the sample.

5.3 Methodology

5.3.1 Materials

H₂ was purchased from Air Liquid with a purity of 99.990 mol%. TBAB and THF were purchased from Aldrich–Sigma with a certified purity of >99.0%. The chemicals were used without any further purification. Double distilled and deionized Millipore quality water was used.

5.3.2 Experimental procedure

The experimental procedure was performed as described in Section 3.3 of Chapter 3. Two concentrations of TBAB in the aqueous solution were studied, 2.6 mol% and 3.7 mol%. Additionally, one single experiment was performed using an aqueous solution of THF at 5.56 mol%. The flushing was carried out with H₂. The temperature conditions T₁ = 289.15 K and T₂ =

281.15 K were chosen on the basis of the hydrate phase equilibrium temperatures of the system at the concentrations tested [12].

5.4 Results and discussion

5.4.1 The T-cycle and the T-constant methods

A typical pressure and temperature (p-T) profile of formation and dissociation of H₂-TBAB semi-hydrates by the T-cycle (constant cooling) method is shown in Figure 5.1. The gray dots correspond to the formation process and the black dots correspond to the dissociation process. At the beginning of the experiment pressure is stabilized (point A) and the system is cooled down at constant cooling rate. Therefore, a less sharp decrease in pressure is observed. During the cooling step, the system overshoots the hydrate equilibrium point indicated by B in Figure 5.1 without hydrate formation, due to the metastability of the system [13]. At point C the H₂-TBAB semi-hydrates begin to form. Here, a temperature increase takes place since hydrate formation is an exothermic process [13]. A sharp decrease of pressure also takes place due to the incorporation of H₂ molecules into the hydrate phase. The formation of semi-hydrates begins rapidly and the rate decreases with time until maximum sorption is reached [14] (point D). At this point the stationary pressure and temperature are achieved. Then, the system is heated from point D to point A whereby the hydrate phase dissociates. At the same time, the pressure increases due to the release of H₂ from the hydrate phase.

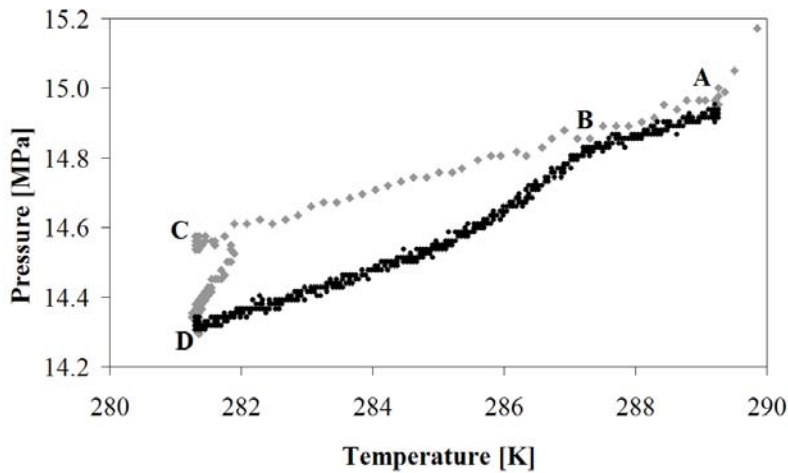


Figure 5.1. Typical pressure and temperature (p-T) profile of formation and dissociation of H₂-TBAB semi-hydrates by the T-cycle method.

The typical (p-T) data of formation and dissociation of H₂-TBAB semi-hydrates by the T-constant (constant temperature) method are graphically shown in Figure 5.2. Similar to the T-cycle method, a sharp decrease of pressure is observed at the beginning of the experiment (point A) due to the contraction of the gas phase and dissolution of H₂. Thereafter, unlike the T-cycle method, another sharp decrease of pressure is observed, but this time it is due to the hydrate formation (point B). At the same time, the temperature increases (point B'), also as a result of hydrate formation. When the maximum sorption is reached (point C), the system is heated from point C to point D, whereby the hydrate phase dissociates and the pressure increases due to H₂ release.

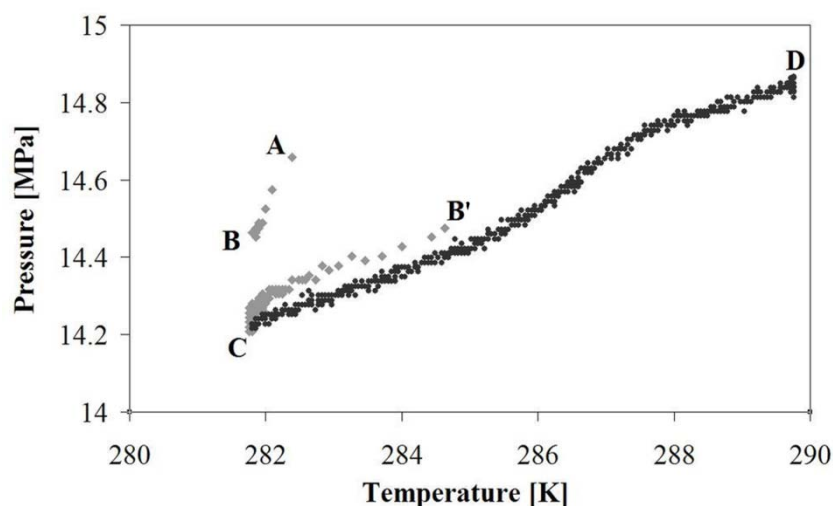


Figure 5.2. Typical pressure and temperature (p-T) profile of formation and dissociation of H₂-TBAB semi-hydrates by the T-constant method.

5.4.2 Induction time

As it was mentioned in Chapter 2, hydrate formation is commonly regarded as a crystallization process, which requires a supersaturation environment to take place [12]. The degree of supersaturation is a function of temperature, pressure and solution concentration. Usually the crystallization kinetics is divided into two separate phases. The first phase involves the formation of hydrate nuclei, whereas the second phase involves the hydrate growth which starts after stable nuclei have been formed. The induction time is defined as the time taken for the second phase to start. It is thus the time needed for hydrate nuclei to be detected macroscopically [13].

In this study the induction time was calculated as the time elapsed from the moment when the gas component is introduced in the system until, a significant pressure drop (~ 0.03 MPa) was detected in the system, the so-called turbidity point. Figure 5.3 displays the raw data of induction time for both concentrations (2.6 mol% and 3.7 mol%) at different pressures obtained by the T-cycle method. From Figure 5.3 it is possible to observe that a higher pressure results in a shorter induction time due to the higher degree of

supersaturation. These results agree well with kinetics reports of other hydrate systems [15-18]. From Figure 5.3 it is also possible to observe that the induction time of the system is less dependent on TBAB concentration and displays a less stochastic nature at higher pressures (above 10 MPa). The induction times obtained by the T-constant method displayed a more stochastic nature; the standard deviation in repeated measurements at high pressures was +/- 20 min. The induction time values varied from 28 minutes for the highest investigated pressure (15 MPa) to 434 minutes at pressure of 5 MPa. These observations agree well with those of Ohmura *et al.* [19], who demonstrated a higher degree of random behavior using the T-constant method.

5.4.3 Rate of formation and amount of H_2 consumed

The number of moles of H_2 consumed per time was calculated from the (p-T) data using the Peng-Robinson equation of state [20]. From this information the rate of hydrate formation was calculated as the ratio of H_2 uptake from the turbidity point to the stationary point (the point when the maximum amount of H_2 has been consumed) over the formation time. Figure 5.4 depicts the influence of pressure and solution concentration on the semi-hydrate formation rate obtained by the T-cycle method. It can be noticed that an increase in pressure and/or TBAB concentration results in an increase on the formation rate. The reason for this is that the formation rate is proportional to the driving force (supersaturation) [15], which rises with increasing H_2 pressure and TBAB concentration. The T-constant method gave similar results, so the hydrate formation rate is not affected by the formation method.

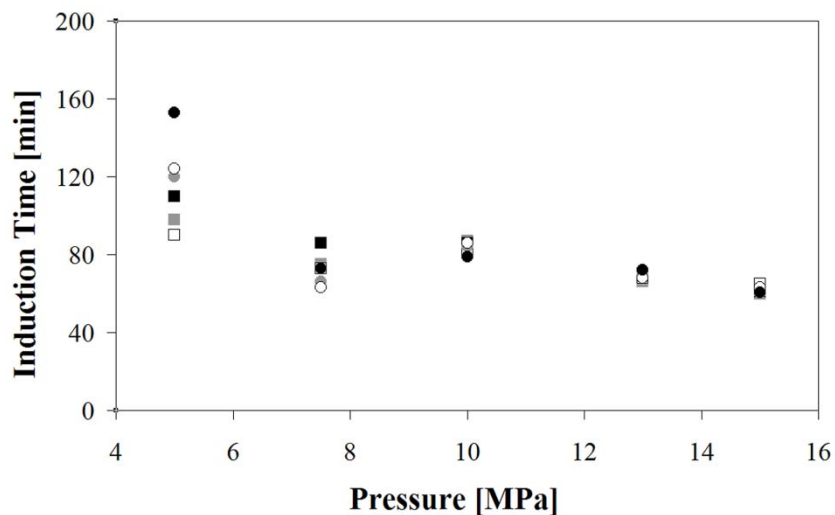


Figure 5.3. Influence of pressure and solution concentration on the induction time obtained by the T-cycle method. The squares correspond to a solution concentration of 2.6 mol% of TBAB and the circles correspond to a solution concentration of 3.7 mol% of TBAB.

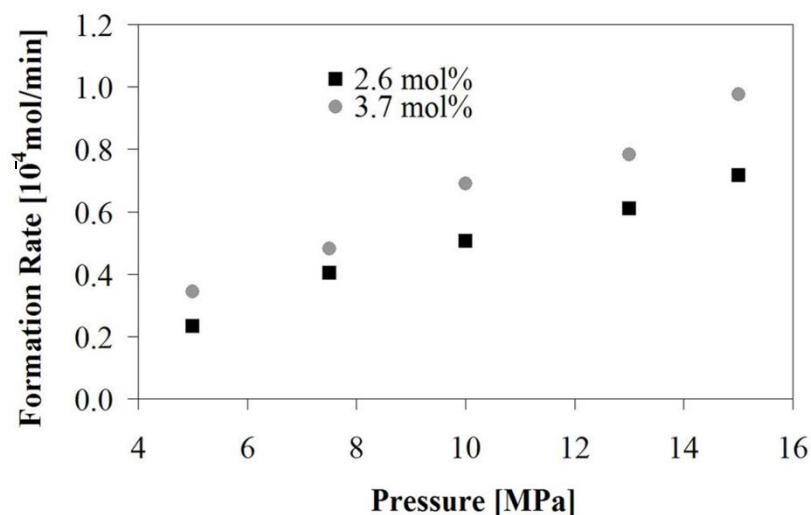
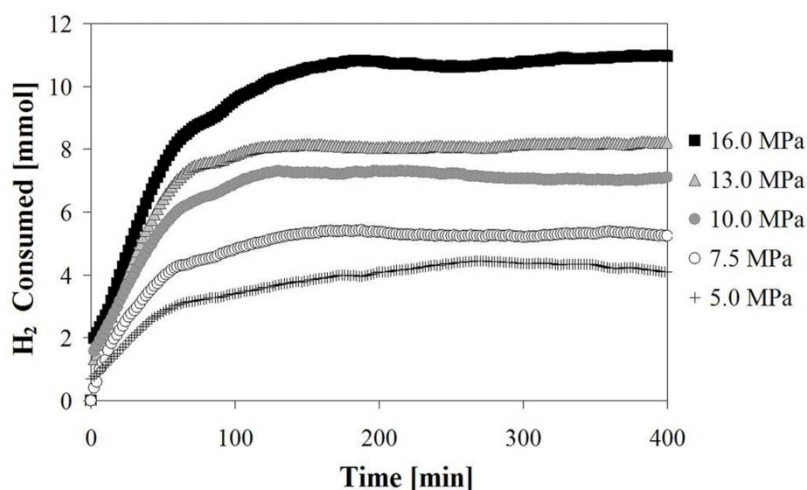


Figure 5.4. Influence of pressure and solution concentration on the H₂-TBAB semi-hydrate formation rate obtained by the T-cycle method.

Figures 5.5 and 5.6 display the amount of H₂ entrapped in the hydrate phase at different pressures for a solution of 3.7 mol% and 2.6 mol% of TBAB, respectively. The results were obtained by the T-cycle method. The amount

of H_2 consumed was calculated only considering the change in the amount of H_2 in the gas phase from the turbidity point to the stationary point; the change in the amount of H_2 in the gas phase from the beginning of the experiment to the turbidity point (due to dissolution of H_2 in the liquid phase) was not taken into account. The T-constant method gave similar results; therefore, the amount of H_2 consumed is not affected by the formation method.

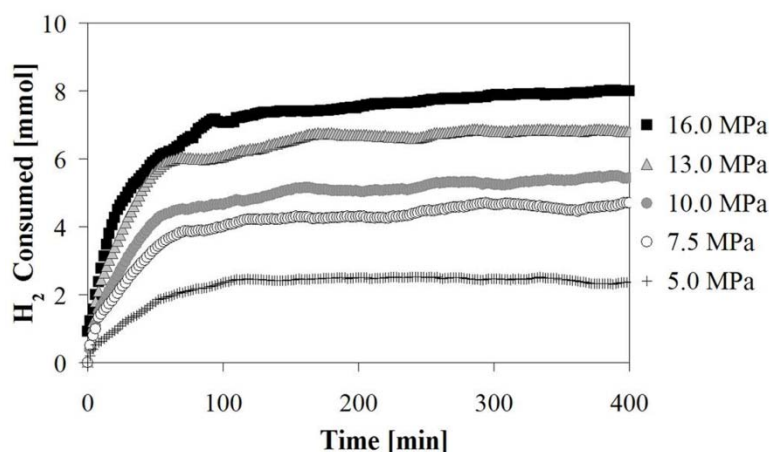
From Figures 5.5 and 5.6 it can be noticed that a higher pressure results in an increasing amount of H_2 consumed. Moreover, the highest concentration (3.7 mol% of TBAB) showed a higher amount of H_2 consumed. It was calculated that for a solution with a concentration of 3.7 mol% of TBAB the amount of H_2 stored was 0.046 wt% at 16 MPa and 281.15 K. Similarly, for a solution with a concentration of 2.6 mol% of TBAB, the amount of H_2 stored at 16 MPa and 281.15 K was 0.031 wt%.



Figures 5.5. Amount of H_2 entrapped in the hydrate phase at different pressures for a solution of 3.7 mol% of TBAB.

Both amounts are significantly lower than those reported by Strobel *et al.* [2]. They calculated the amount of H_2 stored in the bulk of TBAB semi-hydrates as a function of TBAB concentration at 13.8 MPa and 279.5 K. According to their results the highest H_2 storage capacity of 0.22 wt% corresponds to

the solution with a concentration of 2.6 mol% of TBAB, while for more concentrated solutions the capacity was reduced below 0.1 wt%. This contradicts the results obtained in this work, where the amount of H₂ stored was higher for the highest TBAB concentration.



Figures 5.6. Amount of H₂ entrapped in the hydrate phase at different pressures for a solution of 2.6 mol% of TBAB.

A possible explanation of these differences might be due to the H₂ mass transfer resistance. Strobel *et al.* [2] performed the incorporation of H₂ into the hydrate phase from homogeneously sized crushed particles of TBAB semi-hydrate, while in this study the H₂-TBAB semi-hydrate crystals were formed from a liquid solution. The contact area between gaseous H₂ and the hydrate phase is much larger in the crushed particles. On the other hand, in the liquid solution the contact area with the H₂ gas is limited to the diameter of the vessel. Consequently, the H₂ mass transfer resistance is much larger in this work, resulting in a lower H₂ storage capacity. Additionally, it is harder to diffuse H₂ into the liquid phase than into the hydrate phase [21], which could be another explanation for the lower H₂ storage capacity obtained in this study. Therefore, in order to achieve higher storage capacities, the H₂ mass transfer rate into the hydrate phase should be improved [22]. However, the approach applied in this study seems to be less energy and time consuming and consequently more suitable for a real practical application.

5.4.4 sII H₂-THF clathrate hydrates Raman spectroscopic studies

To confirm the reliability of the experimental set-up, the Raman spectra of an aqueous solution of 5.56 mol% THF were recorded during the formation and dissociation of the hydrate phase at ~13 MPa. The T-cycle method was used for the formation of the hydrate phase, the temperature ranged from 288.15 K to 279.15 K (hydrate phase equilibrium conditions were considered [1]) at a constant cooling rate of 0.1 K/min. The dissociation, starting after 22 h, was performed at a constant heating rate of 0.13 K/min.

Figure 5.7 (a) depicts the H₂ Raman spectra in the different phases during hydrate formation and (b) the Raman spectrum of H₂ in the hydrate phase. Here, the H₂ vibration peaks were normalized to each other to make an easier comparison. At the beginning of the experiment, bubbles of gaseous H₂ were dispersed into the liquid phase. Therefore, four peaks corresponding to the H-H stretching vibration mode in the gas phase are observed at ~4125, ~4145, ~4156 and ~4166 cm⁻¹. As can be seen from Figure 5.7 (a), the peak located at ~4145 cm⁻¹ is overlapped by the emerging vibration peak of H₂ in the liquid phase. As the system is cooled continuously, the H₂ is dissolved. Consequently, the intensity of the Raman signal of gaseous H₂ decreases while the intensity of the H-H stretching vibration mode in the liquid phase (~ 4138 cm⁻¹) [23] increases. After some time, the Raman signal of H₂ in the gas phase disappears and only a single peak indicating the presence of H₂ in the liquid phase is observed. Then, the hydrate formation takes place and the vibration peak is shifted to ~4132 cm⁻¹, indicating that H₂ molecules are trapped in the small cavities of the sII clathrate hydrate. These results are consistent with those of Florusse *et al.* [24] and Hashimoto *et al.* [1].

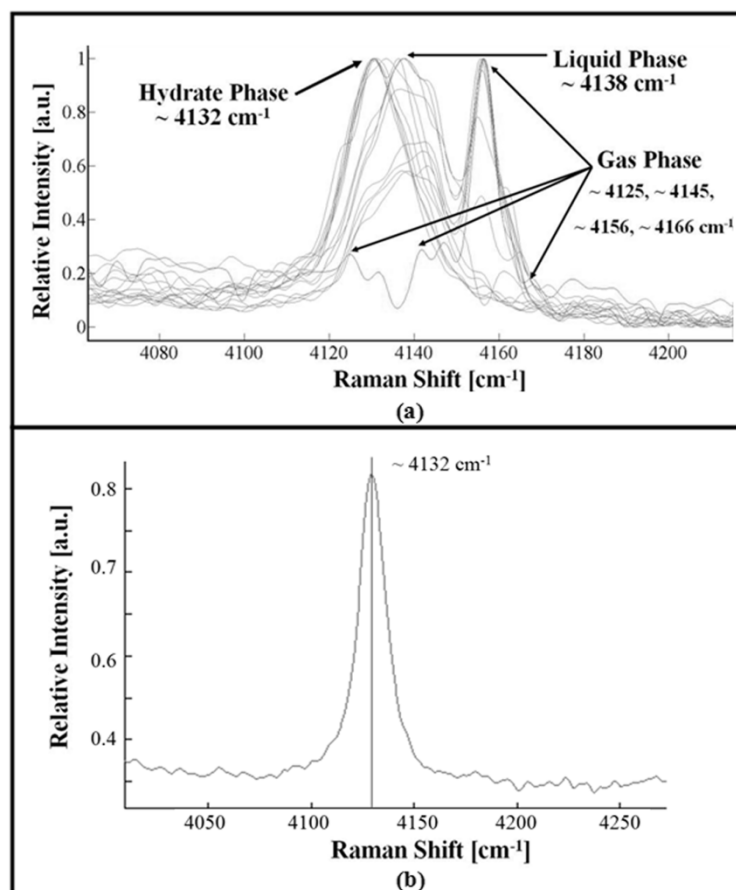


Figure 5.7. Raman relative intensity of the H-H stretching vibration peak (4100 - 4180 cm⁻¹ range) of a solution of 5.56 mol% THF in the different phases during hydrate formation.

After 22 h the system was heated and the sII H₂-THF clathrate hydrates started to dissociate. Figure 5.8 depicts the normalized time-resolved Raman spectra of the H-H vibration peak monitoring the dissociation of the hydrate phase. As can be observed around 23.5 h the vibration peak is shifted again from ~4132 cm⁻¹ to 4138 cm⁻¹, indicating that H₂ is transferred from the hydrate phase into the liquid phase, followed by the appearance of vibration peaks at 4156 cm⁻¹, indicating the desorption of H₂ from the liquid phase into the gas phase. It can be noticed that the H₂ desorption from the liquid phase into the gas phase is not complete; a certain amount of H₂ remains in

the liquid phase after the H_2 is released from the hydrate phase, due to dissolution.

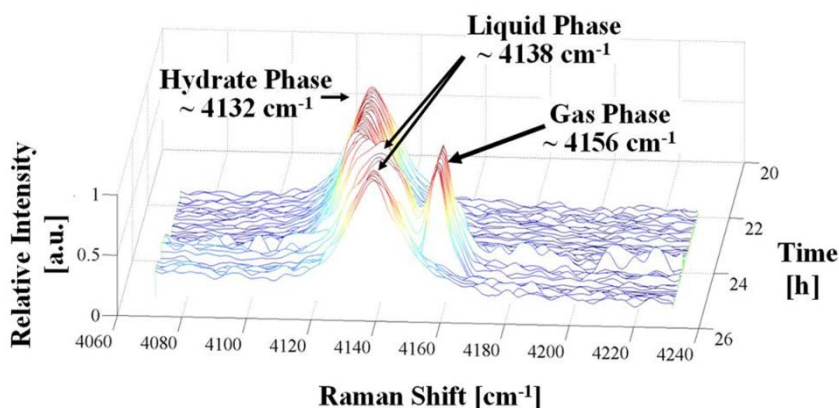


Figure 5.8. Time-resolved Raman spectra of the H-H vibration peak in a solution of 5.56 mol% of THF, during the dissociation of the hydrate phase at 13 MPa and 279.15 K.

5.4.5 H_2 -TBAB semi-hydrate Raman spectroscopic studies

The Raman spectra of an aqueous solution of 2.6 mol% of TBAB at ~13 MPa were recorded during the formation and dissociation of the hydrate phase. The formation was performed using the T-cycle method as described in paragraph 2.3 and the dissociation was performed at a constant heating rate of 0.13 K/min.

Figure 5.9 shows the time-resolved normalized Raman spectra at the surface (~1 mm under the liquid surface) monitoring the formation of the hydrate phase. The peaks were normalized with one of the peaks derived from the TBAB molecule. At the beginning of the experiment (time zero), three peaks located around 2700 – 3000 cm^{-1} indicate the presence of TBAB in the liquid phase [7]. The broad peaks around 3000-3600 cm^{-1} correspond to the O-H stretching vibration of the H_2O molecules [7]. Due to the low concentration of H_2 in the liquid phase, the signal corresponding to the H-H stretching vibration mode in the liquid phase (~4138 cm^{-1} [1]) is not detected. In Figure 5.9, the formation of the hydrate phase is detected by the appearance of a single peak located at ~4132 cm^{-1} corresponding to the H-H stretching

vibration in the hydrate phase, indicating the presence of H₂ hosted in the small cavities.

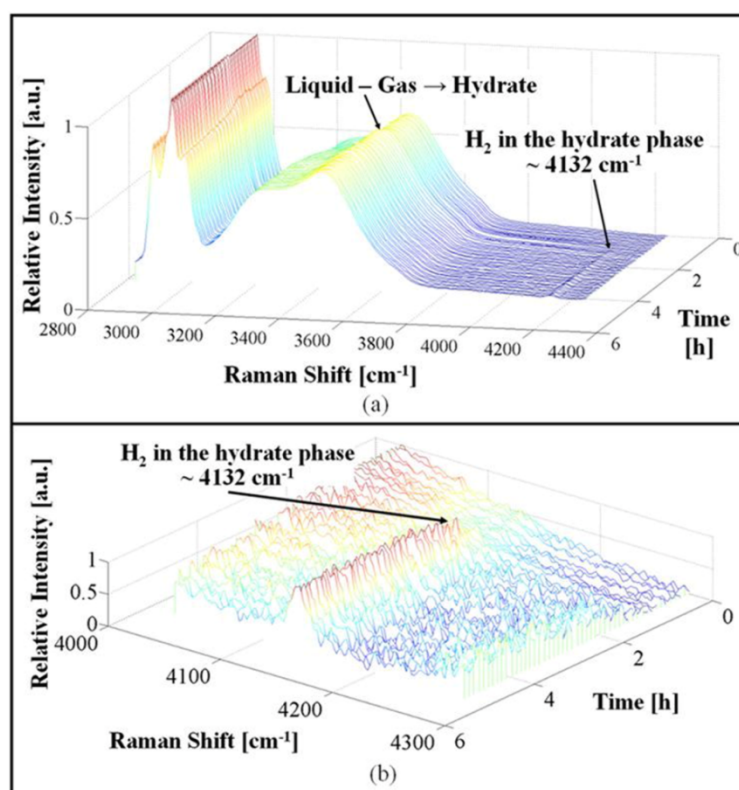


Figure 5.9. Time-resolved Raman spectra at the surface of a solution of 2.6 mol% of TBAB, monitoring the formation of the hydrate phase at ~13MPa and 281.15 K.

Figure 5.10 depicts the normalized time-resolved Raman spectra at the surface (~1 mm under the liquid surface) monitoring the dissociation of the hydrate phase. After ~11 h a sudden change in the peak positions and intensities takes place, indicating the hydrate dissociation. Before that transition, the Raman spectra indicate the presence of TBAB, H₂O and H₂ in the hydrate phase, while the hydrate phase is no longer present after ~11 h. A small single H₂ vibration peak at ~4138 cm⁻¹ remains after hydrate dissociation, corresponding to the H₂ dissolved in the liquid phase.

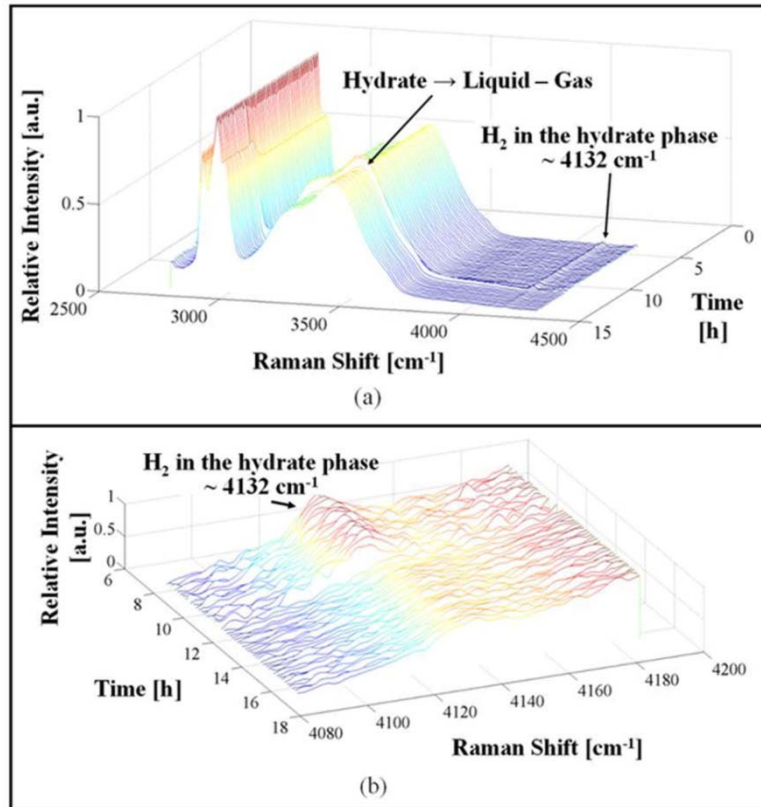


Figure 5.10. Time-resolved Raman spectra at the surface of a solution of 2.6 mol% of TBAB, monitoring the dissociation of the hydrate phase at ~ 13 MPa and 289.15 K.

The influence of H₂ mass transfer into the hydrate phase was studied by changing the position of the Raman probe. This probe was moved from the surface to the bottom of the sample, where the H₂ concentration was expected to be lower due to mass transfer limitations. Figure 5.11 depicts the normalized time-resolved Raman spectra monitoring the formation of the hydrate phase at the bottom of a liquid solution of 2.6 mol% of TBAB at ~ 13 MPa. From Figure 5.11 it is possible to identify the hydrate phase formation due to the shift to lower wavenumbers of the O-H bands in the hydrate phase [36 and due to the small increase of the band located at ~ 3230 cm⁻¹. Such change in shape is similar to the Raman spectra of sII clathrate hydrate [25]. Similarly, the hydrate dissociation is easily identified by the shift to higher wavenumbers of the O-H bands and due to the decrease of the band

located at $\sim 3230\text{ cm}^{-1}$. However, the H_2 vibration peaks were not detected in any of the phases of the experiment. This confirms that the H_2 molecules did not reach the bottom of the hydrate phase, even after 13 h. This observation explains the low amount of H_2 entrapped into the hydrate phase and highlights the importance of mass transfer limitations in the effective H_2 storage capacity of the hydrate phase.

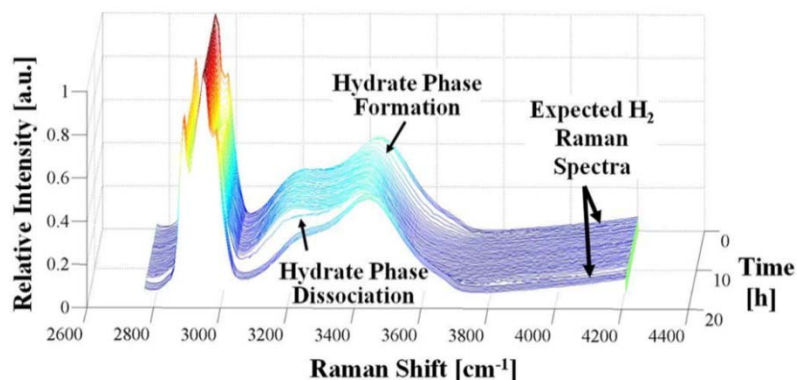


Figure 5.11. Time-resolved Raman spectra monitoring the formation and dissociation of the hydrate phase at the bottom of a liquid solution of 2.6 mol% of TBAB at $\sim 13\text{ MPa}$.

5.5 Conclusions

In this study the kinetics of formation of the H_2 -TBAB semi-hydrates was studied. The results indicate that the induction time, the rate of hydrate formation and amount of H_2 consumed are favored at higher pressures and higher solute concentrations. No influence of the formation method on the hydrate growth and amount of H_2 consumed was observed. Consequently, to develop TBAB semi-hydrate based technology for H_2 storage, higher TBAB concentrations and pressures should be used in order to enhance the H_2 storage capacity and the rate of formation.

The reliability of the experimental set up was confirmed by measuring the formation and dissociation of binary sII H_2 -THF clathrate hydrates and by comparison to literature. The apparatus was also used to measure the Raman

spectra of a solution of 2.6 mol% of TBAB during the formation and dissociation of the hydrate phase. The results confirmed the inclusion of H₂ in the hydrate phase over time and showed that the solubility of H₂ in the liquid phase was almost negligible. The influence of mass transfer limitations was studied by changing the probe position to the bottom of the sample, showing that H₂ molecules did not reach the bottom at all. Therefore, the maximum storage capacity was not reached. In order to reach optimal H₂ storage capacity, mass transfer limitations should be eliminated, this can be done by increasing the contact area by either the liquid and gas phases before hydrate phase formation or hydrate and gas phases after hydrate phase formation.

Acknowledgements

The authors gratefully acknowledge the financial support of the ACTS Sustainable Hydrogen Programme, Reg. Nr. H2 2007.

5.6 References

- [1] Hashimoto S., Murayama S., Sugahara T., Ohgaki K. Phase equilibria for H-2 plus CO2 plus tetrahydrofuran plus water mixtures containing gas hydrates. *Journal of Chemical Engineering Data*. 2006;51:1884-6.
- [2] Strobel T. A., Koh C. A., Sloan E. D. Hydrogen storage properties of clathrate hydrate materials. *Fluid Phase Equilibria*. 2007;261:382-9.
- [3] Shimada W., Ebinuma T., Oyama H., Kamata Y., Takeya S., Uchida T., et al. Separation of gas molecule using tetra-n-butyl ammonium bromide semi-clathrate hydrate crystals. *Journal of Applied Physics Part 2 - Letters*. 2003;42:L129-L31.
- [4] Strobel T. A., Hester K. C., Koh C. A., Sum A. K., Sloan E. D. Properties of the clathrates of hydrogen and developments in their applicability for hydrogen storage. *Chemical Physics Letters*. 2009;478:97-109.

- [5] Chapoy A., Anderson R., Tohidi B. Low-pressure molecular hydrogen storage in semi-clathrate hydrates of quaternary ammonium compounds. *Journal of the American Chemical Society*. 2007;129:746-7.
- [6] Arjmandi M., Chapoy A., Tohidi B. Equilibrium Data of Hydrogen, Methane, Nitrogen, Carbon Dioxide, and Natural Gas in Semi-Clathrate Hydrates of Tetrabutyl Ammonium Bromide. *Journal of Chemical & Engineering Data*. 2007;52:2153-8.
- [7] Hashimoto S., Sugahara T., Moritoki M., Sato H., Ohgaki K. Thermodynamic stability of hydrogen plus tetra-n-butyl ammonium bromide mixed gas hydrate in nonstoichiometric aqueous solutions. *Chemical Engineering Science*. 2008;63:1092-7.
- [8] Ohgaki K., Makihara Y., Takano K. Formation of CO₂ hydrate in pure and sea waters. *Journal of Chemical Engineering of Japan* 1993;26:558-64.
- [9] Aladko L. S., Dyadin Y. A., Rodionova T. V., Terekhova I. S. Clathrate hydrates of tetrabutylammonium and tetraisoamylammonium halides. *Journal of Structural Chemistry*. 2002;43:990-4.
- [10] Oyama H., Shimada W., Ebinuma T., Kamata Y., Takeya S., Uchida T., et al. Phase diagram, latent heat, and specific heat of TBAB semiclathrate hydrate crystals. *Fluid Phase Equilibria*. 2005;234:131-5.
- [11] Oshima M., Shimada W., Hashimoto S., Tani A., Ohgaki K. Memory effect on semi-clathrate hydrate formation: A case study of tetragonal tetra-n-butyl ammonium bromide hydrate. *Chemical Engineering Science*. 2010;65:5442-6.
- [12] Natarajan V., Bishnoi P. R., Kalogerakis N. Induction phenomena in gas hydrate nucleation *Chemical Engineering Science*. 1994;49:2075-87.
- [13] Sloan E. D., Koh C. A. *Clathrate Hydrates of Natural Gases*. 3rd ed. Florida: CRC Press; 2008.
- [14] Sabil K. M., Duarte A. R. C., Zevenbergen J., Ahmad M. M., Yusup S., Omar A. A., et al. Kinetic of formation for single carbon dioxide and mixed carbon dioxide and tetrahydrofuran hydrates in water and sodium chloride aqueous solution. *International Journal of Greenhouse Gas Control*. 2010;4:798-805.

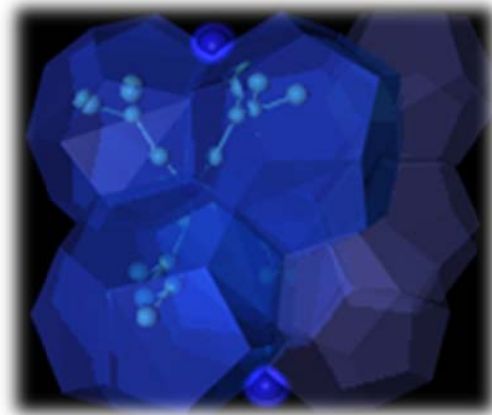
- [15] Englezos P., Kalogerakis N., Dholabhai P. D., Bishnoi P. R. Kinetics of gas hydrate formation from mixtures of methane and ethane. *Chemical Engineering Science*. 1987;42:2659-66.
- [16] Giavarini C., Maccioni F., Santarelli M. L. Formation kinetics of propane hydrates. *Industrial & Engineering Chemistry Research*. 2003;42:1517-21.
- [17] Nagai Y., Yoshioka H., Ota M., Sato Y., Inomata H., Smith R. L. Binary Hydrogen-Tetrahydrofuran Clathrate Hydrate Formation Kinetics and Models. *AIChE Journal*. 2008;54:3007-16.
- [18] He Y. Y., Rudolph E. S. J., Zitha P. L. J., Golombok M. Kinetics of CO₂ and methane hydrate formation: An experimental analysis in the bulk phase. *Fuel*. 2011;90:272-9.
- [19] Ohmura R., Ogawa M., Yasuoka K., Mori Y. H. Statistical study of clathrate-hydrate nucleation in a water/hydrochlorofluorocarbon system: Search for the nature of the "memory effect". *Journal of Physical Chemistry B*. 2003;107:5289-93.
- [20] Peng D., Robinson D. B. New 2-Constant Equation of State. *Industrial and Engineering Chemistry Fundamentals*. 1976;15:59-64.
- [21] Lokshin K. A., Zhao Y. S. Fast synthesis method and phase diagram of hydrogen clathrate hydrate. *Applied Physics Letters*. 2006;88:131909-3.
- [22] Talyzin A. Feasibility of H₂-THF-H₂O clathrate hydrates for hydrogen storage applications. *International Journal of Hydrogen Energy*. 2008;33:111-5.
- [23] Ziparo C., Giannasi A., Ulivi L., Zoppi M. Raman spectroscopy study of molecular hydrogen solubility in water at high pressure. *International Journal of Hydrogen Energy*. 2011;36:7951-5.
- [24] Florusse L. J., Peters C. J., Schoonman J., Hester K. C., Koh C. A., Dec S. F., et al. Stable low-pressure hydrogen clusters stored in a binary clathrate hydrate. *Science*. 2004;306:469-71.
- [25] Schicks J. M., Erzinger J., Ziemann M. A. Raman spectra of gas hydrates differences and analogies to ice 1h and (gas saturated) water. *Spectrochimica Acta Part A: Molecular and Biomolecular Spectroscopy*. 2005;61:2399-403.

Chapter 6

Kinetic Measurements and

In situ Raman

Spectroscopy Study of the
Formation of TBAF Semi-
Hydrates with Hydrogen
and Carbon Dioxide



6.1 Introduction

In the present chapter the kinetics of semi-clathrate hydrates of tetra n-butyl ammonium fluoride (TBAF) with hydrogen (H_2) and carbon dioxide (CO_2) were studied in order to elucidate their potential for H_2 storage as well as for CO_2 sequestration. Section 6.2 provides a general background of the study. Section 6.3 presents the materials used and a brief description of the methodology. Sections 6.4.1-2 presents the results and respective discussions on induction time, rate of formation and amount of H_2 and CO_2 stored. Sections 6.4.3-4 provide the results of Raman spectroscopic measurements of hydrate formation together with the respective discussion. Finally section 6.5 presents the conclusions of the study. The present chapter is a modified version of the article published in International Journal of Hydrogen Energy, volume 38, issue 18, page 7326.

6.2 Background

Several studies have been conducted in order determine the hydrate phase equilibrium of tetra n-butyl ammonium salts (TBAF, tetra n-butyl ammonium bromide (TBAB) and tetra n-butyl ammonium chloride (TBAC)) with CO_2 [1-4] and H_2 [5-10]. Only few attempts have been made to study their potential for CO_2 sequestration or H_2 storage [10-13]. However, most of these studies are focused on TBAB semi-hydrates. To the best of our knowledge, kinetic studies of H_2 -TBAF semi-hydrates are entirely absent. Nevertheless, phase equilibrium measurements have shown that TBAF semi-hydrates are stable at higher temperatures than TBAB semi-hydrates [5] [6] [14] [10, 15]. Moreover, Fan *et al.* [14] reported that CO_2 -TBAF semi-hydrates showed higher rate of formation over conventional CO_2 clathrate hydrates and CO_2 -TBAB semi-hydrates.

Therefore, in this work, the potential of TBAF semi-hydrates for CCS and H_2 storage has been studied. Motivated by data scarcity, the kinetics of hydrate formation of the systems CO_2 -TBAF- H_2O and H_2 -TBAF- H_2O

were measured to determine the effect of TBAF concentration in the aqueous solution, pressure and formation method on the hydrate nucleation, hydrate growth and gas storage capacity. Coupled with the kinetic results, the Raman spectra studying the structural changes that take place during the formation and dissociation of the H₂-TBAF and CO₂-TBAF semi-hydrates were recorded *in situ* by Raman spectroscopy.

6.3 Methodology

6.3.1 Materials

CO₂ and H₂ were both purchased from Air Liquid. The purity of H₂ and CO₂ was 99.999 mol%. TBAF hydrate was purchased from Sigma-Aldrich with a purity of 98%. The water content of TBAF hydrate (~16.6 wt %) was obtained by using Karl Fisher method. This water content of the TBAF hydrate was taken into account during the preparation of the liquid solutions at the specified concentration. The chemicals were used without any further purification. Double distilled and deionized Millipore quality water was used.

6.3.2 Experimental apparatus and procedure

The experimental apparatus and procedure have been previously described in Chapter 3. However, in this particular case two concentrations of TBAF in the aqueous solution were studied i.e., 3.4 mol% and 1.8 mol%. The former corresponds to the stoichiometric concentration of the cubic structure of TBAF hydrate with hydration number 28.6 [16]. The second concentration is lower than the stoichiometric concentration (3.0 mol%) of the tetragonal structure of TBAF hydrate with hydration number 32.3. This concentration was selected in order to study the structural transition observed by Sakamoto *et al.* [10] in the H₂-TBAF semi-hydrates. For comparison purposes the same concentrations were selected to study the formation of the CO₂-TBAF semi-hydrates.

For the system H₂-H₂O-TBAF, the initial temperature (T_1) was 306.15 K and the final temperature (T_2) was 294.15 K. Both temperatures were chosen taking into account the hydrate phase equilibrium temperatures of the system at the concentrations tested [10]. For the system CO₂-H₂O-TBAF, T_1 was 303.15 K and T_2 was either 293.15 K or 295.15 K. Due to scarcity of phase equilibrium data of the system CO₂-H₂O-TBAF at the concentrations tested, these temperature conditions were chosen on basis of the hydrate phase equilibrium data of the system CO₂-H₂O-TBAB at similar concentrations [15]. The T-constant method was only applied for the system H₂-H₂O-TBAF. In that case, the temperature was first stabilized at T_2 (294.15 K) and then the high pressure vessel was pressurized with H₂. For the T-cycle method a cooling rate of 0.1 K/min was used for both systems, H₂-H₂O-TBAF and CO₂-H₂O-TBAB. All the experiments were repeated three times for each pressure, temperature and concentration condition.

6.4 Results and discussion

6.4.1 Induction time

The induction time was calculated as in our previous study [17]; this is the time elapsed from the moment the gaseous component is introduced in the system until the so-called turbidity point was reached. Table 6.1 and 6.2 display the experimental conditions for semi-hydrate formation of the systems H₂-H₂O-TBAF and CO₂-H₂O-TBAF, respectively. The induction times for both systems were obtained by the T-cycle method. Figure 6.1 and 6.2 display the induction time for the systems H₂-H₂O-TBAF and CO₂-H₂O-TBAF, respectively, where the variations (standard deviations) in measured induction times are shown as error bars.

From Figure 6.1 it can be noticed that the TBAF concentration and pressure play an important role in the induction time of the system H₂-H₂O-TBAF. At isobaric conditions for a simple hydrate the driving force depends on the difference between the operation temperature and the equilibrium temperature (T_{Eq}) also known as subcooling (ΔT_{Sub}) [18]. The influence of

pressure on the induction time was strong at low TBAF concentrations, where higher pressures resulted in shorter induction times and a less stochastic nature. This is because the equilibrium temperature is higher at higher pressures increasing the subcooling and consequently the driving force. Table 6.1 shows the increase in subcooling at higher pressures for the system H₂-H₂O-TBAF at the concentrations studied. Similarly, the highest TBAF concentration shows shortest induction time and less stochastic behavior. This is because the equilibrium curve at high concentration presents higher equilibrium temperatures therefore the subcooling (or driving force) is higher. Moreover, at high TBAF concentrations the influence of pressure was not significant. This might be because at these conditions concentration is the main driving force. These results are in agreement with similar reports of other hydrate systems [18-20].

Table 6.1. Experimental conditions of the system H₂-H₂O-TBAF

H ₂ -H ₂ O-TBAF			
TBAF		Temperature	
Concentration [mol%]	Initial Pressure [MPa]	Difference $\Delta T = T_2 - T_1$ [K]	Subcooling $\Delta T_{\text{Sub}} = T_{\text{Eq}}^{\text{a}} - T_1$
1.8	5.0	12.0	4.6
1.8	7.5	12.0	5.0
1.8	10.0	12.0	5.3
1.8	13.0	12.0	5.7
3.4	5.0	12.0	7.0
3.4	7.5	12.0	7.1
3.4	10.0	12.0	7.3
3.4	13.0	12.0	7.5

^a T_{Eq}, Equilibrium temperature taken from Sakamoto *et al.* [10]

Table 6.2. Experimental conditions of the system CO₂- H₂O-TBAF

CO ₂ - H ₂ O-TBAF		
TBAF Concentration [mol%]	Initial Pressure [MPa]	Temperature Difference $\Delta T = T_2 - T_1$ [K]
1.8	1.6	10.0
1.8	1.8	10.0
1.8	2.3	10.0
1.8	2.6	10.0
1.8	1.6	8.0
1.8	1.8	8.0
1.8	2.1	8.0
3.4	1.6	10.0
3.4	2.0	10.0
3.4	2.3	10.0

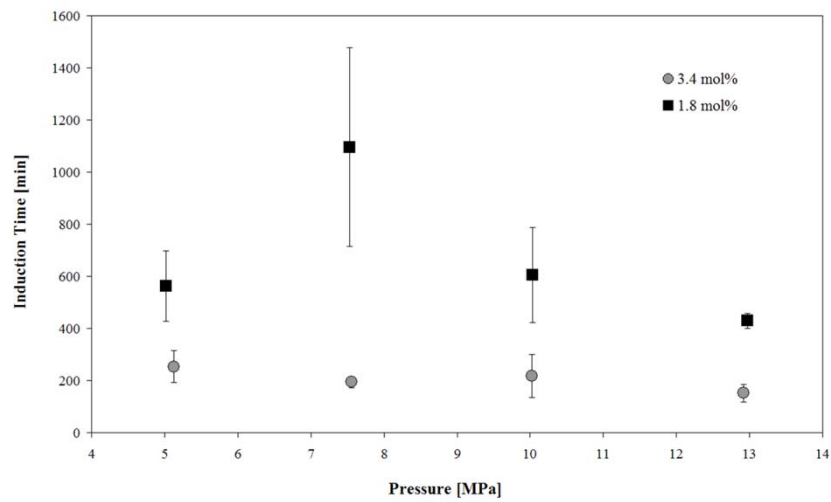


Figure 6.1. Influence of pressure and solution concentration on the induction time of the H₂-TBAF semi-hydrate.

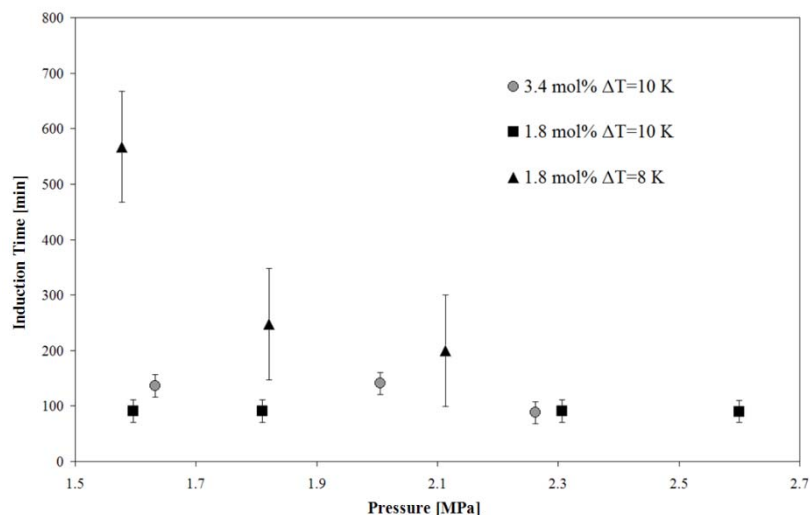


Figure 6.2. Influence of pressure, solution concentration and temperature on the induction time of the CO₂-TBAF semi-hydrate.

On the other hand, from Figure 6.2 it can be observed that the system CO₂-H₂O-TBAF displayed shorter induction times that were independent of the TBAF concentration and pressure. However, strong dependence of the induction time on the semi-hydrate formation temperature or operation temperature (T_2) was found, where lower operation temperatures displayed shorter induction times and less stochastic nature. The reason is also the increase in subcooling due to the lower operation temperature. Unfortunately, due to the lack of equilibrium data the subcooling of the system CO₂-H₂O-TBAF at the concentrations studied is not reported.

There is a significant difference between the induction times of the systems H₂-H₂O-TBAF and CO₂-H₂O-TBAF, which can be explained by the difference of subcooling between both systems. CO₂ hydrates are stable at higher temperatures and lower pressures than H₂ hydrates. Therefore the subcooling is higher for the CO₂ system for both concentrations. For instance, the system H₂-H₂O-TBAF displayed induction times between 150 and 250 min in a pressure range of 5.0-13.0 MPa, while the system CO₂-H₂O-TBAF displayed induction times between 90 and 150 min in a pressure range of 1.6-2.3 MPa, at the same TBAF concentration conditions (3.4

mol%) and similar temperature (294.15 K for H₂ and 293.13 K for CO₂). Another factor that might influence the difference between the induction times for both systems is the solubility of the gas guest. The solubility of CO₂ is higher in aqueous solutions therefore the supersaturation of CO₂ in the liquid phase might be reached faster than the supersaturation of H₂.

6.4.2 Rate of formation and total amount of guest gas consumed

The number of moles of gas consumed was calculated as in our previous study. Figure 6.3 depicts the influences of pressure and TBAF concentration on the H₂-TBAF semi-hydrate formation rate obtained by the T-cycle and T-constant method. It can be noticed that an increase in pressure and/or TBAF concentration results in an increase of the formation rate. Thus, the formation rate is proportional to the driving force (supersaturation) [18], as it was explained previously the driving force rises with increasing H₂ pressure and TBAF concentration. Figure 6.3 also shows that the formation method does not have a strong influence on the formation rate.

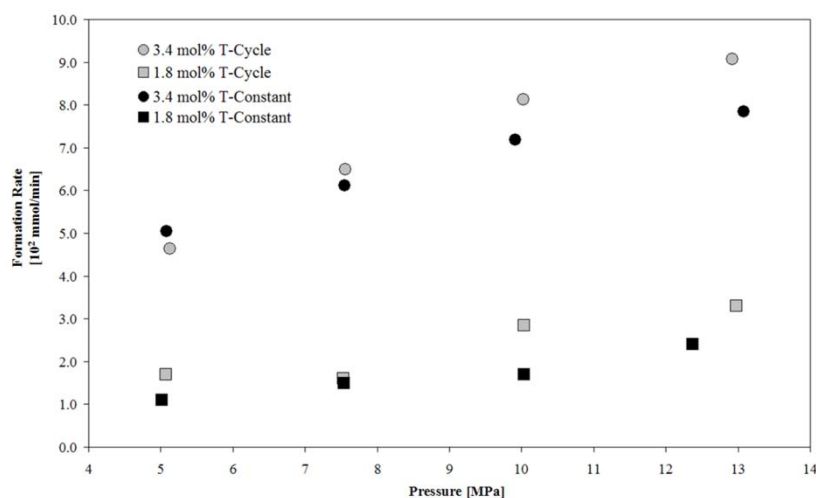


Figure 6.3. Influence of pressure and solution concentration on the H₂-TBAF semi-hydrate formation rate.

Figure 6.4 shows the influence of pressure and TBAF concentration on the CO₂-TBAF semi-hydrate formation rate obtained by the T-cycle method. It can be observed that the TBAF concentration and formation temperature do not display a significant influence on the formation rate of CO₂-TBAF semi-hydrate. However, the pressure seems to have a major influence, mainly above 2.3 MPa. This might be because the supersaturation of CO₂ is increased at higher pressures.

Figure 6.5 displays the amount of H₂ entrapped in the hydrate phase at different pressures and at two different TBAF concentrations (3.4 mol% and 1.8 mol%) using the T-cycle method. The amount of H₂ consumed was calculated only considering the change in the amount of the gas phase from the turbidity point to the stationary point. The change in the amount of gas phase from the beginning of the experiment to the turbidity point (due to dissolution of guest gas in the liquid phase) was not taken into account. Dissolution of gas in the liquid phase after reaching the turbidity point is considered to be negligible, because the hydrate formation occurs much faster than dissolution. Therefore, we have assumed that the amount of gas dissolved in this time is negligible and does not have a significant effect on the gas uptake experiments.

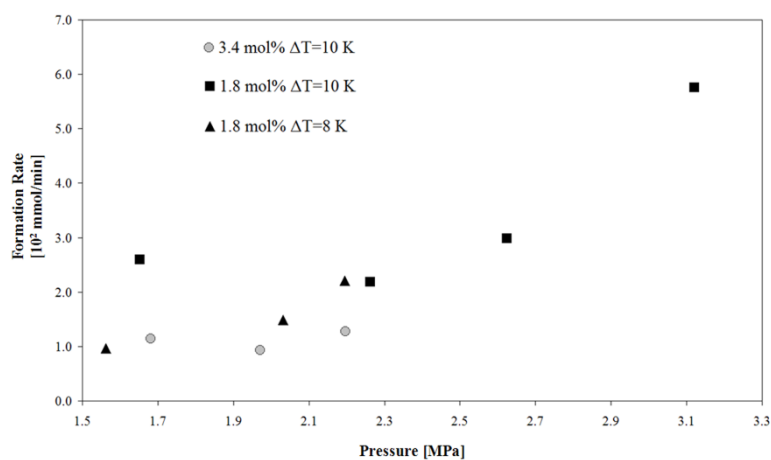


Figure 6.4. Influence of pressure, solution concentration and temperature on the CO₂-TBAF semi-hydrate formation rate.

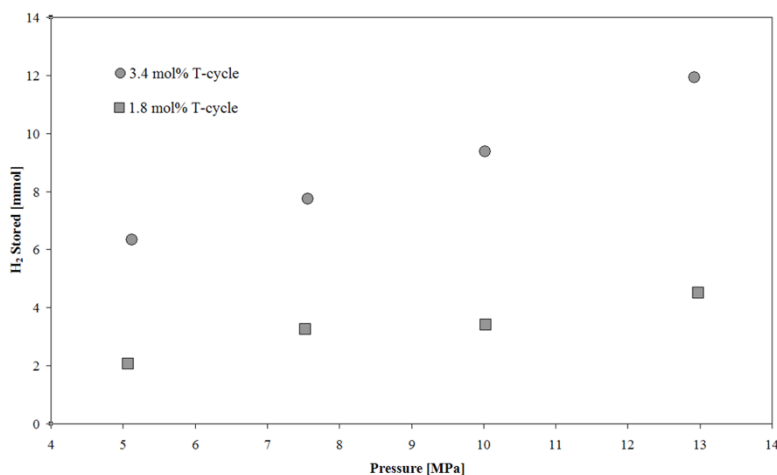


Figure 6.5. Amount of H₂ entrapped in the hydrate phase at different pressures and two solute concentrations of TBAF.

From Figure 6.5 it can be noticed that a higher pressure resulted in an increasing amount of H₂ consumed. Furthermore, the highest TBAF concentration (3.4 mol% of TBAF) showed the highest amount of H₂ stored i.e., 12.0 mmol (0.024 wt%) at 13.0 MPa compared to 4.5 mmol for the lower TBAF concentration (1.8 mol% of TBAF) at the same pressure and temperature conditions.

Previous studies performed on TBAF semi-hydrates report that two unit cell structures are possible: the cubic structure I (C_{ss}-I) and the tetragonal structure I (T_s-I). The C_{ss}-I consists of 344 H₂O molecules forming 16 pentagonal dodecahedrons (5¹²) and 12 large cavities (T₄). These large cavities are composed by four T-type (5¹²6²) cavities hydrogen-bonded together with a hollow center to host the TBA⁺ cation while the F⁻ anion replaces a water molecule in the hydrate lattice [10, 21, 22]. T_s-I is composed by 172 H₂O molecules forming 10 pentagonal dodecahedrons (5¹²) and five large cavities. Four of the large cavities are composed by 3 T-type (5¹²6²) cavities and 1 P-type cavity (5¹²6³) and one large cavity is composed by 4 T-type (5¹²6²) cavities [16, 21, 23]. Under the conditions tested in the present study the stable structure is C_{ss}-I at the high TBAF concentration, which is also the stoichiometric concentration (3.4 mol%). At the low TBAF

concentration (1.8 mol %) and high pressures (>10 MPa), Sakamoto *et al.* [10] reported that a structural transition from C_{ss}-I to T_s-I of the H₂-TBAF semi-hydrate phase may take place. The T_s-I has higher potential for H₂ storage due to the larger number of small cavities relative to the large ones. The maximum theoretical gas storage capacity as a function of the small cavity occupancy at stoichiometric concentrations (each large cavity is filled by one TBA cation) of the C_{ss}-I and T_s-I is: 0.34 wt% for H₂ and 6.97 wt% for CO₂ and 0.45 wt% for H₂ and 9.02 wt% for CO₂ respectively. Figure 5 shows that the highest concentration of TBAF presents the highest amount of H₂ consumed (0.024 wt%), indicating that T_s-I has not been formed at low TBAF concentrations. Therefore, we assume that the C_{ss}-I structure was mainly present at all the experimental conditions used in this study, also at the low TBAF concentrations. The highest storage capacity at highest TBAF concentrations can then be explained by the higher H₂ supersaturation at high TBAF concentration. It is important to notice that under the current experimental conditions only ~7.0 % of the maximum theoretical gas storage capacity was achieved. This might be as a result of mass transfer limitations. Finally, it was observed that the formation method did not have a significant influence on the amount of H₂ consumed.

Figure 6.6 displays the amount of CO₂ entrapped in the hydrate phase at different pressures and TBAF concentrations (3.4 mol% and 1.8 mol% of TBAF) by the T-cycle method. The total amount of CO₂ consumed was calculated as described for H₂ before. From Figure 6.6 it can be noticed that a higher pressure results in an increasing amount of CO₂ consumed. However, above 2.6 MPa the amount of CO₂ stored remained stable and did not increase any further. At this pressure the maximum CO₂ storage capacity was reached. The TBAF concentration does not have a significant influence on the amount of CO₂ consumed. However, the temperature showed the largest influence on the CO₂ storage capacity, where lower temperatures increased the CO₂ consumption by the hydrate phase. The results are in accordance with previous reports [14]. It was calculated that the CO₂ content in the CO₂-TBAF semi-hydrate formed at the low concentration of TBAF (1.8 mol%) and at 2.6 MPa and 293.15 K was 0.45 wt%, this amount is only

~6.5% of the maximum theoretical storage capacity. Therefore as in the case of H₂ mass transfer might play a major influence in the amount of gas uptake.

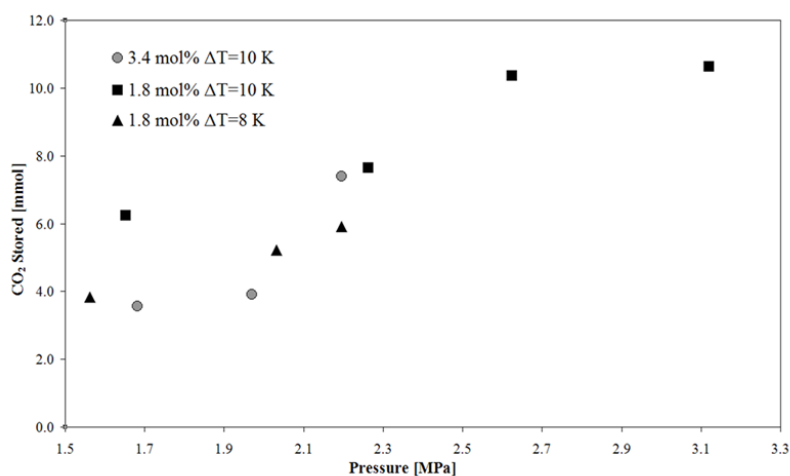


Figure 6.6. Amount of CO₂ entrapped in the hydrate phase at different pressures, temperatures and two solute concentrations of TBAF.

6.4.3 H₂-TBAF semi-hydrate Raman spectroscopic studies

Figure 6.7 depicts the H₂ Raman spectra in the gas, liquid and hydrate phases. The spectra in the liquid and hydrate phases were obtained from an initial solution of 1.8 mol% of TBAF. The peaks were normalized with one of the peaks derived from the TBAF molecule. Three peaks corresponding to the H-H stretching vibration mode in the gas phase are observed at ~4125, ~4145 and ~4156 cm⁻¹, one peak at ~4166 cm⁻¹ overlaps with the peak at ~4156 cm⁻¹. It is important to mention that under the temperature conditions ortho hydrogen is the dominant isomer in a proportion 3:1. Raman spectra of gaseous H₂ displays four frequencies of vibrational transition Q₁(0), Q₁(1), Q₁(2) and Q₁(3). The intensity of the peak Q₁(1) is dominated by the ortho-para ratio. The H-H stretching vibration mode in the liquid phase was observed at ~4138 cm⁻¹ and the H-H stretching vibration in the hydrate phase was located at ~4132 cm⁻¹, indicating the presence of H₂ hosted in the small cavities (pentagonal dodecahedron) [24]. Both peaks correspond to the

$Q_1(1)$ vibrational transition. It should be noticed that the signal of H_2 in the liquid phase was easily identified. In our previous study [17], the signal of H_2 in the system H_2 -TBAB- H_2O (2.6 mol% of TBAB) at 13 MPa was not detected before hydrate phase formation. Therefore, it can be concluded that the solubility of H_2 in the liquid solution of H_2O -TBAF is higher than in the solution of H_2O -TBAB. Also TBAF semi-hydrate presented a higher amount of H_2 than TBAB semi-hydrate. For example, the amount of H_2 stored in the H_2 -TBAB semi-hydrate was ~8.0 mmol at a TBAB concentration of 3.7 mol% and 13.0 MPa [17], while this work shows that ~12.0 mmol of H_2 can be stored in the H_2 -TBAF semi-hydrate at a TBAF concentration of 3.4 mol% at 13.0 MPa. Although H_2 -TBAB semi-hydrate has more small cavities available to be occupied by H_2 , H_2 -TBAF seems to be kinetically favored due to the higher solubility of H_2 in the TBAF semi-hydrate.

Figures 6.8 and 6.9 show the Raman peaks derived from the TBAF molecule in the liquid and hydrate phases at the low and high Raman shifts, respectively. The spectra were recorded at ~13 MPa and 294.15 K. At the low Raman shift the TBAF peaks are detected around 700 – 1500 cm^{-1} , while at the high Raman shift the TBAF peaks are detected around 2700 – 3100 cm^{-1} . The wide broad peak of O-H vibration of water is located next to the TBAF peak in the high Raman shift around 3100 – 3700 cm^{-1} . It can be observed in Figures 6.8 and 6.9 that there are no significant changes in the Raman spectra at the two concentrations. The main differences are detected in the region located around 1120 and 1194 cm^{-1} at the low Raman shift and in the peak located at 2989 cm^{-1} in the high Raman shift. The CH_m ($m=2,3$) stretching bands appear in the region between 2963-2875, the CH_m deformation bands in the region between 1486-1376 while the CH_m waggings and rockings, CH_2 twistings and CC stretchings are displayed in region between 1347-750 cm^{-1} . Sakamoto *et al.* [10] suggested that the little change in the spectra at both TBAF concentrations is due to the minor change in the cage size that entraps the TBA molecule as a function of concentration.

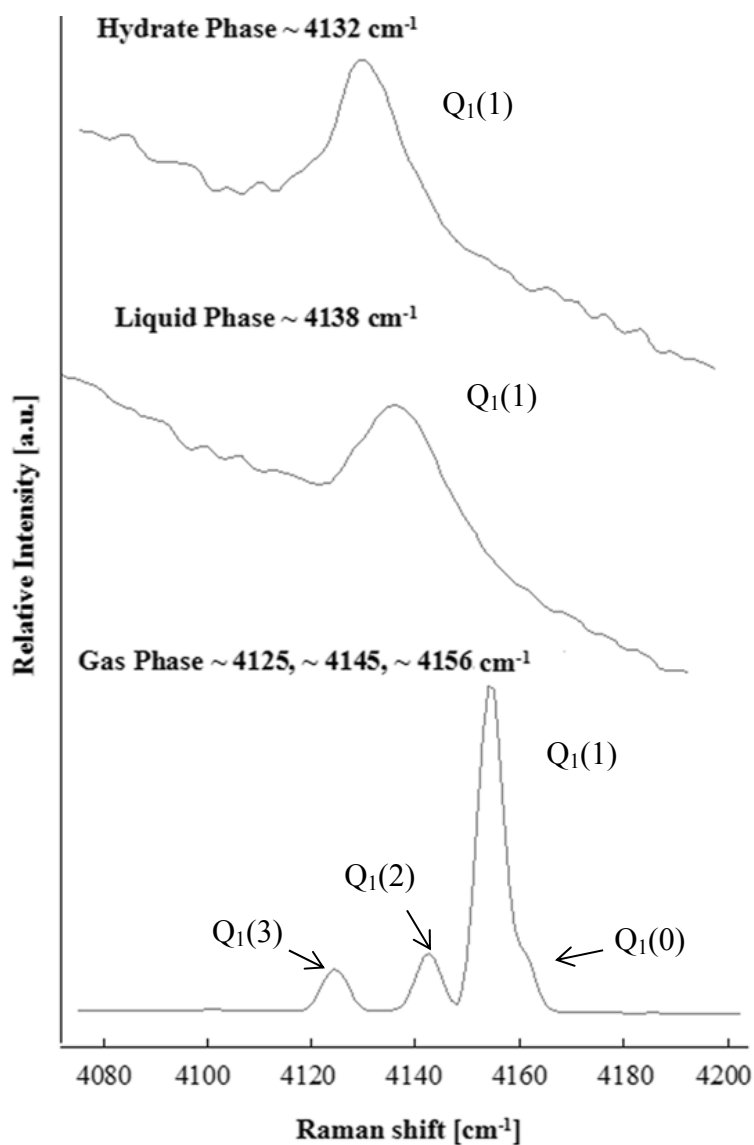


Figure 6.7. H₂ Raman spectra in the gas, liquid and hydrate phases obtained from an initial solution of 1.8 mol% of TBAF at 5 MPa and 293.15 K.

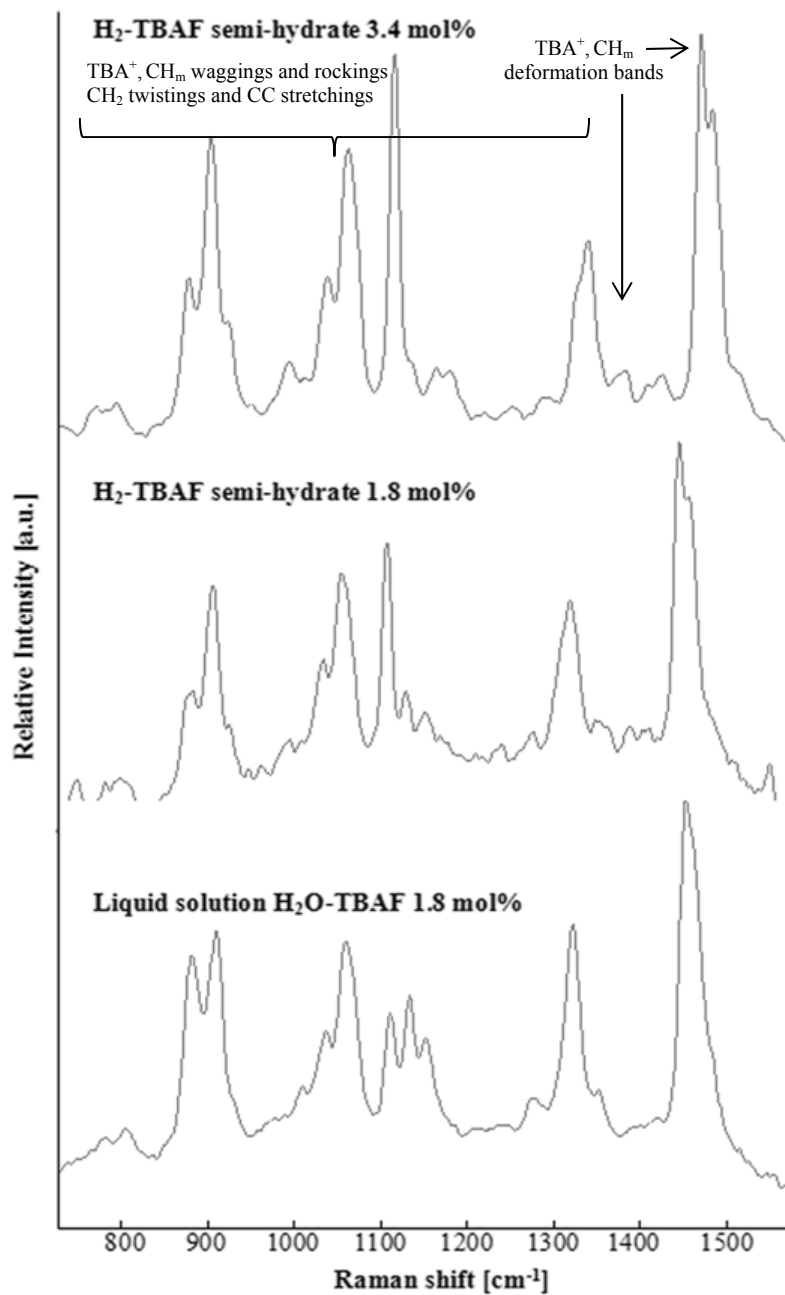


Figure 6.8. The Raman peaks derived from the TBAF molecule in the liquid and hydrate phases at the low Raman shift.

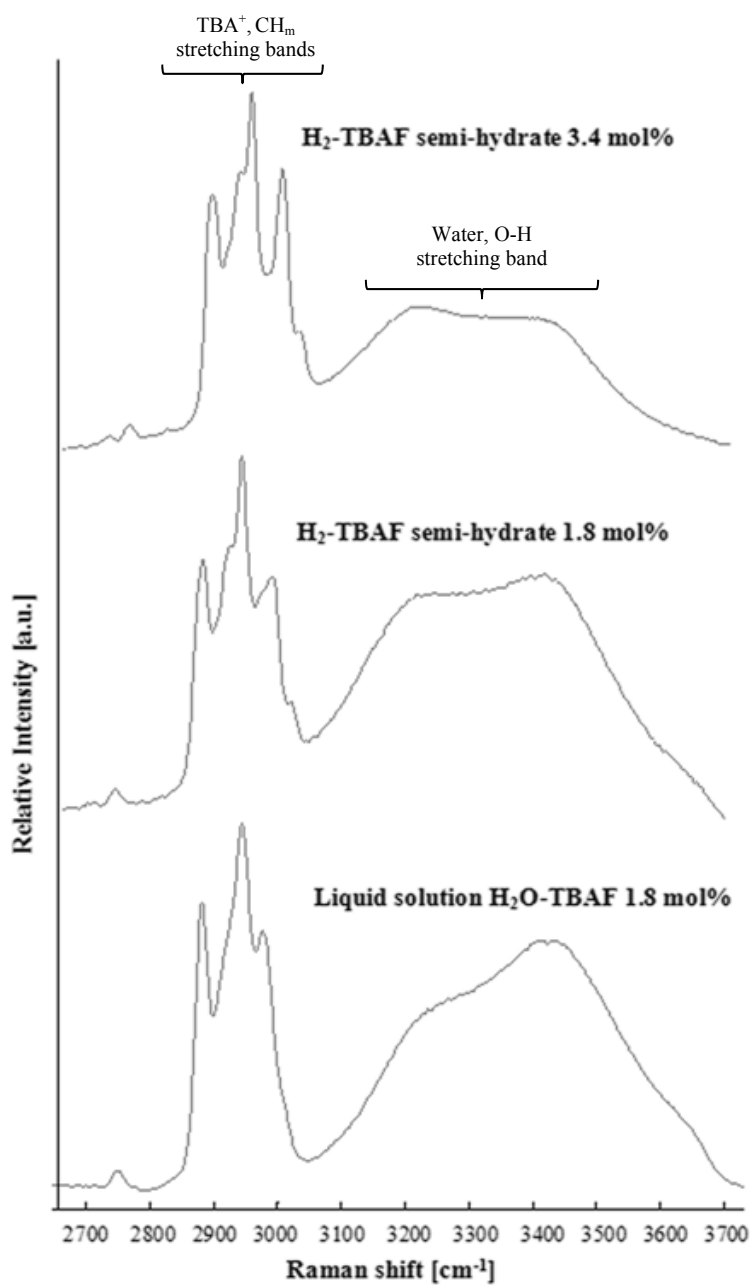


Figure 6.9. The Raman peaks derived from the TBAF molecule in the liquid and hydrate phases at the high Raman shift.

6.4.4 CO₂-TBAF semi-hydrate Raman spectroscopic studies

The Raman spectra of the CO₂-TBAF semi-hydrate at two concentrations of TBAF (1.8 and 3.4 mol%) are depicted in Figure 6.10. The peaks were normalized with one of the peaks derived from the TBAF molecule. The spectra were recorded at ~5 MPa and 293.15 K. CO₂ in the hydrate phase typically displays two peaks at 1277 and 1381 cm⁻¹ [25, 26]. However, in Figure 6.10 only the peak at 1381 cm⁻¹ can be clearly identified, while the peak at 1277 cm⁻¹ overlaps with the signal of TBAF. Similar to the H₂-TBAF semi-hydrate, there is no significant change in the Raman spectra of CO₂-TBAF semi-hydrate upon a change in TBAF concentration.

Figure 6.11 displays the time-resolved normalized Raman spectra of a liquid solution of H₂O-TBAF (1.8 mol% of TBAF) at ~5 MPa during the formation of the CO₂-TBAF semi-hydrate. The formation was performed using the T-cycle method. The peaks were normalized with one of the peaks of the TBAF molecule. At the beginning of the experiment (time zero), only the peaks of TBAF in the liquid phase are observed. The CO₂ peak corresponding to CO₂ in the liquid phase (1382 cm⁻¹) [25] is detected few minutes after the beginning of the experiment due to the high solubility of CO₂ in the liquid phase. Around 150 min the hydrate phase formation takes place, because a shoulder is formed in the TBAF peak at ~1310 cm⁻¹. However, the peaks of TBAF and CO₂ in the liquid and hydrate phase are overlapping so that it is difficult to distinguish the structural transitions. After ~ 200 min the hydrate phase is completely formed, and the peak located at 1381 cm⁻¹ corresponding to CO₂ in the hydrate phase displays the highest intensity.

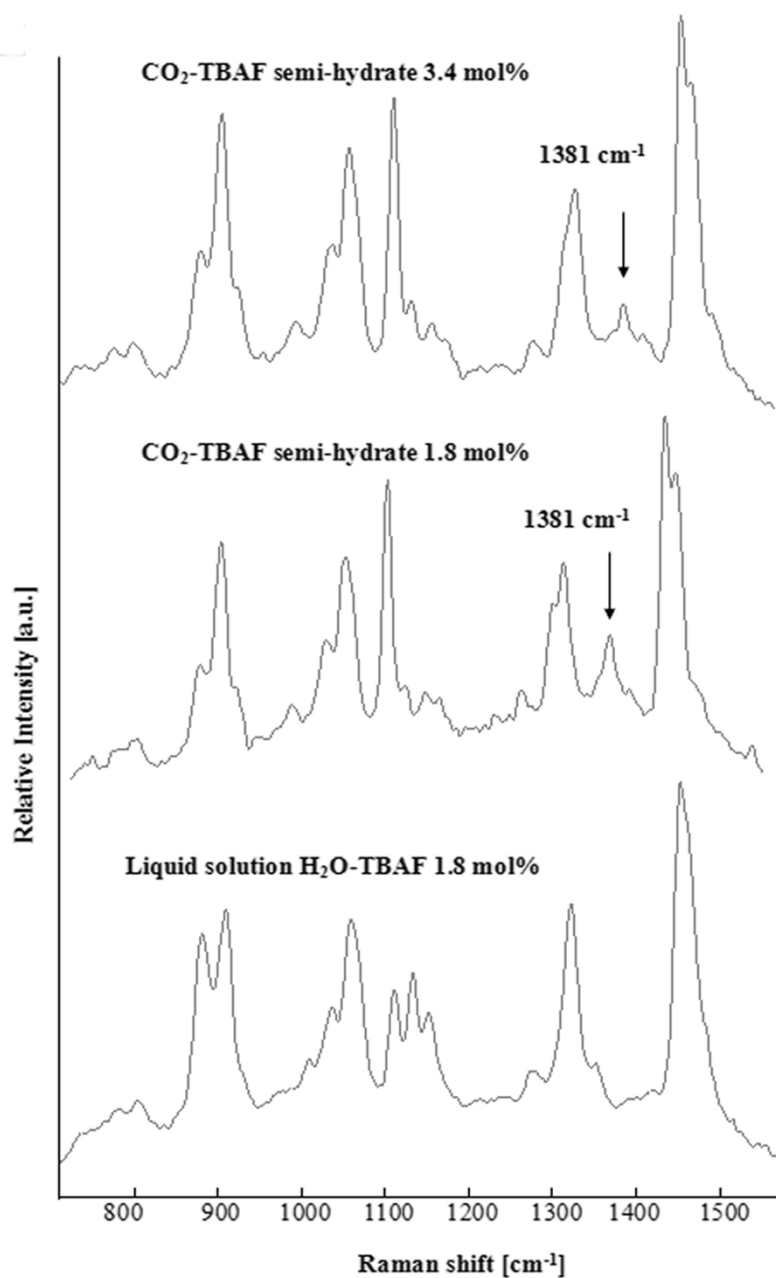


Figure 6.10. Raman spectra of CO₂-TBAF semi-hydrate at two concentrations of TBAF (1.8 and 3.4 mol%).

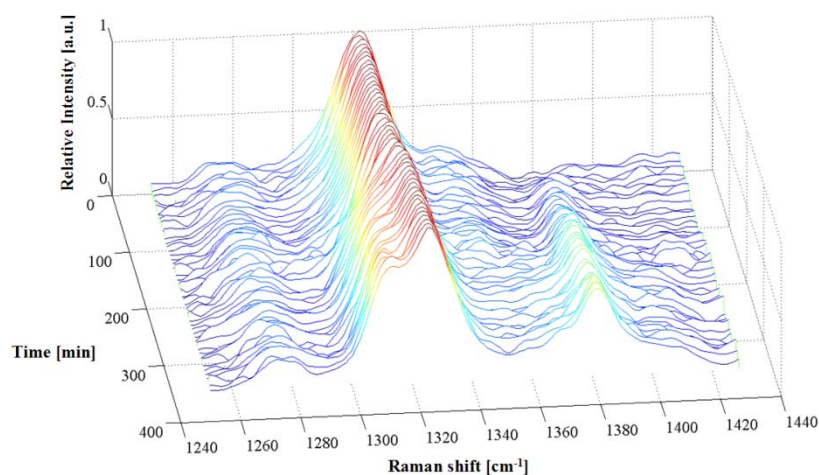


Figure 6.11. Time-resolved Raman spectra of a solution of 1.8 mol% of TBAF, monitoring the formation of the CO₂-TBAF semi-hydrate at ~5MPa and 293.15 K.

6.5 Conclusions

The kinetics of formation of H₂-TBAF and CO₂-TBAF semi-hydrates were studied. The induction time, the rate of hydrate formation and the amount of H₂ consumed during H₂-TBAF formation are favored at higher pressures and higher TBAF concentrations due to the increase in supersaturation, while for CO₂-TBAF semi-hydrates the TBAF concentration did not show a large influence and pressure only displayed a major influence on the formation rate. Instead, the induction time and the amount of CO₂ consumed were favored at low temperatures as a result of the increase in subcooling. No influence of the formation method on the hydrate growth and amount of H₂ consumed was observed.

The H₂-TBAF semi-hydrate formation was compared to the formation of H₂-TBAB semi-hydrates. H₂ presented a higher solubility in the liquid solution of H₂O-TBAF, which was confirmed by Raman spectroscopy. Due to the higher solubility of H₂ in the liquid solution, mass transfer and therefore kinetics are favored for the H₂-TBAF semi-hydrate.

Despite the fact that the H₂ content in H₂-TBAF semi-hydrates is too low to be feasible as H₂ storage materials, the results indicate that CO₂-TBAF semi-hydrates have the potential to be applied in novel separation technologies e.g., for the purification of flue gases (CO₂ removal). CO₂-TBAF semi-hydrate formation displays short induction times, high formation rates and at low pressures the CO₂ content in the hydrate phase is considerable higher than the H₂ content. Further research will be performed on mixtures of CO₂/H₂ using TBAF semi-hydrates in order to elucidate their potential as a separation technology.

6.6 References

- [1] Li X. S., Xia Z. M., Chen Z. Y., Wu H. J. Precombustion Capture of Carbon Dioxide and Hydrogen with a One-Stage Hydrate/Membrane Process in the Presence of Tetra-n-butylammonium Bromide (TBAB). *Energy Fuels*. 2011;25:1302-9.
- [2] Duc N. H., Chauvy F., Herri J. M. CO₂ capture by hydrate crystallization - A potential solution for gas emission of steelmaking industry. *Energy Conversion and Management*. 2007;48:1313-22.
- [3] Lin W., Delahaye A., Fournaison L. Phase equilibrium and dissociation enthalpy for semi-clathrate hydrate of CO(2) plus TBAB. *Fluid Phase Equilibria*. 2008;264:220-7.
- [4] Mohammadi A. H., Eslamimanesh A., Belandria V., Richon D. Phase Equilibria of Semiclathrate Hydrates of CO(2), N(2), CH(4), or H(2) + Tetra-n-butylammonium Bromide Aqueous Solution. *Journal of Chemical Engineering Data*. 2011;56:3855-65.
- [5] Chapoy A., Anderson R., Tohidi B. Low-pressure molecular hydrogen storage in semi-clathrate hydrates of quaternary ammonium compounds. *Journal of the American Chemical Society*. 2007;129:746-7.
- [6] Aladko E., Larionov E., Rodionova T., Aladko L., Manakov A. Double clathrate hydrates of tetrabutylammonium fluoride + helium, neon, hydrogen and argon at high pressures. *Journal of Inclusion Phenomena and Macrocyclic Chemistry*. 2010;68:381-6.

- [7] Deschamps J., Dalmazzone D. Hydrogen Storage in Semiclathrate Hydrates of Tetrabutyl Ammonium Chloride and Tetrabutyl Phosphonium Bromide. *Journal of Chemical & Engineering Data*. 2010;55:3395-9.
- [8] Arjmandi M., Chapoy A., Tohidi B. Equilibrium data of hydrogen, methane, nitrogen, carbon dioxide, and natural gas in semi-clathrate hydrates of tetrabutyl ammonium bromide. *Journal of Chemical Engineering Data*. 2007;52:2153-8.
- [9] Hashimoto S., Murayama S., Sugahara T., Sato H., Ohgaki K. Thermodynamic and Raman spectroscopic studies on H₂+tetrahydrofuran+water and H₂+ tetra-n-butyl ammonium bromide+water mixtures containing gas hydrates. *Chemical Engineering Science*. 2006;61:7884-8.
- [10] Sakamoto J., Hashimoto S., Tsuda T., Sugahara T., Inoue Y., Ohgaki K. Thermodynamic and Raman spectroscopic studies on hydrogen plus tetra-n-butyl ammonium fluoride semi-clathrate hydrates. *Chemical Engineering Science*. 2008;63:5789-94.
- [11] Strobel T. A., Koh C. A., Sloan E. D. Hydrogen storage properties of clathrate hydrate materials. *Fluid Phase Equilibria*. 2007;261:382-9.
- [12] Hashimoto S., Sugahara T., Moritoki M., Sato H., Ohgaki K. Thermodynamic stability of hydrogen plus tetra-n-butyl ammonium bromide mixed gas hydrate in nonstoichiometric aqueous solutions. *Chemical Engineering Science*. 2008;63:1092-7.
- [13] Sabil K. M., Duarte A. R. C., Zevenbergen J., Ahmad M. M., Yusup S., Omar A. A., et al. Kinetic of formation for single carbon dioxide and mixed carbon dioxide and tetrahydrofuran hydrates in water and sodium chloride aqueous solution. *International Journal of Greenhouse Gas Control*. 2010;4:798-805.
- [14] Fan S. S., Li S. F., Wang J. Q., Lang X. M., Wang Y. H. Efficient Capture of CO(2) from Simulated Flue Gas by Formation of TBAB or TBAF Semiclathrate Hydrates. *Energy Fuels*. 2009;23:4202-8.
- [15] Li S. F., Fan S. S., Wang J. Q., Lang X. M., Wang Y. H. Semiclathrate Hydrate Phase Equilibria for CO(2) in the Presence of Tetra-n-butyl Ammonium Halide (Bromide, Chloride, or Fluoride). *Journal of Chemical Engineering Data*. 2010;55:3212-5.

- [16] Dyadin Y. A., Terekhova I. S., Polyanskaya T. M., Aladko L. S. Clathrate hydrates of tetrabutylammonium fluoride and oxalate. *Journal of Structural Chemistry*. 1976;17:566-71.
- [17] Trueba A. T., Radovic I. R., Zevenbergen J. F., Kroon M. C., Peters C. J. Kinetics measurements and in situ Raman spectroscopy of formation of hydrogen-tetrabutylammonium bromide semi-hydrates. *International Journal of Hydrogen Energy*. 2012;37:5790-7.
- [18] Englezos P., Kalogerakis N., Dholabhai P. D., Bishnoi P. R. Kinetics of gas hydrate formation from mixtures of methane and ethane. *Chemical Engineering Science*. 1987;42:2659-66.
- [19] Giavarini C., Maccioni F., Santarelli M. L. Formation kinetics of propane hydrates. *Industrial & Engineering Chemistry Research* 2003;42:1517-21.
- [20] Nagai Y., Yoshioka H., Ota M., Sato Y., Inomata H., Smith R. L. Binary Hydrogen-Tetrahydrofuran Clathrate Hydrate Formation Kinetics and Models. *AIChE Journal*. 2008;54:3007-16.
- [21] Aladko L. S., Dyadin Y. A., Rodionova T. V., Terekhova I. S. Clathrate hydrates of tetrabutylammonium and tetraisoamylammonium halides. *Journal of Structural Chemistry*. 2002;43:990-4.
- [22] Komarov V. Y., Rodionova T. V., Terekhova I. S., Kuratieva N. V. The Cubic Superstructure-I of Tetrabutylammonium Fluoride (C₄H₉)₄NF·29.7H₂O Clathrate Hydrate. *Journal of Inclusion Phenomena and Macrocyclic Chemistry*. 2007;59:11-5.
- [23] McMullan R. K., Jeffrey G. A., Bonamico M. Polyhedral Clathrate Hydrates. 5. Structure of Tetra-n-butyl ammonium fluoride hydrate *Journal of Chemical Physics*. 1963;39:3295-&.
- [24] Florusse L. J., Peters C. J., Schoonman J., Hester K. C., Koh C. A., Dec S. F., et al. Stable low-pressure hydrogen clusters stored in a binary clathrate hydrate. *Science*. 2004;306:469-71.
- [25] Nakano S., Moritoki M., Ohgaki K. High-pressure phase equilibrium and Raman microprobe spectroscopic studies on the CO₂ hydrate system. *Journal of Chemical Engineering Data*. 1998;43:807-10.

[26] Hashimoto S., Murayama S., Sugahara T., Ohgaki K. Phase equilibria for H₂ plus CO₂ plus tetrahydrofuran plus water mixtures containing gas hydrates. *Journal of Chemical Engineering Data*. 2006;51:1884-6.

Chapter 7

Inter-cage Dynamics in sII
and sH Fluoromethane
Hydrates as Studied by ^{13}C
and ^2H NMR



7.1 Introduction

In this chapter the ability of the two dodecahedral cages (D-5¹² and D'-4³⁵⁶6³) of structure H (sH) hydrate, with t-butylmethylether (TBME) as large cage guest, to distinguish between methane (CH₄) and fluoromethane (CH₃F) guest molecules was studied by ¹³C NMR and ²H NMR. Section 7.2 presents the background and justification of the study. Section 7.3 presents the methodology while section 7.4 presents the results and the respective discussion. Finally the conclusions are presented in section 7.5. The present chapter is a modified version of the article submitted for publication in the Journal of Physical Chemistry (2013).

7.2. Background

Prospective utilizations of clathrate hydrates have been considered for industrial application as materials for gas separation [1-4] and the storage and transport of energy gases [5]. For gas separation processes, in particular for separation of methane gas from a mixture, the difference in the relative number of cavities of different sizes in each structure becomes a key factor for the performance of the hydrate phase. For instance, sI hydrate has three times as many large as small cavities, whereas sII has twice as many small as large cavities. sH has three small, two medium and one large cavity [6]. Moreover, the cavities in each structure present different features. For example, the small 5¹² cavity, also denoted as the D cavity [7], despite being common to the three clathrate hydrate structures, exhibits different size and symmetry in each structure, and consequently its behavior toward guest molecules is also different [8]. As a result, the D cavity can host small molecules like hydrogen and helium as well as larger molecules, e.g. CH₄, hydrogen sulfide and fluoromethanes. The large cavity of sI, also denoted as the T cavity, has oblate geometry with a major axis of 6.12 Å and minor axis of 5.07 Å for the ellipsoidal void [7], due to this feature, the guest shape is essential in framework stability [9]. This cavity can host molecules with average diameters ≤ 6.0 Å. The large 5¹²6⁴ cavity of sII, also denoted as the H

cavity, hosts molecules with an average diameter $\leq 6.6 \text{ \AA}$ and it is the most spherical of all clathrate hydrate cavities. The large $5^{12}6^8$ cavity of sH, also denoted as the E cavity, is the largest of the three main clathrate hydrate structures, it can hosts molecules of size between 7.1 and 9 \AA . However due to its particular shape, efficient space filling in addition to suitable size is required for framework stability [10, 11]. The medium $4^35^66^3$ cavity of sH is an irregular dodecahedron also denoted as D', which includes water molecules hydrogen bonding in square sides. It is significantly less spherical than the D cavity but their average radii are similar [12] and host similar sized guests.

Previous work has shown that fluoromethane (CH_3F) is a viable D-cage guest in sI [13, 14], sII [15, 16] and sH [17]. In the current work the ability of the D and D' cages in sH hydrate to discriminate between two guest molecules that are slightly different in size, CH_4 and CH_3F , is studied. The technique of choice was solid state ^{13}C NMR spectroscopy, as it has been shown that in favorable cases CH_4 in these two small cages can be distinguished from the ^{13}C resonance lines [18]. Molecular dynamics simulations and ^2H NMR will be used to support the conclusions and further study the differences between the distribution of these two guests in the D and D' cages.

7.3 Materials and methods

Methane (CH_4) was obtained from Praxair (UHP grade), fluoromethane- d_3 (CD_3F) (99%), and fluoromethane (CH_3F) (99%) were obtained from Synquest Labs. Tetrahydrofuran (THF) (99%), methylcyclohexane (MCH) (99%) and tert-butylmethylether (TBME) (99%) were purchased from Sigma Aldrich. All the samples were prepared with distilled water and all the chemicals were used without any further purification. The clathrate hydrates were prepared as described in Chapter 3 section 3.3.1 and the measurements were performed as described in sections 3.3.2-3.

7.4 Results and discussion

The clathrate hydrates prepared with CH₃F and CH₄ were first analyzed with PXRD to identify the crystal structure. The PXRD patterns and lattice constants are presented in the Appendix A.

Zilm *et al.* [19] have reported the low temperature ¹³C spectrum of CH₃F in an argon matrix. It is a doublet due to ¹³C – ¹⁹F dipolar coupling (D) plus anisotropic *J* coupling (ΔJ). Spin coupling parameters for ¹⁹F in a rigid C-F bond are: $D_{C-F} = 10$ kHz, $J_{C-F} \sim 158$ Hz, $\Delta\nu_{^{13}C} = 1800$ Hz (at 20.12 MHz = 1.88 T) therefore $\Delta\delta = \sim 90$ ppm, $\Delta J = 1200 \pm 1200$ Hz. With MAS of the rigid ¹³C – ¹⁹F bond, the spectrum becomes a doublet (the components may have different intensities) governed by the *J* coupling, and a manifold of spinning sidebands determined by the interplay of dipolar, chemical shift anisotropic and *J*-coupling interactions [19].

Figure 7.1 shows ¹³C spectra for sI, sII and sH hydrates containing CH₃F. The simplest is that for the sII hydrate, Figure 7.1(b), where the large cages are occupied by THF and CH₃F resides in the small cages. The spectrum is a near-symmetric *J*-coupled doublet at 70-72 ppm with a splitting of 158 Hz. The small sII cage is anisotropic, however, the dynamics appear to be both fast and close to isotropic and complexities appear to be minimal. The sI CH₃F spectrum, Figure 7.1(a), shows two overlapping doublets from molecules in large and small cages in the region between 70-73 ppm. The more intense doublet (70 and ~71.4 ppm) can be attributed to CH₃F in the large cage, which, as for the ¹³C spectrum of CH₄ has the small cage contribution to high field of that for the large cage. The large-cage doublet is asymmetric and this can be ascribed to interference effects, as described above. The spectrum for sH hydrate with both CH₃F and CH₄ in the small cages and TBME in the large cage is shown in Figure 7.1(c). The CH₄ ¹³C resonance at ~ -4 ppm is of interest as it shows just a single line. One might expect two lines, one for CH₄ in each small sH cavity, however, as will be shown below, there are some unexpected features which can be ascribed to

dynamics [18]. The spectrum of *sH* hydrate of MCH and CH_3F , Figure 7.1(d), shows an asymmetric doublet for CH_3F , with a very small splitting due to the slightly different chemical shifts of CH_3F in the D and D' cage types barely discernible. The ^{13}C NMR chemical shifts of CH_3F in the different clathrate hydrate structures are reported in Table 7.1.

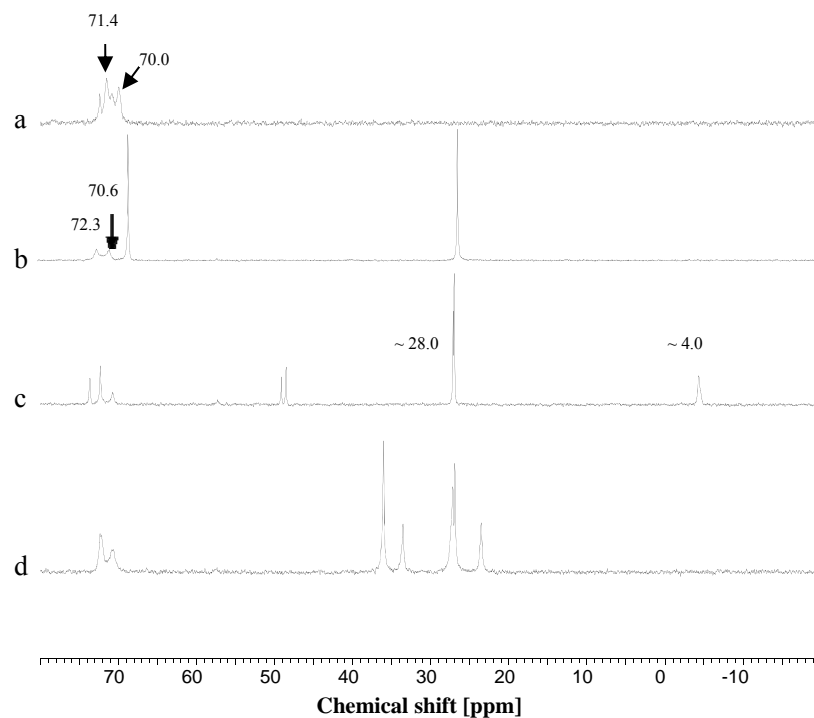


Figure 7.1. ^{13}C CP/MAS NMR spectra at 193.15 K of (a) *sI* CH_3F hydrate; (b) *sII* hydrate of CH_3F and THF; (c) *sH* hydrate of TBME with CH_3F and CH_4 in the small cages; and (d) *sH* hydrate with MCH and CH_3F as the small cage guest at 193.15 K.

Table 7.1. ^{13}C NMR chemical shifts (ppm with respect to TMS) of the CH_3F guest incorporated into different clathrate hydrate structures.

Hydrate	System	^{13}C NMR shifts
sI	CH_3F	70.00, 70.76, 71.46, 72.38
sII	CH_3F -THF	70.61, 72.33
sH	CH_3F -MCH	70.68, 72.19
sH	CH_3F - CH_4 -TBME	70.73, 72.20

So far, with ^{13}C NMR spectra alone, it has not been possible to discern the cage preferences of CH_4 or CH_3F for the D and D' cages of sH hydrate. As mentioned above, it was surprising to see a single line for CH_4 in the D and D' cages of sH TBME hydrate with both CH_4 and CH_3F guests. A more detailed observation of the temperature dependence of the ^{13}C spectrum, concentrating on the small guest molecule regions is given in Figure 7.2. At the lowest temperature, 183 K, the CH_4 populations in the D and D' cages are clearly distinguishable, although this is not the case for CH_3F . Measurement of the relative intensities shows that the ratio of the CH_4 populations is $p(\text{D}')/p(\text{D}) = 0.62$. The usual value for this ratio is close to one if CH_4 is the only small cage guest, suggesting that there is a degree of partitioning with CH_3F having a small preference for the D' cage. The CH_4 doublet collapses as the temperature is increased to ~ 248 K. This was interpreted in terms of the CH_4 populations molecules in the D and D' cages being able to exchange, thus averaging the chemical shift difference of 0.36 ppm (or 36 Hz at the Larmor frequency of the experiment). This process requires an exchange time greater than $\sim 4.4 \times 10^{-3}$ sec, as the condition for a collapse of two signals separated in the absence of exchange by the chemical shift of 36 Hz is $1/2\pi \times 36$ s. This direct observation of cage-to-cage guest exchange in the clathrate hydrate is relatively rare, while guest exchange between neighboring cages may occur in other systems, the timescales are too slow to be seen in the NMR spectrum. It was expected that the relatively rapid intercage dynamics may have some contributions from specific guest-host interactions, in particular related to the hydrogen bonding of TBME with the water lattice, as was the case for CO_2 dynamics in the binary THF

sII clathrate hydrates [20]. Recent work [21-23], after initial suggestions made many years ago [24], has shown that guest molecules capable of accepting hydrogen bonds can introduce Bjerrum L-defects [25] in the water lattice by forming transient hydrogen bonds with a water molecule. Migration of L and D Bjerrum defects in the hydrate lattice occurs through water molecule reorientation [24, 25]. Calculations have suggested that different small cage guests in sII hydrate can either enhance or retard the creation of Bjerrum defects [20]. Although CH_3F is not known as a hydrogen bond acceptor, there is some evidence that there may be special host guest interactions [26] (i.e. halogen bonding as, for example in the hydrates of dihalogens) [27], so that the combination of TBME and CH_3F also may give rise to fast dynamics of the water lattice.

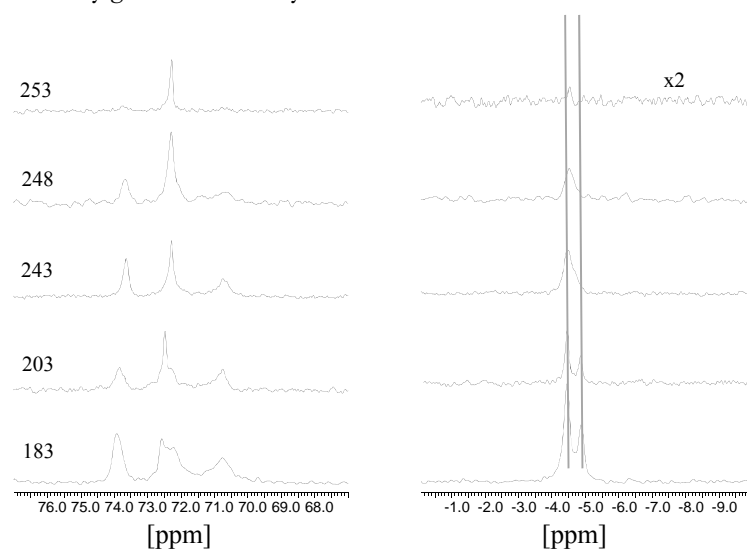


Figure 7.2. Details of the ^{13}C NMR spectra of the sH TBME/ CH_4 / CH_3F hydrate as a function of temperature for the CH_3F (left hand side) and CH_4 (right hand side) guests. At 183 K, the separate spectral signatures of CH_4 in the D and D' cages are clearly visible. However, by 243 K, the two signals have coalesced, indicating that CH_4 in these two cages is exchanging rapidly on a timescale determined by the chemical shift difference of the two signals in the slow motion limit.

Recent calculations of CH_4 diffusivity in a hydrate lattice [27] have introduced a water vacancy in the hydrate in order to get reasonable rates of

transport. Vacancies in the water lattice can be inferred as well from ^1H NMR studies of water molecular motion in THF [28] and ethylene oxide (EO) [29] hydrates, where the equivalent of centre-of-mass diffusion of water molecules was observed from the temperature dependence of the ^1H NMR line shapes and rotating frame relaxation time measurements. Whether such vacancies are intrinsic, or mediated by host-guest interactions remains unknown. The activation energy for water molecule diffusion in the two aforementioned hydrates is only ~20% less than it is in Ice Ih [24] so it appears that the effect of guest - host interactions on water diffusion is rather smaller than it is on reorientation.

In order to further test the idea of cage-to-cage transport, a double hydrate of sII was prepared with THF and CD_3F as guests, as this guest combination may well show intercage transport as well. CD_3F was employed to use the ^2H powder pattern to monitor the guest motions. The relationship between guest dynamics and cage symmetry has been well documented for both chemical shift and quadrupole coupling tensors [13]. The temperature dependence of the ^2H NMR powder pattern of CD_3F in the small cage of sII hydrate is shown in Figure 7.3. At 250 K, the doublet splitting gives a quadrupole coupling constant of 6.0 kHz, as compared with a value of 5.3 kHz for CD_3F in the large cage of sI hydrate at 268 K. These rather similar values are characteristic of extensive motional averaging in the anisotropic sI large and the sII small cages. At 260 K, the powder pattern for the sII hydrate shows the start of further motional averaging which is reasonably complete at the highest temperature of study, 281 K. As observed before for CO_2 in the small cage of sII hydrate [20], the motional averaging requires the breaking of the confining symmetry of the cage which can be achieved by the exchange of CH_3F among a number of different D cages, where some participating small cages in the diffusion process are empty. The minimum path for complete averaging of the quadrupolar tensor would be through a cluster of four neighboring D cages which are tetrahedrally arranged with respect to each other (a situation which exists in sII but not in sI or sH). The estimated correlation time for this motion is 3.5×10^{-5} sec at 260 K.

Figure 7.4 shows ²H NMR line shapes as a function of temperature for the sH hydrate of TBME and CD₃F. At 77 K the line shape is broad and featureless, characteristic of CD₃F guest dynamics in hydrate cages with frozen-in disorder of the water protons. At 160 K and higher temperatures the line shapes are considerably narrower with some discernible features. This means that even at 160 K, water dynamics is fast enough so that the hydrate cages have achieved their high average symmetry [30]. The D and D' cages have quite different symmetries, one axial, the other non-axial (see Table 7.2), so it should be possible to resolve the line shape contributions from guests in the two cages.

Table 7.2. ²H NMR quadrupole coupling parameters of CD₃F in various cages

Hydrate	Cage type	Cage symmetry	Quadrupole		T /K
			coupling constant Q _c /kHz	Asymmetry parameter, η	
sI	D	m3	0	0	261
sI	T	-42m	5.3	0	261
sII	D	3m	6.0	0	250
sH	D	mmm	5.1	0.7	200
sH	D'	-62m	13.2	0	200

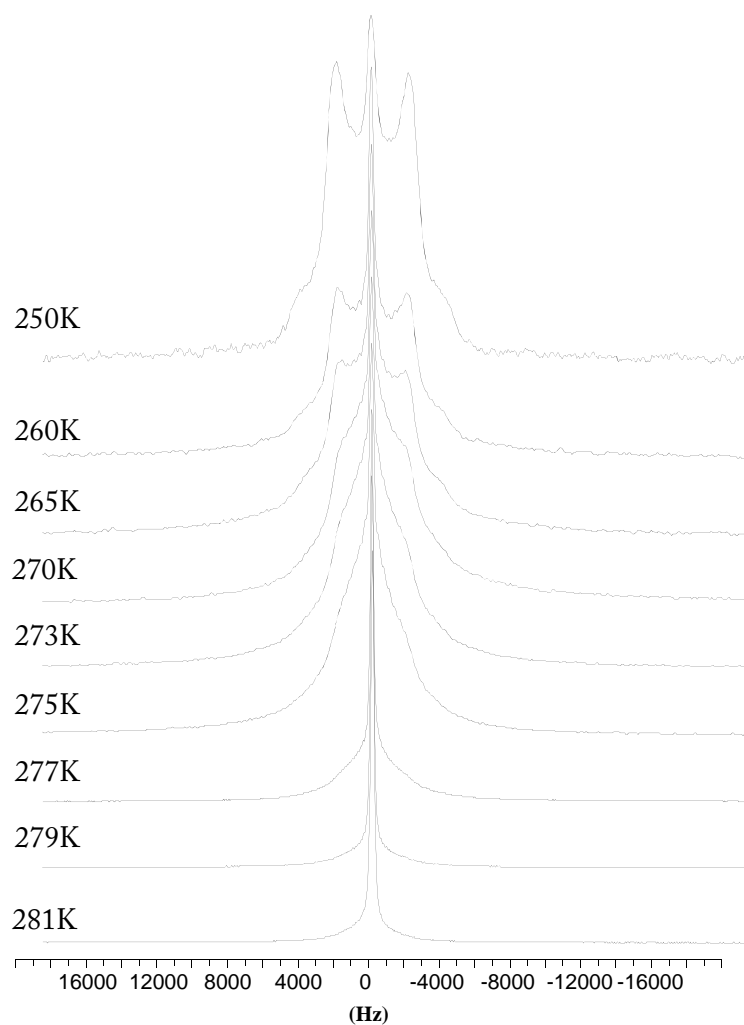


Figure 7.3. ^2H NMR powder line shapes for CD_3F in the small cages of the sII double hydrate of THF and CD_3F . A quadrupolar coupling of 6 kHz is observed at the 250 K. The line shape at 250 K was recorded last in order to confirm reversible behavior of the line shape. The disappearance of the doublet shows that the motion that sets in breaks the symmetry of the cage, hence is indicative of cage-to-cage transport.

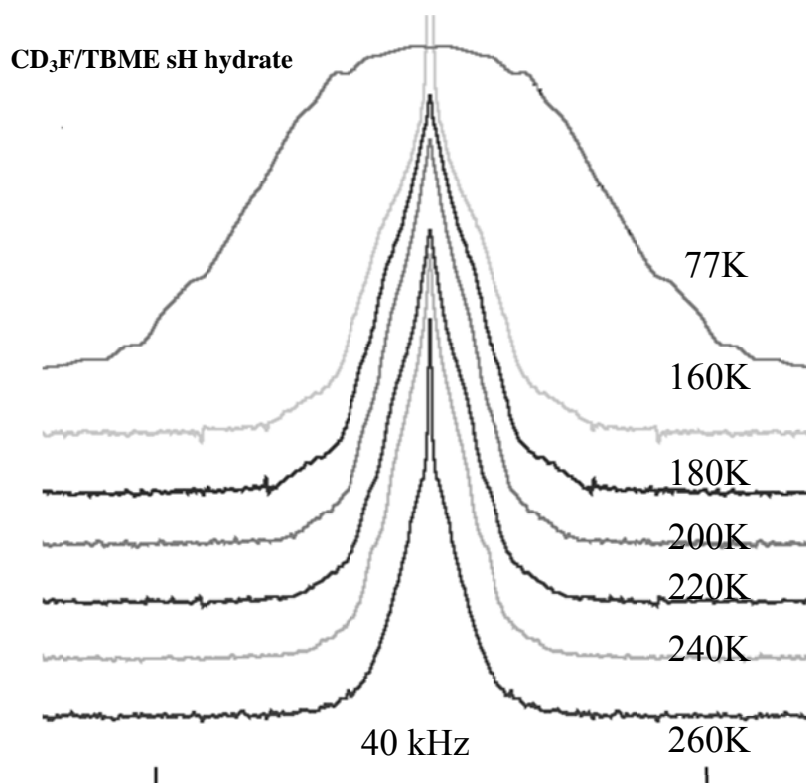


Figure 7.4. ^2H NMR line shapes of CD_3F in the D and D' cages of the *sH* hydrate of TBME/ CD_3F as a function of temperature. The quadrupole coupling parameters are given in Table 7.2.

Figure 7.5 shows the best visual fits when individual contributions from CD_3F in the D and D' cage are added, varying the quadrupole coupling parameters as well as relative intensities. The symmetry of the D' cage is such that the ^2H lineshape for CD_3F in this cage should have a zero asymmetry parameter. This was used as a constraint in the fitting.

Figure 7.6 shows an overlay of the ^2H NMR line shapes for the *sH* hydrates of TBME/ CD_3F and TBME/ $\text{CD}_3\text{F}/\text{CH}_4$. The difference spectrum lineshape has the same non-axial shape determined for CD_3F in the D cage in the fit shown in Figure 7.5. This difference represents reduced intensity from CD_3F in the D cage in the $\text{CD}_3\text{F}/\text{CH}_4/\text{TBME}$ hydrate indicating that

CD_3F has a slight preference for the D' cage whereas CH_4 shows a slight preference for the D cage.

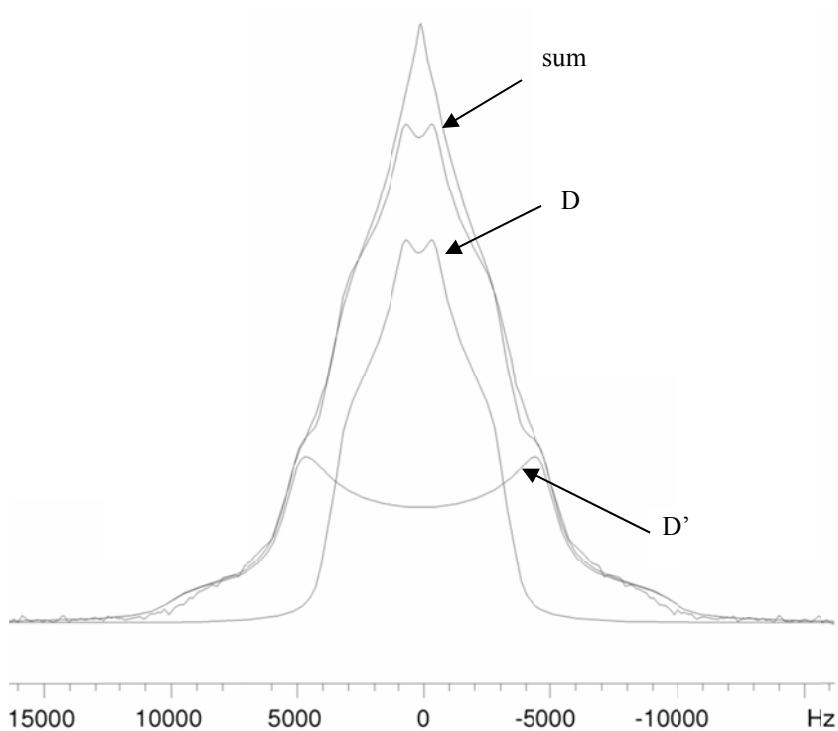


Figure 7.5. Visual fit of the ^2H NMR spectrum at 200K of the two contributions of CD_3F in the D and D' cages of sH hydrate of TBME/ CD_3F . The quadruple coupling parameters of CD_3F in the various hydrates are shown in Table 7.2.

The temperature dependence of the line shapes in Figure 7.4 gives some further insight into the dynamics at higher temperatures. Above ~ 200 K the fine structure associated with the dynamics of the CD_3F molecules in the D and D' cages starts to fade, and it is essentially gone at 260 K. Such disappearance of fine structure can be taken as a sign that the motion of the guest CD_3F molecules breaks the symmetry of the cage, as it would be expected if the CD_3F molecules in the D and D' cages exchanged. (In this case, if higher temperatures could be reached before decomposition one would expect to see a narrowed but structured lineshape) This is in

agreement with the collapse of the ^{13}C NMR lines observed for CH_4 in the D and D' cages in sH TBME/ $\text{CH}_3\text{F}/\text{CH}_4$ hydrate at about 250 K in Figure 7.2.

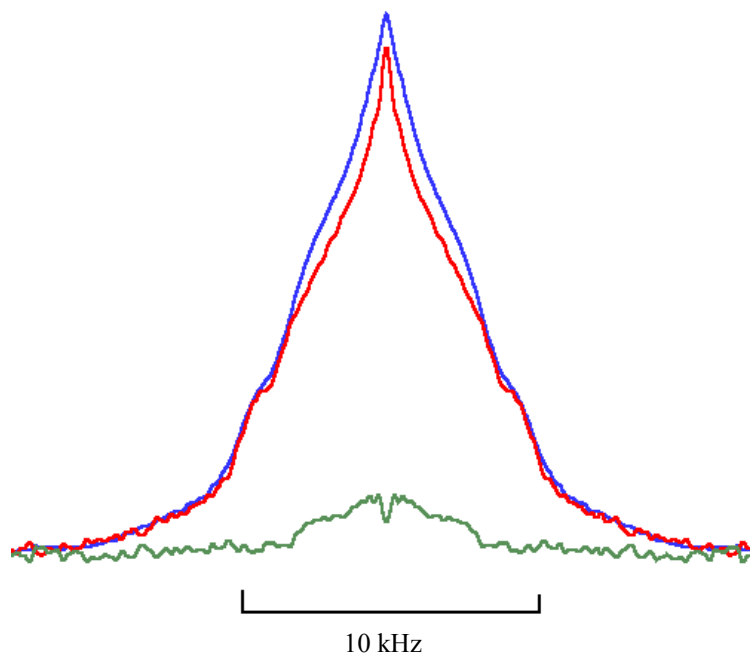


Figure 7.6. Overlay of ^2H NMR line shapes for the sH hydrates of TBME/ CD_3F (blue) and TBME/ $\text{CD}_3\text{F}/\text{CH}_4$ (red). The difference (green) shows the lineshape corresponding to CD_3F in the D cage and indicates a slight preference of CH_4 over CD_3F in the D cage.

7.5 Conclusions

The ^{13}C NMR studies show the incorporation of fluoromethane and methane as help-gas species in the small / medium cages of sH and sII binary clathrate hydrates with TBME and THF, respectively. At low temperatures, the ^{13}C NMR peaks associated with CH_3F show doublet structures, reflecting the non-spherical environments of the sII and sH cages. At high temperature, beginning at ~ 250 K range, these doublet peaks merge into a single peak which implies a local migration of CH_3F and CH_4 between

neighboring cages and the isotropic environment of these guests at high temperatures. The sH clathrate hydrate of CH₃F with the methylcyclohexane does not show the merging of the doublet of peaks. Molecular dynamics simulations show that the TBME and THF guest molecules show enhanced hydrogen bonding in the binary hydrates with CH₃F which could be due to the larger size of these molecules and the resulting weakening of the water hydrogen bonding network in the cages which accommodate CH₃F, which then enhances the hydrogen bonding with the large cage guests.

The ²H NMR powder lineshapes of the THF / CD₃F hydrate at different temperatures also show the transformation of the low temperature doublet peak of CD₃F into a single isotropic peak at temperatures above 270 K or so. This verifies the picture of cage-to-cage transport of the small guests.

Acknowledgements

The authors gratefully acknowledge the financial support of the ACTS Sustainable Hydrogen Program, Reg. Nr. H2 2007. We thank S. Lang for technical support.

7.6 References

- [1] Seo Y., Tajima H., Yamasaki A., Takeya S., Ebinuma T., Kiyono F. A new method for separating HFC-134a from gas mixtures using clathrate hydrate formation. *Environmental Science & Technology*. 2004;38:4635-9.
- [2] Shiojiri K., Okano T., Yanagisawa Y., Fujii M., Yamasaki A., Tajima H., et al. A new type separation process of condensable greenhouse gases by the formation of clathrate hydrates. In: Park S. E., Chang J. S., Lee K. W., editors. *Carbon Dioxide Utilization for Global Sustainability 2004*. p. 507-12.
- [3] Englezos P., Lee J. D. Gas hydrates: A cleaner source of energy and opportunity for innovative technologies. *Korean Journal of Chemical Engineering*. 2005;22:671-81.

- [4] Nohra M., Woo T. K., Alavi S., Ripmeester J. A. Molecular dynamics Gibbs free energy calculations for CO₂ capture and storage in structure I clathrate hydrates in the presence of SO₂, CH₄, N₂, and H₂S impurities. *The Journal of Chemical Thermodynamics*. 2012;44:5-12.
- [5] Gudmundsson J. S., Parlaktuna M., Khokhar A. A. Storing natural gas as frozen hydrate. *SPE Production & Facilities*. 1994;9:69-73.
- [6] Seo Y., Lee J. W., Kumar R., Moudrakovski I. L., Lee H., Ripmeester J. A. Tuning the Composition of Guest Molecules in Clathrate Hydrates: NMR Identification and Its Significance to Gas Storage. *Chemistry – An Asian Journal*. 2009;4:1266-74.
- [7] Alavi S., Udachin K., Ratcliffe C. I., Ripmeester J. A. *Clathrate Hydrates. Supramolecular Chemistry: From Molecules to Nanomaterials*. New York: John Wiley & Sons; 2012.
- [8] Ripmeester J. A., Ratcliffe C. I. The diverse nature of dodecahedral cages in clathrate hydrates as revealed by Xe-129 and C-13 NMR spectroscopy: CO₂ as a small-cage guest. *Energy Fuel*. 1998;12:197-200.
- [9] Sloan E. D., Koh E. D. *Clathrate Hydrates of Natural Gases*. 3rd ed. Florida: CRC Press; 2008.
- [10] Ripmeester J. A., Ratcliffe C. I. Xe-129 NMR-Studies of clathrate hydrates - new guests for structure-II and structure-H. *Journal of Physical Chemistry*. 1990;94:8773-6.
- [11] Tezuka K., Murayama K., Takeya S., Alavi S., Ohmura R. Effect of Guest Size and Conformation on Crystal Structure and Stability of Structure H Clathrate Hydrates: Experimental and Molecular Dynamics Simulation Studies. *Journal of Physical Chemistry C*. 2013;117:10473-82.
- [12] Seo Y. T., Lee H. C-13 NMR analysis and gas uptake measurements of pure and mixed gas hydrates: Development of natural gas transport and storage method using gas hydrate. *Korean Journal of Chemical Engineering*. 2003;20:1085-91.
- [13] Collins M. J., Ratcliffe C. I., Ripmeester J. A. Nuclear Magnetic-Resonance studies of guest species in clathrate hydrates -Line - Shape Anisotropies, Chemical-Shifts, and the Determination of Cage Occupancy Ratios and Hydration Numbers. *Journal of Physical Chemistry*. 1990;94:157-62.

- [14] Davidson D. W., Ratcliffe C. I., Ripmeester J. A. ^2H and ^{13}C NMR study of guest molecule orientation in clathrate hydrates. *Journal of Inclusion Phenomena*. 1984;2:239-47.
- [15] Uchida T., Ohmura R., Hori A. Critical size for guest molecules to occupy dodecahedral cage of clathrate hydrates. *Journal of Physical Chemistry C*. 2008;112:4719-24.
- [16] Takeya S., Ohmura R. Phase Equilibrium for Structure I and Structure H Hydrates Formed with Methylfluoride and Methylcyclohexane. *Journal of Chemical Engineering Data*. 2007;52:635-8.
- [17] Takeya S., Yasuda K., Ohmura R. Phase equilibrium for structure II hydrates formed with methylfluoride coexisting with cyclopentane, fluorocyclopentane, cyclopentene, or tetrahydropyran. *Journal of Chemical Engineering Data*. 2008;53:531-4.
- [18] Susilo R., Ripmeester J. A., Englezos P. Characterization of gas hydrates with PXRD, DSC, NMR, and Raman spectroscopy. *Chemical Engineering Science*. 2007;62:3930-9.
- [19] Zilm K. W., Grant D. M. ^{13}C Dipolar spectroscopy of small organic-molecules in argon matrices. *Journal of the American Chemical Society*. 1981;103:2913-22.
- [20] Alavi S., Ripmeester J. A. Effect of small cage guests on hydrogen bonding of tetrahydrofuran in binary structure II clathrate hydrates. *Journal of Chemical Physics*. 2012;137.
- [21] Alavi S., Udachin K., Ripmeester J. A. Effect of Guest-Host Hydrogen Bonding on the Structures and Properties of Clathrate Hydrates. *Chemistry: A European Journal*. 2010;16:1017-25.
- [22] Alavi S., Susilo R., Ripmeester J. A. Linking microscopic guest properties to macroscopic observables in clathrate hydrates: Guest-host hydrogen bonding. *Journal of Chemical Physics*. 2009;130.
- [23] Susilo R., Alavi S., Moudrakovski I. L., Englezos P., Ripmeester J. A. Guest-Host Hydrogen Bonding in Structure H Clathrate Hydrates. *Chemphyschem*. 2009;10:824-9.
- [24] Davidson D. W., Ripmeester J. A. *Inclusion Compounds: Physical Properties and Applications*: Academic Press; 1984.
- [25] Bjerrum N. Structure and properties of ice. *Science*. 1952;115:385-90.

- [26] Udachin K. A., Ripmeester J. A. Unpublished results on structure of CH₃F hydrate. Ottawa: Steacie Institute for Molecular Sciences, National Research Council Canada.
- [27] Peters B., Zimmermann N. E. R., Beckham G. T., Tester J. W., Trout B. L. Path Sampling Calculation of Methane Diffusivity in Natural Gas Hydrates from a Water-Vacancy Assisted Mechanism. *Journal of the American Chemical Society*. 2008;130:17342-50.
- [28] Garg S. K., Davidson D. W., Ripmeester J. A. NMR behavior of clathrate hydrate of tetrahydrofuran I. Proton measurements. *Journal of Magnetic Resonance*. 1974;15:295-309.
- [29] Ripmeester J. A. Proton and deuteron nuclear magnetic-resonance study of host and guest motions in ethylene oxide d₄ clathrate hydrate. *Canadian Journal of Chemistry*. 1976;54:3677-84.
- [30] Ripmeester J. A., Ratcliffe C. I. On the contributions of NMR spectroscopy to clathrate science. *Journal of Structural Chemistry*. 1999; 40:654-62.
- [31] Susilo R., Ripmeester J. A., Englezos P. Characterization of gas hydrates with PXRD, DSC, NMR, and Raman spectroscopy. *Chemical Engineering Science*. 2007;62:3930-9.

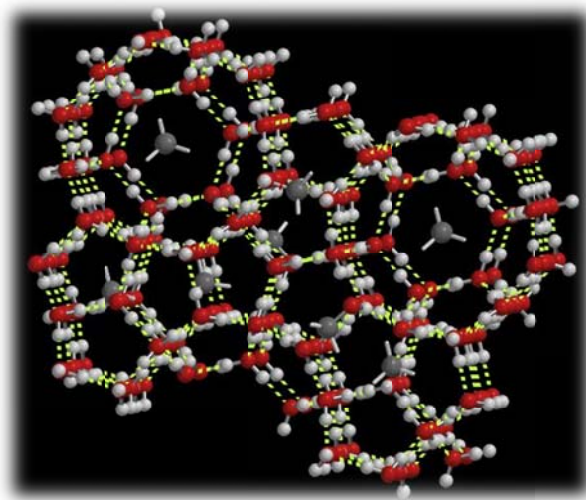
Chapter 8

Molecular Dynamics

Study of sII and sH

Fluoromethane and

Methane Hydrates



8.1 Introduction

The present chapter is a continuation of the previous study on the inter-cage dynamics in sII and sH CH₃F/CH₄ hydrates. The free energy of substitution of CH₄ with CH₃F in the D and D' cages of sH clathrate hydrate was studied via molecular dynamic (MD) thermodynamic integration calculations to determine whether there is cage selectivity between these two guests. Thermodynamic integration has been previously used to study the stability and occupancy of H₂ in sII clathrate hydrates [1], the stability of rare gases in sH [2], CH₄ occupancy and stability in sH clathrate hydrate [3], and most recently the carbon dioxide (CO₂) substitution in sI clathrate hydrates [4, 5]. Finally, the rotational dynamics of CH₄ and CH₃F in the D and D' cages of sH and in the D cage of sII was also calculated at different temperatures and pressures in order to study their effect on the hydrogen bonding between the guest in the large cage and the oxygen of the water molecules composing the large cage [6]. The present chapter is a modified version of the article submitted for publication in the Journal of Physical Chemistry (2013).

8.2 Computational methods

Simulations of the sH hydrates were performed in a 3×3×3 replica of the unit cell with initial dimensions set at 36.84×31.09×29.64 Å³ and sII hydrates in a 2×2×2 replica of the unit cell with initial dimensions of 34.68×34.68×34.68 Å³, imposing periodic boundary conditions in all cases. The DL_POLY molecular dynamics simulation package version 2.20 [7] was used in the *NpT* ensemble using the Nosé–Hoover thermostat-barostat algorithm [8] with thermostat and barostat relaxation times of 0.2 and 0.5 ps, respectively. Time steps of 1 fs are used in all simulations. The initial positions of the water oxygen atoms of the hydrate lattice were obtained from the crystallographic structures of sH [9] and sII hydrate [10]. The disordered water hydrogen atoms were arranged about water oxygen sites subjected to the constraints of the Bernal-Fowler ice rules [11] via a unit-cell dipole-moment minimizing Monte Carlo calculation.

The TIP4P potential was used for water [12]. The structures of TBME, THF, and CH₃F were determined by energy optimization using density function theory at the B3LYP/6-311++G(*d,p*) level with the Gaussian 03 suite of programs [13]. The electrostatic point charges on the optimized TBME, THF, and CH₃F molecules are estimated from “charges from electrostatic potential grid” (CHELPG) method as implemented in Gaussian 03. The intermolecular van der Waals interaction parameters are taken from the general AMBER force field (GAFF) [14]. Methane molecules modeled with the Murad-Gubbins single-point potential [15] (in the free energy calculations) and the TRAPPE all-atom potential [15] (in hydrogen bonding and guest dynamics studies). Standard combination rules, $\epsilon_{ij} = (\epsilon_i \epsilon_j)^{1/2}$ and $\sigma_{ij} = (\sigma_i + \sigma_j)/2$ were used to derive the Lennard-Jones potential parameters between unlike atom-type force centers *i* and *j*. The Ewald summation method was used to calculate long-range Coulombic interactions and all intermolecular interactions in the simulation box within a cutoff distance of 13.0 Å. Table 8.1 shows the atomic electrostatic point charges and the Lennard-Jones parameters of the molecules used in the simulations. The internal degrees of motion of molecules in the clathrate hydrates were considered to be frozen and the molecules moved as a rigid unit in the simulations.

In the sH simulations, initially, all large cages are occupied by a single TBME molecule (27 molecules in total) whereas all small and medium cages are occupied by either CH₃F or CH₄ molecules (135 molecules in total, of which 81 are in the small cages and 54 are in the medium cages). In the sII simulations, all large cages are occupied by a single THF molecule (64 molecules in total) whereas all small cages are occupied by either CH₃F or CH₄ molecules (132 molecules in total). These configurations with all small cages occupied by guests are hypothetical since experimentally some fraction of the small/medium cages remains vacant.

Two sets of simulation studies were performed. In the first set, we studied hydrogen bonding of the ether oxygen (OS) of TBME and THF with water in the binary systems of sH and sII with CH₃F or CH₄. We previously

studied the effect of small cage help-gas guests on the hydrogen bonding of the large cages guests and found that the shape and interaction of the help-gas guests can significantly affect the hydrogen bonding of the large cage guests.[6] This large-guest hydrogen bonding with framework water molecules can in turn lead to the formation of defects in the water hydrogen bonding network which affects the dynamical behavior of the water molecules and small cage guests. We shall use the results of these simulations in the interpretation of the some of the experimental NMR results.

Constant pressure-temperature NpT simulations were performed for the sH and sII hydrates with CH_3F and all-atom representation of the CH_4 molecules. Hydrogen bond dynamics and small guest rotation dynamics were extracted from constant energy/volume NVE simulations and were executed starting with the final NpT configurations previously described. The NVE simulations were performed for a total time of 600 ps, with the first 100 ps used for equilibration. Pressures from 1 to 50 bar at two temperatures 183 and 253 K were studied for each hydrate system in sH, and for the systems in sII simulations were carried out at 250 and 281 K and 1 bar. The guests were considered hydrogen bonded to a water molecule if the OS atom distance to a hydrogen atom of water (HW) was less than 2.1 Å. The average probability of hydrogen bond formation was calculated by averaging the ratio of times during the simulation that TBME or THF were hydrogen bonded to the cage water molecules.

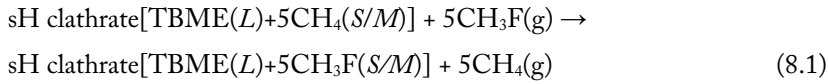
In a second series of molecular dynamics simulations, we determined the free energy for substitution of CH_4 guests in the small and medium cages of the binary sH hydrate with TMBE with CH_3F guests using the thermodynamic integration method. The CH_4 molecules are replaced from both small and medium cages by CH_3F molecules using the alchemic transformation via the coupling factor λ which was varied between 0.0 and 1.0 in intervals of 0.025. Simulations were carried out for 500 ps with the first 200 ps used for equilibration.

Table 8.1. Intramolecular potential parameters.

^a CH₄ modeled with single point potential [15].

Atom	Molecule	q (e)	σ_{ii} (Å)	ϵ_{ii} (kJ/mol)
O (OW)	H ₂ O	0.0	3.153	0.6479
H (HW)	H ₂ O	0.52	0.0	0.0
E (EE)	H ₂ O	-1.040	0.0	0.0
C1 (C3)	TBME	0.1027	3.340	0.4577
H1-H3 (H1)	TBME	0.0256	2.471	0.0657
O (OS)	TBME	-0.5404	3.000	0.7113
C2 (C3)	TBME	0.7721	3.340	0.4577
C3-C5 (C3)	TBME	-0.3474	3.340	0.4577
H4-H12 (HC)	TBME	0.0701	2.650	0.0657
C3	THF		3.3996	0.4577
H1	THF		2.4714	0.0656
OS	THF	-0.4670	3.000	0.7113
HC	THF		2.6496	0.0656
C	CH ₃ F	0.2156	3.3997	0.4577
F	CH ₃ F	-0.2925	3.1181	0.2552
H	CH ₃ F	0.0256	2.4713	0.0657
CH ₄ ^a	CH ₄	0.0	3.640	0.326
C	CH ₄	-0.572	3.35	0.4255
H	CH ₄	0.143	2.61	0.0719

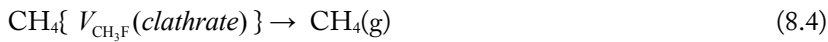
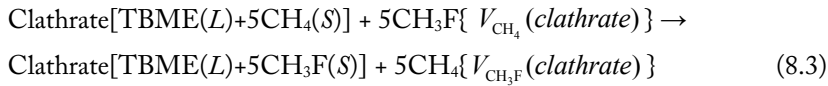
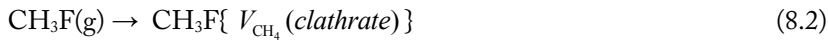
The MD simulations are used to determine the Gibbs free energy associated with the following reaction,



where 5 CH₃F gas molecules at a temperature T and pressure p replace 5 CH₄ molecules from the small and medium cages of the sH clathrate hydrate. The CH₄ molecules originally in the hydrate phase are subsequently released to the gas phase. The methodology for the thermodynamics integration method for free energy calculations is standard and described in the following section.

8.3 Thermodynamics of the guest substitution

To simplify the calculations of the Gibbs free energy, the reaction is separated into three hypothetical stages. Take the volume of the binary sH (CH₄-TBME) hydrate phase as $V_{\text{CH}_4}(\text{clathrate})$ and the volume of the binary sH (CH₃F-TBME) hydrate as $V_{\text{CH}_3\text{F}}(\text{clathrate})$. The volumes of reactant and product gases at temperature T and pressure p are $V_{\text{CH}_3\text{F}}(g; T, p)$ and $V_{\text{CH}_4}(g; T, p)$, respectively. Equation (8.1) is then written as the sum of the following three reactions,



Equation 8.2 is the compression of the CH₃F from the gas volume at T, p to a hypothetical ideal gas state where its volume is equal to that of the sH binary (TBME+CH₄) clathrate hydrate, $V_{\text{CH}_4}(\text{clathrate})$. Equation 8.3 is the release of the CH₄ guests in the hydrate cages and the converting them into non-interacting ideal gas (“ghost”) molecules which occupy the hydrate system with volume $V_{\text{CH}_3\text{F}}(\text{clathrate})$ and the simultaneous capture of non-interacting CH₃F molecules from the ideal gas “ghost” state in a volume $V_{\text{CH}_4}(\text{clathrate})$ and incorporating them into binary sH (TBME+CH₃F)

clathrate hydrate cages. Equation 8.4 is the expansion of the ideal gas CH₄ from the hypothetical state where its volume at T and p is that of the binary sH (TBME+CH₃F) clathrate hydrate, $V_{CH_3F}(clathrate)$ to its real gas volume at T, p .

The Gibbs free energy of Eq. 8.3 determines whether the CH₄-TBME sH hydrate is more stable if CH₄ is replaced by CH₃F. Therefore for CH₃F the Gibbs free energy in the gas phase is,

$$G_{CH_3F}^g = 5kT \ln \left(\frac{\rho_{CH_3F}(g; T, p)}{q_{CH_3F}} \right) + 5\mu [CH_3F(g; T, p)] \quad (8.5)$$

where $\rho_{CH_3F}(g; T, p)$ is the number density of the CH₃F in the gas phase and $q_{CH_3F}(T)$ is the ideal CH₃F(g) partition function. The residual chemical potential for CH₃F(g) is given by the thermodynamic expression,

$$\mu_{res} [CH_3F(g; T, p)] = \int_1^p [V_{CH_3F}(g; p, T) - V_{CH_3F}^{ideal\ gas}(g; T, p)] dp \quad (8.6)$$

where the real gas molar volume for CH₃F(g), $V(p, T)$ can be determined from experimental measurements at T and p , or calculated from MD simulations. For the CH₃F molecules in the hydrate phase at T and p , the Gibbs free energy is,

$$G_{CH_3F}^{clathrate} = 5kT \ln \left(\frac{\rho_{CH_3F}(clathrate; T, p)}{q_{CH_3F}} \right) + 5\mu [CH_3F(clathrate; T, p)] \quad (8.7)$$

where $\rho_{CH_3F}(clathrate; T, p)$ is the number density of the CH₃F in the hydrate phase and the residual chemical potential for CH₃F(clathrate) is calculated by MD thermodynamics integration

Combining Equations 8.5 and 8.7 and the corresponding equations for the Gibbs free energies of CH₄ the resulting expression for the total Gibbs free energy of Eq. 8.3 is,

$$\begin{aligned} \Delta G_{total} = 5kT & \left[\ln \left(\frac{\rho_{CH_4}(clathrate; T, p)}{\rho_{CH_3F}(clathrate; T, p)} \right) + \ln \left(\frac{\rho_{CH_3F}(gas; T, p)}{\rho_{CH_4}(gas; T, p)} \right) \right] \\ & + 5 \{ \mu_{res} [CH_4(clathrate)] - \mu_{res} [CH_3F(clathrate)] \} \\ & + 5 \{ \mu_{res} [CH_3F(g)] - \mu_{res} [CH_4(g)] \} \end{aligned} \quad (8.8)$$

Assuming $\text{CH}_3\text{F}(\text{g})$ and $\text{CH}_4(\text{g})$ behave as ideal gases under the conditions of the current experiment that the volumes of the hydrate phases with $5\text{CH}_3\text{F}$ and 5CH_4 are similar, Eq. 8.8 simplifies to,

$$\Delta G_{\text{Total}} = \left\{ \mu_{\text{res}} [\text{CH}_4(\text{clathrate})] - \mu_{\text{res}} [\text{CH}_3\text{F}(\text{clathrate})] \right\} \quad (8.9)$$

In Eqs. 8.2 and 8.4, it is assumed that CH_3F and CH_4 are ideal under the pressure and temperature conditions of the experiment. It is also assumed that the clathrate phase is incompressible $\rho_{\text{CH}_4}(\text{g}; T, p)$.

In Eq. 8.9 the Hamiltonian which describes the transformation is given as,

$$H_\lambda = (1 - f(\lambda))H_r + f(\lambda)H_p \quad (8.10)$$

where in this case, H_r is the Hamiltonian for a the system of CH_4 interacting with the water of the sH clathrate hydrate lattice with the CH_3F molecules acting as non-interacting ideal gas ghost molecules entrapped in the simulation cell volume. Similarly, H_p is the Hamiltonian for the system of CH_3F interacting with the water of the sH clathrate hydrate lattice with the CH_4 molecules acting as non-interacting ideal gas ghost molecules in the simulation cell volume.

It can be shown that the free energy associated with Eq. 8.3 is calculated from,

$$\Delta G_{\text{TI}} = \int_0^1 \left\langle \frac{\partial H_\lambda}{\partial \lambda} \right\rangle_{\lambda, T, p} d\lambda = \int_0^1 \left\langle (H_p - H_r) \frac{\partial f(\lambda)}{\partial \lambda} \right\rangle_{\lambda, T, p} d\lambda \quad (8.11)$$

where the brackets indicate ensemble averages taken over the duration of the simulation. To numerically evaluate the integral in Eq. 8.11, it is necessary to calculate $\left\langle (H_p - H_r) \frac{\partial f(\lambda)}{\partial \lambda} \right\rangle_{\lambda, T, p}$ at different values of λ and numerically integrate the values between 0 and 1.

8.4 Results and discussion

Hydrogen bonding was observed between framework water molecules and the ether atoms (OS) of the TBME and THF guests in the sH and sII large cages, respectively. Snapshots of hydrogen bonding configurations of these

guests are shown in Figure 8.1. The radial distribution function (RDF) for the OS atom of TBME with the framework water hydrogen atoms (HW) and for the OS atom of THF with the framework water hydrogen atoms (HW) are shown in Figures 8.2 and 8.3 respectively. The peaks in the OS-HW RDF at 1.8 Å in Figure 8.2 show the presence of guest-water hydrogen bonding in these systems. In the TBME hydrate, the height of the first peak in the OS-HW RDF is larger in the CH₃F binary hydrate than in the corresponding CH₄ binary hydrate. The height of the peak shows the greater probability of hydrogen bonding in the former cases. In all cases, OS-HW hydrogen bonding increases at higher temperatures and there is only a small pressure dependence of the hydrogen bonding. In the case of the binary sII hydrates with THF, the first peaks in the OS-HW RDF were smaller in both systems compared to the TBME peaks. However, the peaks for the THF-water hydrogen bonding are also higher in the hydrate with CH₃F than in the hydrate with CH₄.

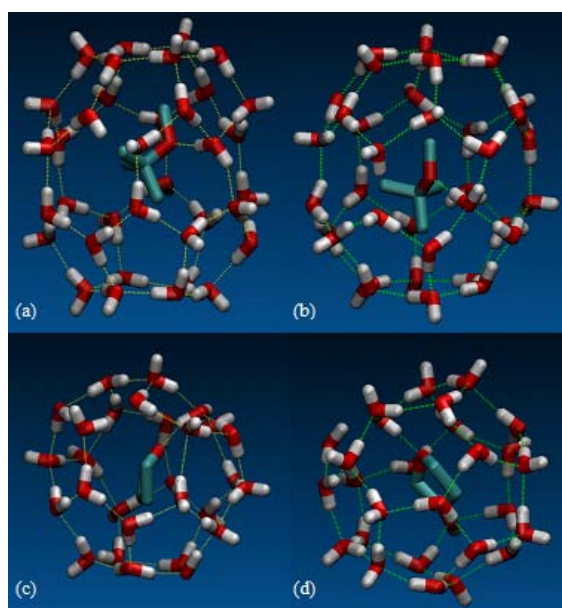


Figure 8.1. Snapshots of the hydrogen bond formed between the TBME guest and the water molecule of the large cavity of sH (a and b) and the THF guest with the water molecule of the large cavity of sII (c and d). The sH snapshots are at 183 K and 1 bar, and the sII snapshots are at 250 K and 1 bar. (a) sH clathrate hydrate of CH₃F and TBME, (b) sH clathrate hydrate

of CH₄ and TBME, (c) sII of CH₃ and THF and (d) sII of CH₄ and THF. The hydrogen atoms of the guest molecules are not shown in these snapshots.

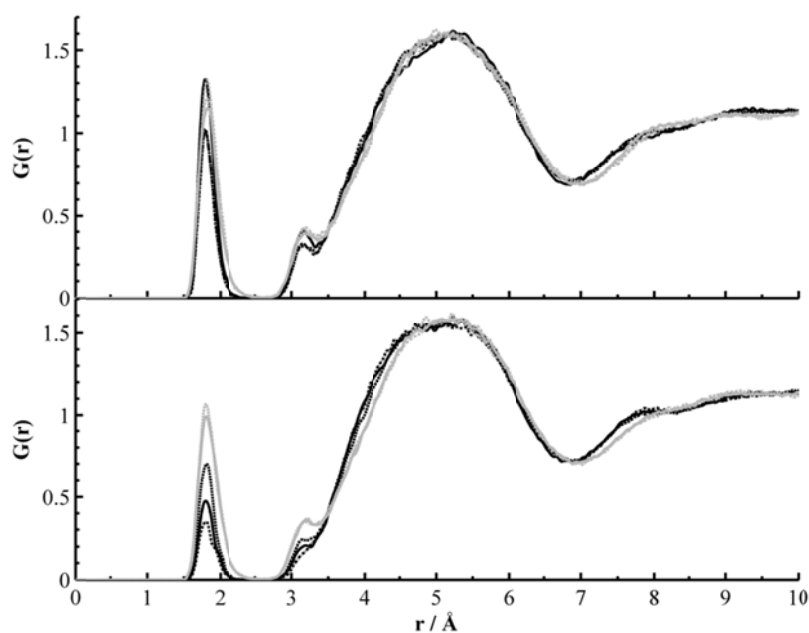


Figure. 8.2. Radial distribution function (RDF) for the guest ether oxygen of TBME with the framework water hydrogen atoms (HW) in the sI hydrate with CH₃F (top) and CH₄ (bottom) at 183 K black curves and 253 K gray curves. The full lines correspond to 1 bar, the dotted lines to 25 bar and the dashed lines to 50 bar.

The probability of hydrogen bonding between the large cage guests and water can be quantified by counting the fraction of snapshots in the simulation where the OS...HW distance is less than 2.1 Å. These probabilities are given in Table 8.2. In the case of the TBME hydrates, the probabilities can also be determined from the integral,

$$p = \int_0^{r_{\min}} \rho g(r) 4\pi r^2 dr, \quad (8.12)$$

where r_{\min} is the location of the first minimum after the peak which represents hydrogen bonding. These values are also given in Table 8.2.

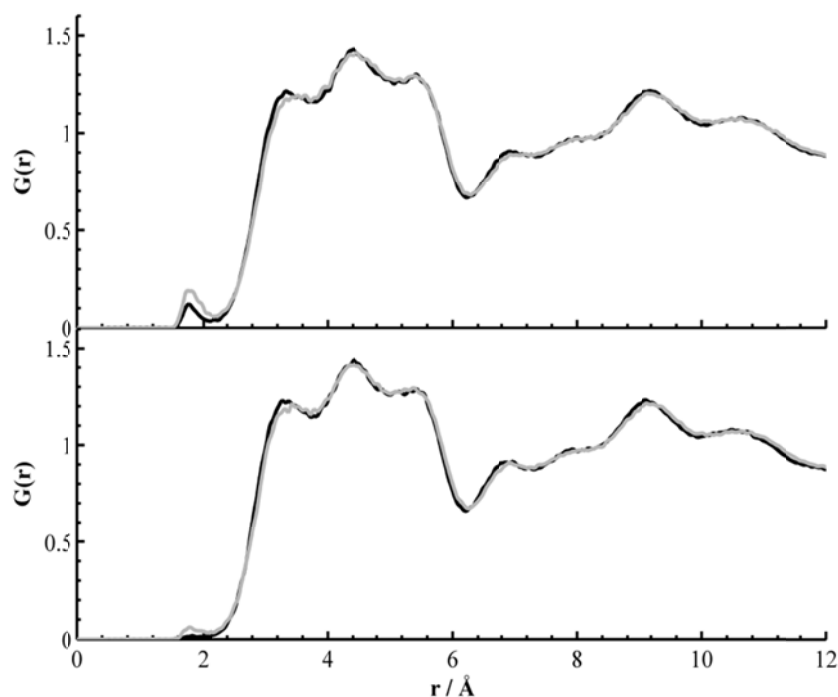


Figure. 8.3. Radial distribution function (RDF) for the guest ether oxygen of THF with the framework water hydrogen atoms (HW) in the sII hydrate with CH₃F (top) and CH₄ (bottom) at 250 K black curves and 281 K gray curves.

In general, the hydrogen bonding probability in the CH₃F clathrate hydrates is greater than the corresponding CH₄ clathrate hydrates. The enhanced hydrogen bonding probability introduces a greater number of Bjerrum defects into the lattice.

In the present simulations no small / medium cage vacancies were introduced in the simulations and therefore direct migrations of CH₃F or CH₄ molecules between neighboring small cages (as inferred from the NMR results presented in the previous chapter) are not observed. However, the contribution of hydrogen bonds of TBME with water on the migration of CH₃F and CH₄ between different cages can partly explain the difference observed between the ¹³C spectra of the TBME + CH₃F / CH₄ hydrate of

Figure 7.1(c), presented in the previous chapter, and the MCH + CH₃F hydrate of Figure 7.1(d). The MCH molecule does not have hydrogen bonding functional groups and CH₃F peaks in the sH small and medium cages in the ¹³C spectrum retained their doublet structure. The CH₃F guest exchange between the small / medium cages, if present in the MCH + CH₃F hydrate, occurs on a time scale slower than the NMR experiment.

Table 8.2. Hydrogen bonding probabilities of TBME and THF in binary clathrate hydrates of CH₃F or CH₄ under different temperature and pressure conditions.

Clathrate	$p(\text{H-bond})$	$p_{\text{RDF}}(\text{H-bond})$	Clathrate	$p(\text{H-bond})$	$p_{\text{RDF}}(\text{H-bond})$
TBME+CH ₃ F			TBME+CH ₄		
T = 183 K			T = 183 K		
$p = 1$ bar	0.7229	0.7581	$p = 1$ bar	0.2617	0.3057
$p = 25$ bar	0.6746	0.5708	$p = 25$ bar	0.3188	0.4326
$p = 50$ bar	0.5505	0.5708	$p = 50$ bar	0.1201	0.2325
T = 253 K			T = 253 K		
$p = 1$ bar	0.7286	0.8580	$p = 1$ bar	0.4299	0.7369
$p = 25$ bar	0.6358	0.9197	$p = 25$ bar	0.7158	0.7604
$p = 50$ bar	0.3363	0.9565	$p = 50$ bar	0.5612	0.7416
THF+CH ₃ F			THF+CH ₄		
T = 250 K			T = 183 K		
$p = 1$ bar	0.0643	0.0722	$p = 1$ bar	0.0127	0.0057
T = 281 K			T = 183 K		
$p = 1$ bar	0.1499	0.1538	$p = 1$ bar	0.0290	0.0447

The free energy of substitution of the CH₄ molecules for CH₃F in the binary sH clathrate hydrate, with TBME as the large cage guests, from thermodynamic integration at different temperature and pressure conditions are given in Table 8.3 and Figure 8.4 shows the variation of $\langle \partial U(\lambda) / \partial \lambda \rangle_{T,p}$

as a function of the coupling parameter λ for Eq. (8.1). Details of the thermodynamic integration process are given in the previous section. The configurational energy of the sH hydrate with TBME and CH₄ and TBME and CH₃F at various pressures and temperatures are also given in Table 8.3. Most of the results in Table 8.3 indicate a small preference for CH₄ over CH₃F in the small and medium sH clathrate hydrate cages, which could be due to the larger effective radius of CH₃F which makes its incorporation in the small / medium cages more difficult, or due to the destabilizing effect of the additional hydrogen bonding of the TBME guest with water when CH₃F is the small guest, see Table 8.2.

To determine the effect of the guest size on the dynamics in the small and medium cages, we studied the velocity autocorrelation function (VACF) of CH₃F and CH₄ in the sH and sII clathrate hydrates. The results are shown in Figures 8.5-8.8.

The VACF for the carbon atoms of the CH₃F and CH₄ in the small and medium cages of the binary sH clathrate hydrate of TBME at different temperature and pressure conditions are shown in Figure 8.5. The long-time behavior of the VACF shown in the inset indicates that the smaller CH₄ molecules have a higher frequency for rattling motion inside the cage. In both hydrates both sets of temperatures have similar mean collision time and the VACF decays to zero at the same speed. However, the long-time behavior of the VACF shows smaller periods at low temperatures.

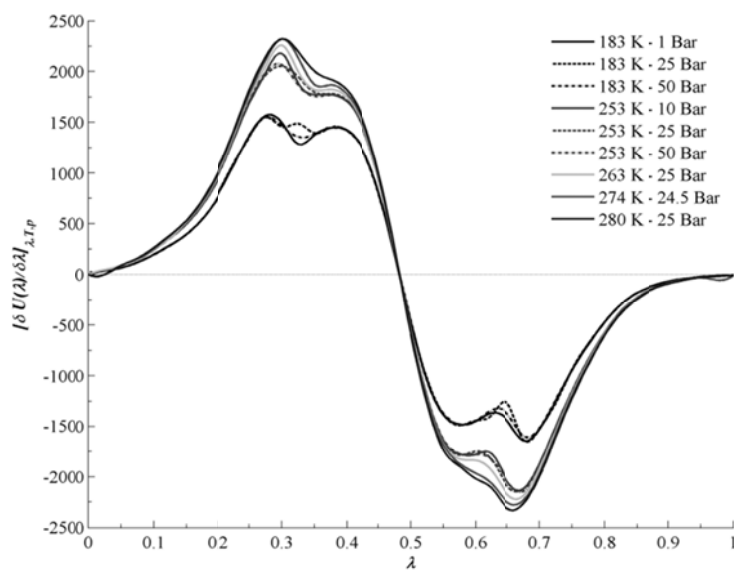


Figure 8.4. The variation of $\langle \partial U(\lambda) / \partial \lambda \rangle_{T,p}$ as a function of the coupling parameter λ for Eq. (8.1) under different pressure and temperature conditions.

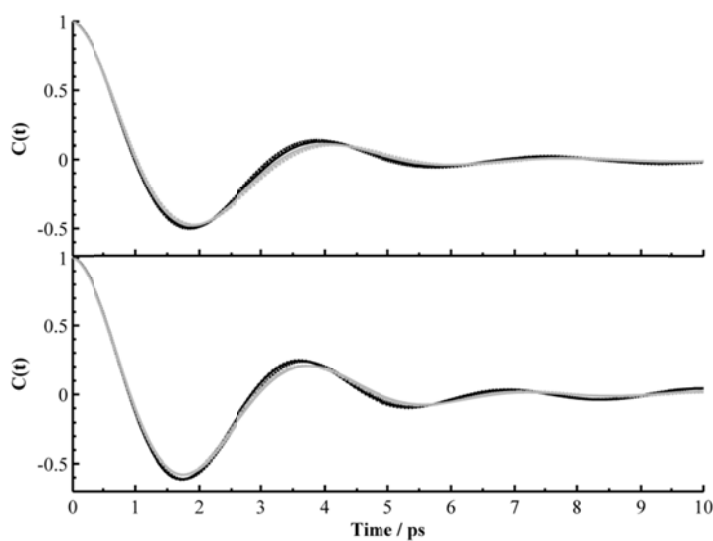


Figure 8.5. The VACFs of the C atom of CH_3F (top) and CH_4 (bottom) in the small and medium cages of sH clathrate hydrate with TBME as large cage guest at 183 K black curves and 253 K gray curves. The full lines correspond to 1 bar, the dotted lines to 25 bar and the dashed lines to 50 bar.

Table 8.3. Configurational energy of sH hydrate with TBME and CH₄ and TBME and CH₃F and at various pressures and temperatures and free energy per unit cell of the chemical substitution of CH₄ with CH₃F under different pressure and temperature conditions. Assuming both species are ideal gases under the pressure and temperature conditions, this will be the total free energy for the substitution reaction.

Temperature K	Pressure bar	$E_{\text{config}}(\text{CH}_4)$ kcal·mol ⁻¹	$E_{\text{config}}(\text{CH}_3\text{F})$ kcal·mol ⁻¹	ΔG_{TI} kcal·mol ⁻¹
183	1	-459.07	-465.36	2.95
183	25	-462.81	-466.10	2.95
183	50	-460.07	-465.23	2.95
253	10	-435.02	-440.31	3.03
253	25	-435.96	-441.23	0.23
253	50	-436.96	-441.50	-1.97
263	25	-435.70	-436.84	2.24
274	24.5	-431.75	-433.43	0.09
280	25	-429.52	-427.60	2.38

The VACF for the carbon atoms of the CH₃F and CH₄ in the small cages of the binary sII clathrate hydrate of THF at different temperatures are shown in Figure 8.6. Once again, the smaller CH₄ guests have a higher rattling frequency in the cages. The VACF for the OS atom of TBME in the binary hydrates is shown in Figure 8.7. The high hydrogen bonding probability of the TBME molecule with the cage water molecules in both binary hydrates (see Table 8.2) indicates that this molecule will be tethered to the cage wall

and undergo small high frequency vibrational motions in the large sH cages. The VACF for the OS atom of THF in the binary hydrates is shown in Figure 8.8. The hydrogen bonding probability of THF with the cage water molecules in the sII binary hydrates is smaller (see Table 8.2) and the THF molecule mostly undergoes free rattling motion in the cage. The VACFs for the OS atoms of THF are must smoother than those of TBME. It is interesting to note that at 281 K, the VACF for THF in the binary hydrate with CH_3F undergoes a noticeable increase in rattling frequency, which correlates with a doubling of hydrogen bond probability at this temperature compared to the 250 K simulation.

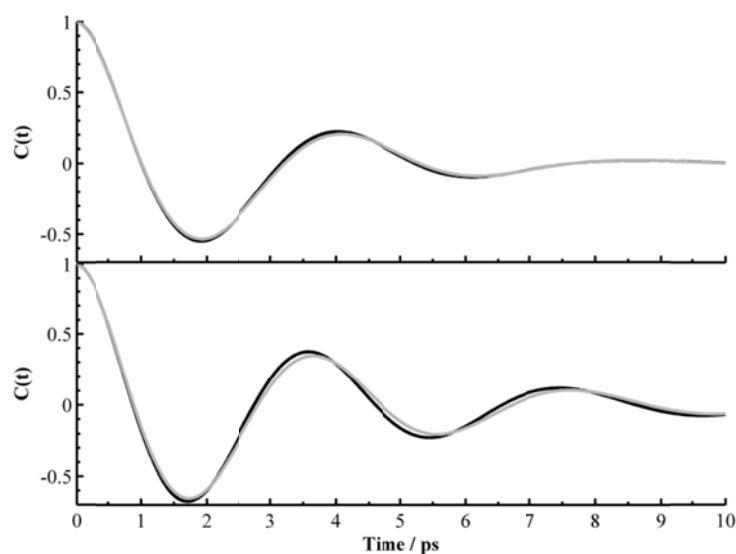


Figure 8.6. The VACFs of the C atom of CH_3F (top) and CH_4 (bottom) in the small cages of sII clathrate hydrate with THF as large cage guest at 250 K black curves and 281 K gray curves.

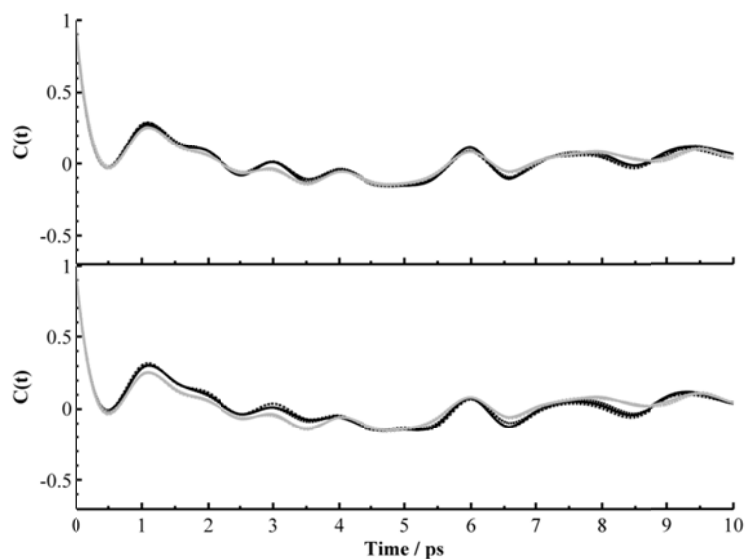


Figure 8.7. The calculated velocity autocorrelation functions (VACFs) of the OS atom of the TBME molecule in the large cage of sH hydrate with (top) CH_3F and (bottom) CH_4 in the small and medium cages at 183 K black curves and 253 K gray curves. The full lines correspond to 1 bar, the dotted lines to 25 bar and the dashed lines to 50 bar.

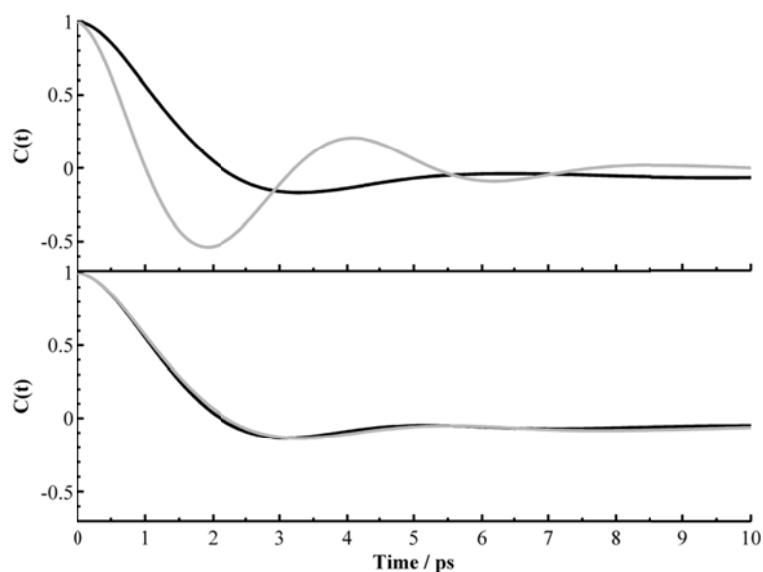


Figure 8.8. The velocity autocorrelation functions (VACFs) of the OS atom of the THF molecule in the large cavity of sII hydrate with (top) CH_3F and (bottom) CH_4 in the small cages at 250 K black curves and 281 K gray curves.

The nature of the VACF for the different hydrates and the changes in guest dynamics at higher temperature correlate well with the changes in the NMR lineshapes and are among the complex changes that occur as the temperature of the hydrate is increased. As mentioned previously, the MD simulations span too short a time period to observe the direct small/medium cage guest exchange between full and empty cages, but nonetheless, they do capture other features which may contribute to the occurrence and rate of guest exchange.

The orientation autocorrelation function (OACF) of the CH₃F and CH₄ molecule in the small cage is a measure of the rotation of a unit vector $\mathbf{u}(t)$ in the direction of the C–F bond for CH₃F or C–H for CH₄ at each time t with respect to a time origin, $\mathbf{u}(0)$. The OACF, $M(t)$ is defined as,

$$M(t) = P_1[\cos\theta(t)] = \langle \mathbf{u}(t) \cdot \mathbf{u}(0) \rangle$$

and represents the ensemble average of P_1 is the first order Legendre polynomial. At any time, $\mathbf{u}(t) \cdot \mathbf{u}(0) = \cos\theta(t)$ represents the angle a molecule has rotated by time t and the brackets represent the ensemble average. It can be observed in Figures 8.9 and 8.10 that the decay of the $M(t)$ CH₄ is faster than that of CH₃F in both hydrate structures. The orientational vector $\mathbf{u}(t)$ of CH₃F maintains its original direction for longer times, whereas CH₄ rotates more freely. As expected both decays are more rapid at higher temperatures.

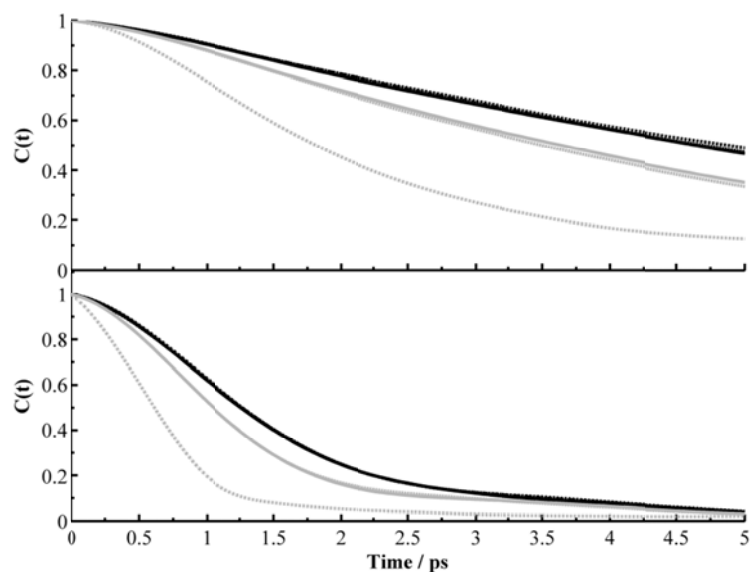


Figure 8.9. The decay of the OACF $M(t)$ with time for (top) CH_3F and (bottom) CH_4 in the sH TBME hydrates at 183 K black curves and 253 K gray curves. The full lines correspond to 1 bar, the dotted lines to 25 bar and the dashed lines to 50 bar.

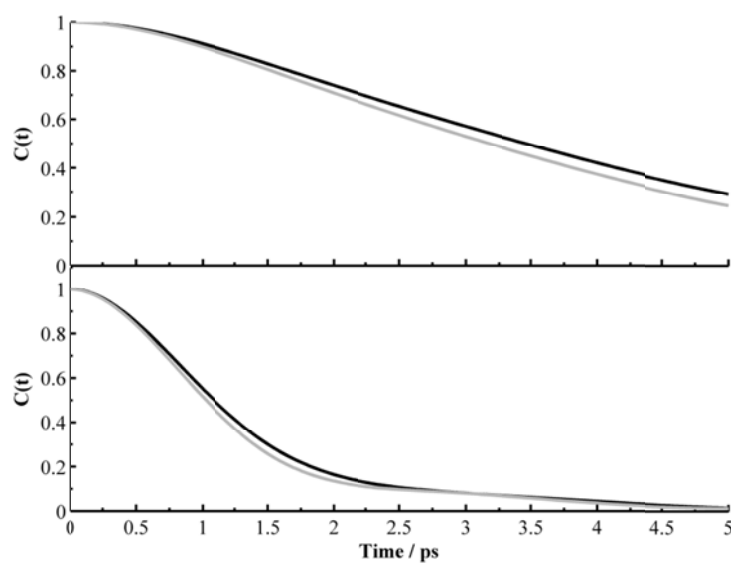


Figure 8.10. The decay of the OACF $M(t)$ with time for (top) CH_3F in the sH TBME and sII THF hydrates and (bottom) CH_4 in the sH TBME and sII THF hydrates at 250 K black curves and 281 K gray curves.

8.5 Conclusions

Molecular dynamics simulations showed that the TBME and THF guest molecules have enhanced hydrogen bonding in the binary hydrates with CH_3F . This could be due to the larger size of these molecules and the resulting weakening of the water hydrogen bonding network in the cages which accommodate CH_3F , which then enhances the hydrogen bonding with the large cage guests.

Additionally, the simulations showed the role of the small/medium cage guests on the hydrogen bonding of the large cage guests with the hydrate framework water molecules. The larger CH_3F molecule which also has a non-zero dipole moment interacts with the cage water molecules to a greater extent, leading to slower translational and rotational dynamics of this molecule in the small / medium cages. This in turn leads to greater hydrogen bonding probability of the large guests in the binary hydrates which have CH_3F as the help-gas. In the simulations, CH_3F molecules do not themselves show a tendency to form hydrogen bonds with the water molecules.

The thermodynamic integration free energy calculations showed that there is a small systematic preference for CH_4 in the small and medium cages compared to CH_3F .

8.6 References

- [1] Alavi S., Ripmeester J. A., Klug D. D. Molecular-dynamics study of structure II hydrogen clathrates. *The Journal of Chemical Physics*. 2005;123:024507-7.
- [2] Alavi S., Ripmeester J. A., Klug D. D. Stability of rare gas structure H clathrate hydrates. *Journal of Chemical Physics*. 2006;125:10.

- [3] Alavi S., Ripmeester J. A., Klug D. D. Molecular dynamics study of the stability of methane structure H clathrate hydrates. *The Journal of Chemical Physics*. 2007;126:124708-6.
- [4] Nohra M., Woo, T. K., Alavi, S., Ripmeester, J. A. Molecular dynamics Gibbs free energy calculations for CO₂ capture and storage in structure I clathrate hydrates in the presence of SO₂, CH₄, N₂, and H₂S impurities. *The Journal of Chemical Thermodynamics*. 2012;44:5-12.
- [5] Dornan P., Alavi S., Woo T. K. Free energies of carbon dioxide sequestration and methane recovery in clathrate hydrates. *Journal of Chemical Physics*. 2007;127.
- [6] Alavi S., Ripmeester, J. A. Effect of small cage guests on hydrogen bonding of tetrahydrofuran in binary structure II clathrate hydrates. *Journal of Chemical Physics*. 2012;137.
- [7] Smith W., Forester, T. R., Todorov, I. T. . *The DL_Poly_2 User Manual, Version 2.20*. 2009.
- [8] Nose S. A Unified Formulation of the Constant Temperature Molecular Dynamics Methods. *Journal of Chemical Physics*. 1984;81:511-9.
- [9] Sasaki S., Hori S., Kume T., Shimizu H. Microscopic observation and in situ Raman scattering studies on high-pressure phase transformations of a synthetic nitrogen hydrate. *Journal of Chemical Physics*. 2003;118:7892-7.
- [10] Alavi S., Susilo R., Ripmeester J. A. Linking microscopic guest properties to macroscopic observables in clathrate hydrates: Guest-host hydrogen bonding. *Journal of Chemical Physics*. 2009;130.
- [11] Bernal J. D., Fowler R. H. A theory of water and ionic solution, with particular reference to hydrogen and hydroxyl ions. *Journal of Chemical Physics*. 1933;1:515-48.
- [12] Abascal J. L. F., Sanz E., Fernandez R. G., Vega C. A potential model for the study of ices and amorphous water: TIP4P/Ice. *Journal of Chemical Physics*. 2005;122.
- [13] Frisch M. J., Trucks, G. W., Schlegel, H. B., Scuseria et al. *GAUSSIAN 03*. Wallingford, CT: Gaussian Inc. ; 2003.
- [14] McQuarrie D. A. *Statistical Mechanics* In: Row H., editor. New York 1976.

[15] S. Murad K. E. G. Computer Modeling of Matter: American chemical society; 1978.

Chapter 9

Conclusions and Outlook



This thesis presents the study of several properties of clathrate hydrate and semi-clathrate hydrate systems with the purpose to elucidate their potential and technical feasibility for H₂ storage.

The aim of the first study was to determine the influence of several organic compounds (also called additives or promoters) on the phase equilibrium conditions of the hydrate phase. For this purpose, the hydrate equilibrium conditions of five mixed (H₂ + organic volatile compound) clathrate hydrates at the stoichiometric concentration of the organic compound were studied. The results showed that the mixed (H₂+organic volatile compound) clathrate hydrates presented a considerably higher stability, not only in comparison with the pure H₂ hydrate but also in comparison with the single clathrate hydrates of the organic compounds tested. The following trend was observed in increasing stability: 1,3-dioxolane < 2,5-dihydrofuran < tetrahydropyran < furan, THF < cyclopentane. This trend was explained in terms of molecular size and geometry of the organic compound. The organic compound with the symmetry that better fits the large cavity seems to be able to produce the most stable clathrate hydrate. Although the results are encouraging in terms of stability, numerous studies have reported that the maximum H₂ storage capacity of sII mixed (H₂+organic volatile compound) is not higher than ~1.0 wt% at the stoichiometric concentration of the organic volatile compound. The US Department of Energy (DOE)'s target for a viable H₂ storage technology for transportation by 2017 is a H₂ storage system with an energy generation to weight ratio of 1.8 kWh/kg. This requires a material possessing 5.5 wt% of H₂. From the results it is evident that a mixed (H₂ + additive) sII clathrate hydrate is still far from reaching this goal. The pressure, temperature and specifically the H₂ storage capacity under the current state of the art do not meet the requirements of a viable H₂ storage technology.

Consequently, in the second and third study, the kinetics of formation of the H₂-TBAB, H₂-TBAF and CO₂-TBAB semi-hydrates was studied. The aim was to determine the factors influencing the amount of H₂ and CO₂ stored in the semi-clathrate hydrate. The results indicated that the induction time, the rate of hydrate formation and amount of H₂ consumed were favored at higher

pressures and higher solute concentrations. No influence of the formation method on the hydrate growth and amount of H₂ consumed was observed. The maximum amount of H₂ stored in the hydrate phase was 0.046 wt% for the TBAB system (16 MPa and 281.1 K in a solution with a concentration of 3.7 mol% of TBAB) and 0.024 wt% for the TBAF system (13 MPa and 294.15 K in a solution with a concentration of TBAF of 3.4 mol%). However, the results showed that mass transfer limitations hindered the gas transport into the hydrate phase and consequently the amount of gas stored was significantly reduced. For the CO₂-TBAF semi-hydrates the TBAF concentration did not show a large influence, and pressure only displayed a major influence on the formation rate. Instead, the induction time and the amount of CO₂ consumed were favored at low temperatures as a result of the increase in subcooling. It was calculated that the CO₂ content in the CO₂-TBAF semi-hydrate formed at the most favorable conditions (1.8 mol% of TBAF, 2.6 MPa and 293.15 K) was 0.45 wt%, this amount is only ~6.5% of the maximum theoretical storage capacity. Therefore, as in the case of H₂, mass transfer played a major role in the total amount of gas uptake. Although, it also seems unlikely that semi-clathrate hydrates can be used to develop a viable H₂ storage technology, the results indicated that CO₂-TBAF semi-hydrates have the potential to be applied in novel separation technologies e.g., for the purification of flue gases (CO₂ removal). CO₂-TBAF semi-hydrate formation displayed shorter induction times and higher formation rates than that of H₂-TBAF semi-hydrate. Moreover, at low pressures the CO₂ content in the hydrate phase is considerable higher than the H₂ content.

The fourth and fifth study applied NMR spectroscopy and molecular dynamic simulations to identify specific features of the CH₃F-CH₄-TBME sH clathrate hydrate. The original aim was to determine the ability of the two dodecahedral cages (D-5¹² and D'-4³⁵⁶⁶) of sH to discriminate between the two guest molecules (CH₄ and CH₃F) that are slightly different in size. ¹³C NMR studies showed a small preference of CH₃F for the D' cage compared to the D cage. However, a more interesting feature was observed. At high temperatures, the ¹³C NMR spectra associated with CH₃F, showed a

merging of the doublet structures characteristic of CH_3F in the non-spherical environments of the sII and sH cages. The merging of the doublet peaks implies a local migration of CH_3F and CH_4 between neighboring cages. Additional measurements of the ^2H NMR powder lineshapes of the THF/ CD_3F hydrate at different temperatures confirmed the migration of CD_3F between neighboring cages. This phenomenon of rapid motion of the guest between cages can be attributed to water vacancies in the confining symmetry of the cages. It is uncertain if the water vacancies are intrinsic or the result of host-guest interactions. However, previous studies have reported that certain features of the guests can contribute to specific guest-host interactions, in particular to hydrogen bonds formation between the large cage guest and the water molecules of the cage framework. Hydrogen bonds can introduce Bjerrum L-defects in the water lattice and migration of L and D Bjerrum defects in the hydrate lattice can occur through water molecule reorientation. Therefore, the results suggest that the combination of TBME and CH_3F and THF and CH_3F at temperatures above 250 K gives rise to fast dynamics of the water lattice in sII and sH. Although guest exchange between neighboring cages may occur in other systems, this is the first time that such motion in a NMR spectrum is reported. Consequently, it would be advisable to perform further research in order to find evidence of similar behavior in other systems, a starting point could be exploring the system difluoromethane-TBME. This would help to increase the understanding of the factors affecting the dynamics of the guest and the guest-host interactions. It would also be interesting to perform complementary research to understand the influence of CH_3F on the stability and kinetics of clathrate hydrates using polar and non-polar large guest molecules.

Molecular dynamics calculations of the hydrogen bond dynamics and small guest rotation dynamics showed that CH_3F enhances hydrogen bonding between TBME and THF with the water framework. This could be due to the larger size of CH_3F molecules and the resulting weakening of the water hydrogen bonding network in the cages hosting CH_3F , resulting in the enhanced hydrogen bonding of the large cage guests with the water framework. The previous findings represent a step forward in the

understanding of clathrate hydrate systems. However, it is advisable to explore the specific features of CH_3F responsible for the high probability of defects formation on the hydrate lattice. It would also be interesting to complement the study calculating the probability of hydrogen bond formation using a non-polar large molecule guest.

Despite the unfavorable results for H_2 storage in clathrate hydrates, the knowledge gained over the last few years on the subject can open opportunities to new technological developments. For instance, a deep understanding of the structure and interactions among guest molecules and host molecules is of particular importance. From this knowledge, new materials with higher H_2 storage capacity can be developed. As it was shown in the previous chapters, the interactions of guest molecules with the H_2O molecules of the hydrate framework can induce defects in the structure. These defects affect the mechanical and physical properties of the structure and the behavior and motion of the guest molecules. This study proves that in order to fully understand the behavior of these materials, further research addressing specific targets such as the effect of certain guest molecule or guest mixture on the cell volume and structure, the development of methods for the incorporation of molecules on the framework and the study of the factors affecting cage occupancy, etc. is necessary.

Appendix A

PXRD Patterns

The PXRD patterns were fitted to standard sI, sII and sH hydrate patterns to obtain the lattice constants which are presented in Table A.1. The PXRD patterns are presented in the Figures A.1-A.4. Unreacted ice was present in all the samples. The lattice parameters suggest that the presence of CH₃F causes an expansion of the lattice.

Table A.1. Lattice constants of CH₃F and CH₄ sI and sH hydrates obtained at 183.15 K.

System	Hydrate structure	Lattice constants / Å
CH ₄ -TBME-H ₂ O	sH	a = 12.2452(6)Å c = 10.0452(7)Å
CH ₄ -H ₂ O*	sI	a = 11.85 Å
CH ₃ F-TBME-H ₂ O	sH	a = 12.2756(5)Å c = 10.0225(2)Å
56 % excess TBME	sI	a = 11.8945(9)Å
CH ₃ F-H ₂ O	sI	a = 11.8993(1)Å
CH ₃ F-CH ₄ -TBME- H ₂ O	sH	a = 12.2624(1)Å c = 10.0408(6)Å
50-50 mol% CH ₃ F-CH ₄ 56 % excess TBME		

* The lattice constant of sI CH₄-H₂O is taken from Susilo et al. Chemical Engineering Science. 2007;62:3930-9.

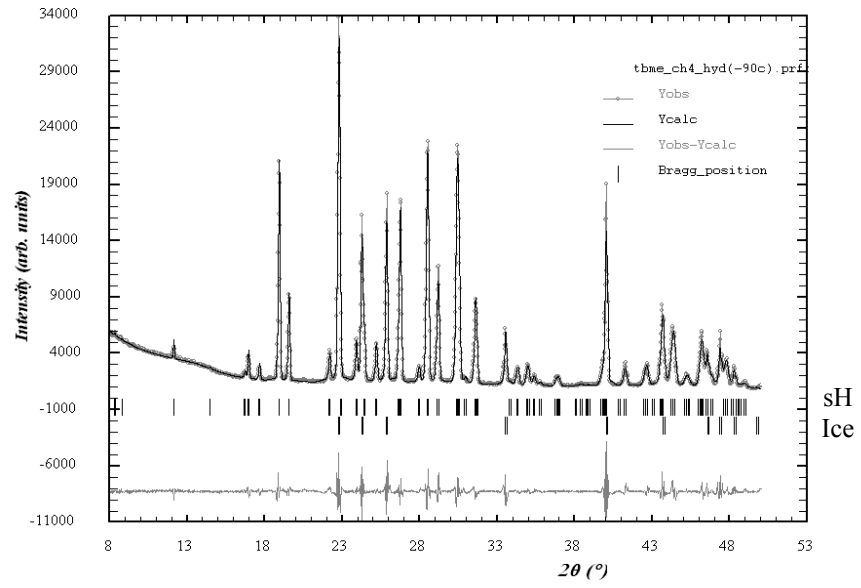


Figure A.1. PXRD pattern of sH hydrate CH₄-TBME-H₂O at 183.15 K

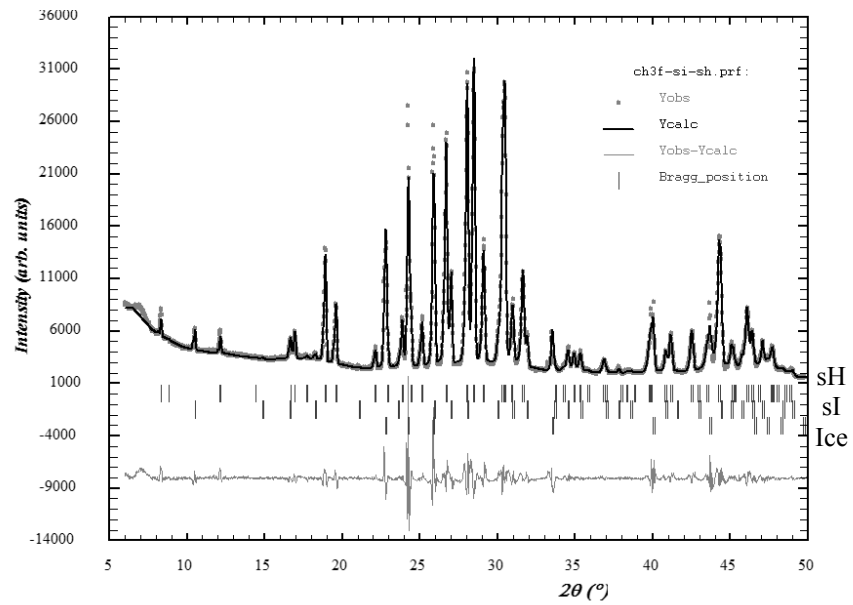


Figure A.2. PXRD pattern of sH hydrate CH₃F-TBME-H₂O (56% excess TBME) at 183.15 K

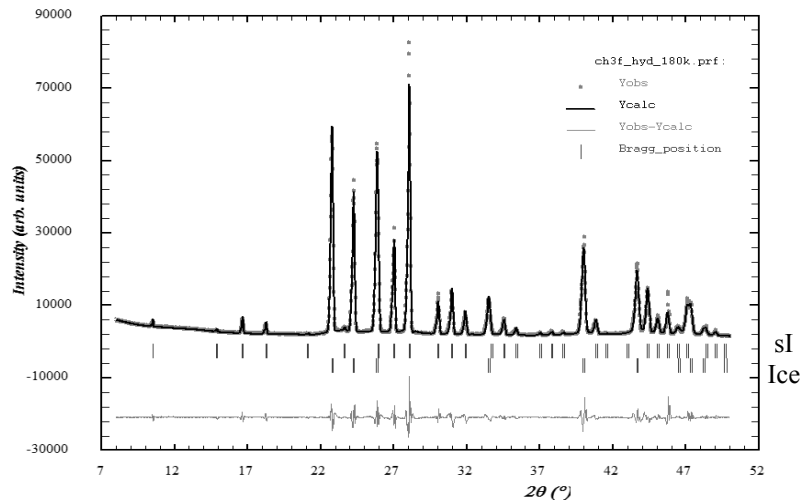


Figure A.3. PXRD pattern of sI hydrate $\text{CH}_3\text{F}-\text{H}_2\text{O}$ at 183.15 K

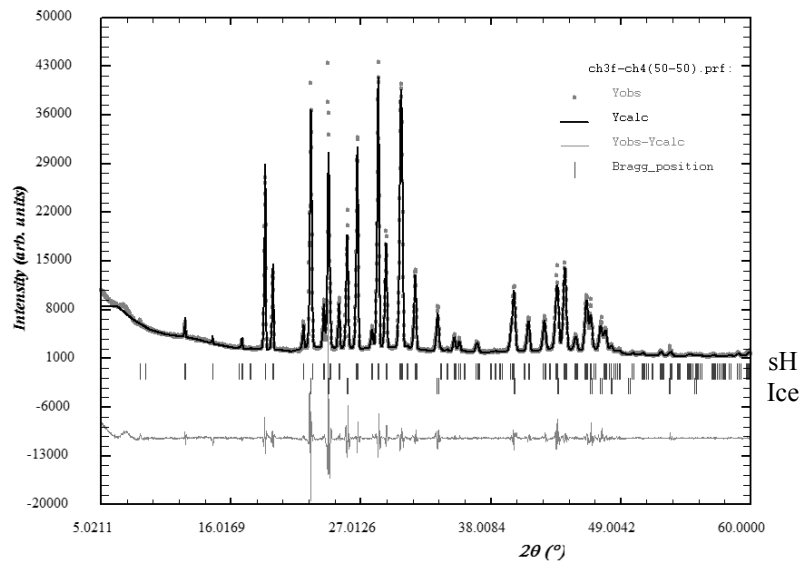


Figure A.4. PXRD pattern of sI hydrate $\text{CH}_3\text{F}-\text{CH}_4-\text{TBME}-\text{H}_2\text{O}$ 50-50 mol% $\text{CH}_3\text{F}-\text{CH}_4$ (56 % excess of TBME) at 183.15 K.

Personal Information

Alondra Torres Trueba was born on the 27th of September 1982 in Mexico City. After finishing her Bachelor Degree on Chemical Engineering in 2005 at Universidad Autonoma del Estado de Mexico, in Toluca Mexico, she studied a Master in Science in Chemical Engineering at Universidad Iberoamericana in Mexico City. In 2007 she graduated with Cum Laude within the Thermodynamics and Process Engineering group on Formation of Polymeric Membranes with Supercritical Carbon Dioxide with Applications for Gas Separation. From 2009 she started a PhD project at Delft University of Technology and continued it at Eindhoven University of Technology at Eindhoven in the Netherlands of which the results are presented in this dissertation. In 2011 she won a prize for best poster and best poster presentation at the 5th International Symposium on Hydrogen Energy and in 2012 she participate in the foundation of the Mexican Student Association at Delft University of Technology.

List of Publications

- Alondra Torres Trueba, Maaïke C. Kroon, Cor J. Peters, Igor L. Moudrakovski, Christopher I. Ratcliffe, Saman Alavi, John A. Ripmeester, *Inter-cage Dynamics in Structure I, II, and H Fluoromethane Hydrates as studied by ^{13}C and ^2H NMR*, Journal of Physical Chemistry, To be submitted (2013)
- Alondra Torres Trueba, Maaïke C. Kroon, Cor J. Peters, Igor L. Moudrakovski, Christopher I. Ratcliffe, Saman Alavi, John A. Ripmeester, *Molecular dynamics study of sII and sH Fluoromethane and Methane Hydrates*, Journal of Physical Chemistry, To be submitted (2013)
- Torres Trueba, A., Radovic, I., Zevenbergen, J., Kroon, M. C. & Peters, C. J., *Kinetic Measurements and In situ Raman Spectroscopy Study of the Formation of TBAF Semi- Hydrates with Hydrogen and Carbon Dioxide*, International Journal of Hydrogen Energy, **2013**, Vol.38, Issue 18, pp. 7326- 7334
- Torres Trueba, A., Radovic, I., Zevenbergen, J., Kroon, M. C. & Peters, C. J., *Kinetics Measurements and In situ Raman Spectroscopy of Formation of Hydrogen-Tetrabutylammonium Bromide Semi-Hydrates*, International Journal of Hydrogen Energy, **2012**, Vol. 37, Issue 7, pp. 5790-5797
- Torres Trueba, A., Witkamp, G. J., Rovetto, L. J., Florusse, L. J., Kroon, M. C. Peters, C. J., *Phase Equilibrium Measurements of Structure II Clathrate Hydrates of Hydrogen with Various Promoters*, Fluid Phase Equilibria, **2011**, Vol. 307, Issue 1, pp. 6-10
- Torres Trueba, A., Ortiz Estrada, C., Barcenas, G. L., Ruiz Trevino, A. F., *Formation of Integrally Skinned Asymmetric*

Polysulfone Gas Separation Membranes by Supercritical CO₂, Journal of Membrane Science, 2008, Vol. 320, No 1-2, pp. 431-435.

Conference Proceedings/ Book Abstracts

- Torres Trueba, A., Radovic, I., Zevenbergen, J., Kroon, M. C. & Peters, C. J., *Carbon dioxide sequestration and hydrogen storage in TBAB and TBAF semi-clathrate hydrates: Kinetics and crystal evolution by in situ Raman spectroscopy*, Properties and Phase Equilibria for Process and Product Design, May, 2013, Argentina.
- Torres Trueba, A., Radovic, I., Zevenbergen, J., Kroon, M. C. & Peters, C. J., *Hydrogen Storage in Tetra n-Butyl Amonium Bromide Semi-Clathrate Hydrates: Kinetics and Evolution of Hydrate-Phase Composition by in situ Raman Spectroscopy*, 6th International Symposium Hydrogen & Energy, January, 2012, Switzerland.
- Torres Trueba, A., Radovic, I., Zevenbergen, J., Kroon, M. C. & Peters, C. J., *Hydrogen storage and Carbon Dioxide sequestration in TBAF Semi-Clathrate Hydrates: Kinetics and Evolution of Hydrate-Phase Composition by in situ Raman Spectroscopy*, AIChE Annual Meeting, October, 2012, United States of America.
- Torres Trueba, A., Radovic, I., Zevenbergen, J., Kroon, M. C. & Peters, C. J., *Hydrogen storage and carbon dioxide sequestration in TBAF semi-clathrate hydrates: Kinetics and evolution of hydrate-phase composition by in situ Raman spectroscopy*. Proceedings of the 26th European Symposium on Applied Thermodynamics (ESAT 2012), October 2012, Germany
- Torres Trueba, A., Radovic, I., Zevenbergen, J., Kroon, M. C. & Peters, C. J., *Kinetics of Tetra-n-Butylammonium Bromide + Hydrogen Semi-Clathrate Hydrate Formation*. AIChE Annual Meeting. October, 2011, United States of America.

- Torres Trueba, A., Radovic, I., Zevenbergen, J., Kroon, M. C. & Peters, C. J., *Hydrogen Semi-Clathrate Hydrate Formation from TBAB aqueous solutions: Kinetics and Evolution of Hydrate-Phase Composition by in situ Raman Spectroscopy*, Netherlands Process Technology Symposium 2011. October, 2011, Netherlands.

- Torres Trueba, A., Radovic, I., Zevenbergen, J., Kroon, M. C. & Peters, C. J., *Kinetics Measurements of Hydrogen + Tetra-n-Butylammonium Bromide Semi-Clathrate Hydrates*, 17th International Conference on Gas Hydrates, July, 2011, United Kingdom

- Torres Trueba, A., Witkamp, G. J., Rovetto, L. J., Florusse, L. J., Kroon, M. C. Peters, C. J., *Hydrogen Storage in Structure II Clathrate Hydrates with various Promoters*, 5th International Symposium Hydrogen & Energy. January, 2011, Switzerland.

- Torres Trueba, A., Witkamp, G. J., Rovetto, L. J., Florusse, L. J., Kroon, M. C. Peters, C. J., *Phase Equilibrium Measurements of Structure II Clathrate Hydrates of Hydrogen with Various Promoters*, Netherlands Process Technology Symposium 2010. October, 2010, Netherlands.

- Torres Trueba, A., Ortiz, C., Ruiz, A., *Formation of Asymmetric Polysulfone Membranes with Supercritical CO₂*, XXVIII Encuentro Nacional de la Academia Mexicana de Investigación y Docencia en Ingeniería Química. May 2007, Manzanillo, México.

Acknowledgements

Many individuals have provided advice, encouragement, and support for the completion of this thesis. Therefore, first I would like to thank my supervisor Cor J. Peters for giving me the unique opportunity to take part in this project and for his invaluable support during all these years. I also thank my co-supervisor Maaïke C. Kroon for her feedbacks and valuable comments on my manuscripts and for the welcome in her group at Eindhoven University of Technology. My appreciation is also extended to the ACTS Sustainable Hydrogen committee for their financial support.

My next gratitude goes to my colleague and friend Ivona R. Radović, not only for her guidance and notable contributions, but also for her friendship and constant encouragement. Also to John Zevenbergen for the hospitality in his laboratory at TNO Defense, and for his contagious enthusiasm on the project. Special thanks to Eugene Straver for his assistance during the phase equilibrium measurements.

I wish to express my sincere gratitude to John A. Ripmeester for the privilege to work in his group at the National Research Council of Canada (NRC). The input from him and his highly skilled team was an invaluable contribution to this thesis. Appreciation is also extended to Igor L. Moudrakovski and Christopher I. Ratcliffe for their assistance and contributions in the measurements and interpretation of the NMR experiments. To Saman Alavi for having the enormous patience to explain all the details of the Fortran codes by e-mail, and for his valuable feedback and input on the manuscript. I also want to thank my office mates in Ottawa - Kyuchul, Sanehiro and Litao- for their valuable advices and assistance, and to Steve and Graham for their help in the lab. Special thanks go to Nagu Daraboina for introducing me to the group.

I would also like to thank the people of Eindhoven University, especially Caroline, for her extraordinary assistance with all the paperwork and

procedures and to all my PhD colleagues -Lawien, Nerea and Adriaan- for the warm reception.

Special thanks go to all the people of P&E, starting with the kind services provided by the secretaries -Helma, Leslie and Ilona-, Rob van den Boogaard for the extension of my status as a visitor, Theo W. de Loos for the invitation to the European course in supercritical fluids, Thijs Vlugt and Sondre K. Schnell for their assistance in using the cluster, Wim Buijs for his help in using Spartan and for his friendship, Jaap van Spronsen and Geer-Jan Witkamp for their useful comments during the section meetings.

Thanks to all my friends and colleagues from P&E for complementing the PhD experience with a full set of interesting chats, lunch gatherings, parties, trips, dinners, barbeques, etc. Thanks to Helene, Jessica, Elif and Marcos for being excellent officemates; to Somayeh, Stevia, Kamarza, Mariette, Ernesto Bernardo, Sara and Jorge for the great trips we made together; to Albert, Marloes and Michel for the lunch gatherings; to my group colleagues Selva, Khalik, Mayte, Mamoun, Sona and Ali for their friendship; to Camiel, Orchidea, Aylin, Ana Maria, Sebastian, Nafiseh for the nice chats, parties and gatherings and to Denis and Guido for the candy shop (which was fundamental in finishing this thesis). Special thanks go to Stephanie, Sergio and Carsten for the discussions on my propositions.

The list continues with my friends Jan, Monika and to Adri Peters who made my arrival in the Netherlands a very welcoming experience and to my friend Rick from TNO for the super nice dinners.

To all my friends from the Mexican and international community, thanks for enriching my PhD experience with creativity, exploration of artistic talents, leadership, entrepreneurship and entertainment. I will never forget the parties, artistic events and the creation of the Mexican student association. Mainly, I want to thank: Hugo, Omar, Antonio Ramos, Antonio Jarquin, Adonis, Ileana, Diana, Zeus, Fabian, Manuel, Wilson, Gabriel and Lucie.

Acknowledgements

Special thanks to Alberto for his support, patience and caring during the first years of our stay in the Netherlands.

To my dearest parents and sister, thanks for your encouragement and unconditional love.

Special gratitude goes out to Tiemo, who has provided constant support and encouragement during the final stages, as well as continuously editing my manuscripts and for translating the summary. Thank you!!

Finally, my sincerest appreciation to Eric Fromm and Albert Ellis for their ideas.